TAMPEREEN TEKNILLINEN YLIOPISTO
TAMPERE UNIVERSITY OF TECHNOLOGY

KRISTIAN KONTTINEN

DETERMINING THE AMPLITUDE DEPENDENCE OF NEGATIVE CONDUCTANCE IN A TRANSISTOR OSCILLATOR

Master of Science Thesis

Examiners: University Lecturer Olli-Pekka Lundén and Lecturer Jari Kangas
Examiners and topic approved by the Faculty Council of the Faculty of Computing and Electrical Engineering on 6th May 2015

ABSTRACT

KRISTIAN KONTTINEN: Determining the Amplitude Dependence of Negative Conductance in a Transistor Oscillator
Tampere University of Technology
Master of Science Thesis, 49 pages, 34 Appendix pages
June 2016
Master's Degree Programme in Electrical Engineering
Major: RF Engineering
Examiners: University Lecturer Olli-Pekka Lundén and Lecturer Jari Kangas
Keywords: oscillator, negative resistance, negative conductance

An electronic oscillator is an autonomous circuit that generates a periodic electronic signal. In practice, an oscillator should provide a voltage signal with a certain frequency and amplitude to a resistive load. Predicting the output voltage amplitude typically involves complicated nonlinear equations. One popular simplified approach to amplitude prediction uses the concept of negative output conductance. It assumes that the output conductance of the oscillator is a function of the output voltage amplitude. This function can then be used to predict the output voltage amplitude.

In literature, it is commonly assumed that the output voltage amplitude dependence of the negative conductance or resistance in a transistor oscillator can be approximated sufficiently accurately with a certain straight-line equation. Then a rule for maximizing the oscillator output power is derived based on this straight-line approximation. However, the straight-line equation has not been shown to be valid for transistor oscillators. Instead, the straight-line approximation was originally found to be suitable in describing the negative conductance of an IMPATT (IMPact Avalanche and Transit Time) diode. The validity of the rule for maximizing the output power is questionable for transistor oscillators.

This work studies the output voltage amplitude dependence of negative conductance in a transistor oscillator by simulations, measurements and analytical methods. Simulations are based on the harmonic balance technique. One simulation method determines the amplitude dependence by using a varying test voltage source, and the other method uses a varying load. The measurement method involves terminating the oscillator with a resistive load. The output voltage amplitude and the corresponding negative conductance are calculated from the measured output power for varying load conductance values. The analytical methods are based on a function describing the negative conductance of the transistor oscillator. This function is derived in this work. The results show that the straight-line based rule for maximizing the output power is inapplicable for transistor oscillators.

TIIVISTELMÄ

KRISTIAN KONTTINEN: Transistorioskillaattorin negatiivisen konduktanssin amplitudiriippuvuuden määrittäminen
Tampereen teknillinen yliopisto
Diplomityö, 49 sivua, 34 liitesivua
Kesäkuu 2016
Sähkötekniikan koulutusohjelma
Pääaine: Suurtaajuustekniikka
Tarkastajat: yliopistonlehtori Olli-Pekka Lundén ja lehtori Jari Kangas
Avainsanat: oskillaattori, negatiivinen resistanssi, negatiivinen konduktanssi

Elektroninen oskillaattori on autonominen piiri, joka tuottaa jaksollisen, elektronisen signaalin. Oskillaattorin tehtävä on tuottaa resistiiviselle kuormalle jännitesignaali, jolla on haluttu taajuus ja amplitudi. Lähtöjännitteen amplitudin ennustaminen vaatii tyypillisesti monimutkaisia epälineaarisia yhtälöitä. Eräs yleinen yksinkertaistus lähtöjännitteen amplitudin ennustamiseen perustuu negatiiviseen lähtökonduktanssiin. Tässä yksinkertaistuksessa oskillaattorin lähtökonduktanssin oletetaan olevan lähtöjännitteen amplitudin funktio. Tätä funktiota voidaan käyttää lähtöjännitteen amplitudin ennustamiseen.

Kirjallisuudessa oletetaan yleisesti, että transistorioskillaattorin negatiivisen konduktanssin tai resistanssin riippuvuutta lähtöjännitteen amplitudista voidaan arvioida riittävän tarkasti suoran yhtälön avulla. Tästä arviosta johdetaan edelleen sääntö, jolla oskillaattorin lähtöteho voidaan maksimoida. Suoran yhtälön sopivuutta transistorioskillaattoreille ei ole todettu, vaan alun perin suoran yhtälö todettiin sopivaksi kuvaamaan IMPATT-diodin (IMPact Avalanche and Transit Time) negatiivisen konduktanssin amplitudiriippuvuutta. Tehon maksimointisäännön toimivuus transistorioskillaattoreille on kyseenalainen.

Tässä työssä tutkitaan erään transistorioskillaattorin negatiivisen konduktanssin amplitudiriippuvuutta simuloinneilla, mittauksilla ja analyyttisillä menetelmillä. Simuloinneissa käytetään harmonisen balanssin menetelmää. Toisessa simulointimenetelmässä amplitudiriippuvuus määritetään vaihtelevan testijännitelähteen avulla ja toisessa vaihtelevan kuorman avulla. Mittausmenetelmässä oskillaattoriin kytketään resistiivinen kuorma. Lähtöjännitteen amplitudi ja sitä vastaava negatiivinen konduktanssi lasketaan mitatun tehon ja kuormakonduktanssin avulla vaihtelevilla kuormakonduktanssiarvoilla. Analyyttiset menetelmät perustuvat tässä työssä johdettuun, transistorioskillaattorin negatiivista konduktanssia kuvaavaan funktioon. Tulosten perusteella suoran yhtälöön perustuva tehon maksimointisääntö ei sovellu transistorioskillaattoreille.

PREFACE

I wrote this thesis at Tampere University of Technology during 2015–2016. I would like to thank the supervisor and examiner, Olli-Pekka Lundén, for this interesting topic and for providing valuable suggestions and advice. I would also like thank examiner Jari Kangas for useful comments and advice.

Finally, I would like to thank my parents for their support and kindness.

Tampere, 23rd May 2016

Kristian Konttinen

CONTENTS

LIST OF SYMBOLS AND ABBREVIATIONS

FET	field-effect transistor
IMPATT	IMPact Avalanche and Transit Time

B_L	load susceptance
B_{out}	output susceptance
C_1	capacitance of oscillator feedback capacitor 1
C_2	capacitance of oscillator feedback capacitor 2
C_1'	total base-emitter capacitance
C_2'	total collector-emitter capacitance
C_{bc}	small-signal base-collector capacitance of a transistor
C_{be}	small-signal base-emitter capacitance of a transistor
C_{ce}	small-signal collector-emitter capacitance of a transistor
f	frequency
ϕ	transadmittance phase angle
G_L	load conductance
G_m	small-signal output conductance
G_{out}	output conductance
ω	angular frequency
P_L	load power
P_{SA}	spectrum analyzer input power
r_π	base-emitter resistance of a transistor
r_o	collector-emitter resistance of a transistor
$\hat{v}_{be}$	base-emitter voltage amplitude
$\hat{v}_{out}$	oscillator output voltage amplitude
$\hat{v}_{test}$	voltage amplitude of the test voltage source
x	$\frac{C_1'}{C_2'}$
y_m	transadmittance
Y_L	load admittance
Y_{out}	output admittance
Z_L	load impedance
Z_{out}	output impedance

LIST OF FIGURES

LIST OF TABLES

1. INTRODUCTION

An oscillator can be defined as a circuit which generates "a periodic signal of constant amplitude and frequency f_0 from the energy delivered by direct-current (dc) sources" [1, p. 1]. Oscillators have several applications in radio-frequency circuits. For example, frequency conversion can be performed with an oscillator and a mixer [2, p. 616]. Oscillators are also used to generate the carrier signal in radio transmitters [2, p. 577].

The nonlinearity of the oscillator complicates the design [2, p. 577]. An oscillator involves an active device which is typically a transistor or a negative-resistance diode. Often the voltage and current waveforms in the oscillator circuit are nonsinusoidal and the active device is in "nonlinear" operation.

One common approach to oscillator analysis in textbooks uses the concept of negative resistance. In that approach, the oscillator consists of an active part which has negative resistance connected to a passive part which has positive resistance [3, p. 562]. The passive part can be a resonant circuit (e.g. an LC-resonator) or the external load to which the oscillator delivers power. The active part may use a diode which intrinsically has negative resistance, e.g. an IMPATT (IMPact Avalanche and Transit Time) diode. Alternatively, a circuit consisting of a transistor and suitable reactive elements can be used to generate negative resistance. During oscillation, the sum of the active- and passive-part impedances is zero.

The negative resistance is commonly considered to depend on the oscillation amplitude. Initially, when the circuit is switched on, the magnitude of the negative resistance is assumed to exceed the positive resistance. This causes current at a certain frequency to develop from the noise present in the circuit. As the amplitude increases, the magnitude of the negative resistance decreases. Finally, when the circuit is oscillating in steady state, the sum of the negative and positive resistance is zero. [3, p. 562]

In some textbooks and papers, it is assumed that the magnitude of the negative resistance decreases with increasing oscillation amplitude according to an equation of a straight line. This straight-line assumption is then used to derive an optimum load resistance value which maximizes the output power [3, p. 571].

In some oscillators, it is more appropriate to view the active device as having *negative conductance* instead of *negative resistance*. In this case, the negative conductance is typically assumed to decrease according to the equation of a straight line, and the optimum load value is expressed as a conductance.

The straight-line assumption of the negative conductance was originally presented for oscillators which use an IMPATT diode as the active device [4]. However, textbooks and papers have used the optimum load conductance value derived from the straight-line assumption also for transistor oscillators. This is despite the fact that the straight-line assumption has not been shown to be valid for transistor oscillators.

This thesis aims to determine the validity of the straight-line assumption in a transistor oscillator. The output voltage amplitude dependence of the negative conductance is studied with measurements, simulations and analytical methods.

This thesis is structured as follows. Chapter 2 discusses the concepts of negative resistance, negative conductance and the amplitude dependence. Previous research on the amplitude dependence of negative conductance in oscillators is also reviewed. Chapter 3 describes the simulation methods, and Chapter 4 discusses the measurement procedure. Chapter 5 derives a function which predicts the amplitude dependence of negative conductance by using circuit analysis. Chapter 6 presents the results. The validity of the optimum load conductance assumption is assessed based on the measurement results. The chapter also discusses the agreement between the methods. Chapter 7 summarizes the main results and concludes the thesis.

2. THE CONCEPT OF NEGATIVE RESISTANCE

This chapter begins by showing the existence of negative resistance and negative conductance in steady-state oscillation. Section 2.2 presents the startup conditions for oscillation. Section 2.3 discusses the origin of the straight-line approximation and reviews previous research on the amplitude dependence of negative conductance.

2.1 Existence of negative resistance and conductance

Oscillators can be analyzed and designed using the concept of negative resistance. The oscillating circuit can be considered a combination of an active one-port circuit and a passive one-port circuit. The active circuit has negative port resistance, and the passive circuit has positive port resistance. The resistance of the active part must be understood as dynamic or "differential" resistance.

Figure 2.1 illustrates this idea. The impedance of the active circuit is $Z_{out} = R_{out} + jX_{out}$ and the impedance of the passive circuit is $Z_L = R_L + jX_L$ at the oscillation frequency.

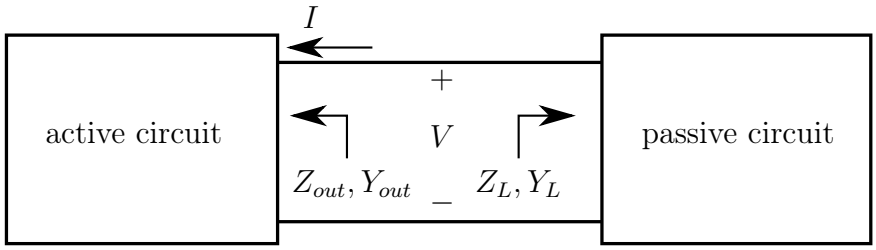

Figure 2.1. *The oscillator consists of an active circuit connected to a passive circuit. The impedances of the circuits are denoted with Z_{out} and Z_L and the admittances with Y_{out} and Y_L.*

The existence of negative resistance can be shown by writing Kirchhoff's voltage law for loop current I [3, p. 562]:

$$I(Z_{out} + Z_L) = 0. \tag{2.1}$$

When the circuit is oscillating, I is nonzero. Therefore, the sum of the impedances

is necessarily zero:

$$Z_{out} + Z_L = R_{out} + jX_{out} + R_L + jX_L = 0. \tag{2.2}$$

Separating the resistances and the reactances yields two necessary conditions for the existence of oscillation:

$$\begin{cases} R_{out} + R_L = 0 \\ X_{out} + X_L = 0. \end{cases} \tag{2.3}$$

It is assumed that the passive circuit is lossy: $R_L > 0$. Therefore, the resistance of the active circuit is negative during the oscillation: $R_{out} = -R_L < 0$.

The oscillation conditions can also be written in terms of admittances [1, p. 14]. Writing Kirchhoff's current law yields

$$V(Y_{out} + Y_L) = 0, \tag{2.4}$$

where V is the oscillation voltage, $Y_{out} = G_{out} + jB_{out}$ the admittance of the active circuit and $Y_L = G_L + jB_L$ the admittance of the passive circuit. Since V is nonzero, it follows that $Y_{out} + Y_L = 0$ and

$$\begin{cases} G_{out} + G_L = 0 \\ B_{out} + B_L = 0. \end{cases} \tag{2.5}$$

Since the conductance of the passive circuit is positive, the conductance of the active circuit is negative.

The active circuit with negative resistance can be constructed using a two-terminal negative-resistance device such as an IMPATT, tunnel or Gunn diode. Alternatively, the negative resistance circuit can be built from a transistor, resistors and capacitors. In that case, reactive elements are connected between the transistor terminals to make the resulting circuit exhibit negative resistance between two nodes. [1, p. 12]

An example of a transistor oscillator is the Colpitts oscillator [5, p. 38] in Figure 2.2. With suitably chosen values of reactive elements L, C_1 and C_2, the output conductance G_{out} is negative.

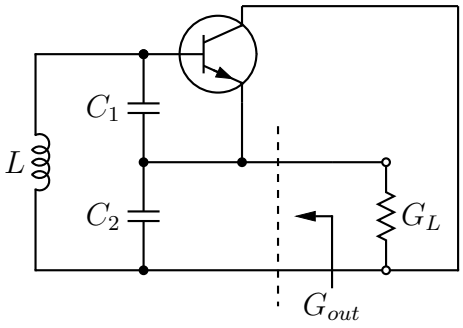

Figure 2.2. *Colpitts oscillator without a biasing network.*

The Colpitts oscillator can be modified by adding a capacitor in series with the inductor to increase the frequency stability [5, p. 40]. The resulting circuit in Figure 2.3 is known as the Clapp oscillator.

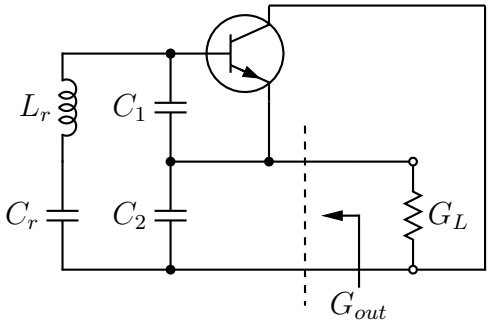

Figure 2.3. *Clapp oscillator.*

2.2 Startup of oscillations

Conditions (2.3) and (2.5) are valid in steady-state oscillation. When the oscillator is switched on, the oscillation amplitude increases from zero until it saturates and reaches the steady-state value. This increase of the amplitude requires that the circuit is initially unstable [1, p. 19]. The instability of the circuit can be determined with the oscillation startup conditions. These conditions can be formulated in terms of Z_{out} and Z_L (*impedance formulation*) or alternatively in terms of Y_{out} and Y_L (*admittance formulation*).

The startup conditions assume an amplitude and frequency dependence of Z_{out} and Y_{out}. In the impedance formulation, Z_{out} depends on the amplitude of the oscillation current $\hat{i}$ and the angular frequency ω such that $Z_{out} = R_{out}(\hat{i}, \omega) + jX_{out}(\hat{i}, \omega)$ [6, p. 251]. The impedance of the passive circuit usually is, to a great extent, independent of the amplitude: $Z_L = R_L(\omega) + jX_L(\omega)$. The admittance formulation uses the amplitude of the oscillation voltage, $\hat{v}$, such that the admittances are written as $Y_{out} = G_{out}(\hat{v}, \omega) + jB_{out}(\hat{v}, \omega)$ and $Y_L = G_L(\omega) + jB_L(\omega)$ [6, p. 256].

In some oscillators, R_{out} becomes less negative when $\hat{i}$ increases. This kind of a circuit requires a negative small-signal loop resistance to start oscillating: $R_{out}(\hat{i}, \omega) + R_L(\omega) < 0$ when $\hat{i} \approx 0$ [3, p. 562]. When the circuit is switched on, the instability causes the noise present in the circuit to be amplified, which makes $\hat{i}$ increase. As $\hat{i}$ increases, R_{out} becomes less negative until $R_{out}(\hat{i}_0, \omega_0) + R_L(\omega_0) = 0$, where $\hat{i}_0$ and ω_0 are the steady-state amplitude and frequency. The startup conditions for these kinds of oscillators are given as the impedance formulation [5, p. 55]

$$\begin{cases} R_{out}(\hat{i} \approx 0, \omega) + R_L(\omega) < 0 \\ X_{out}(\hat{i} \approx 0, \omega) + X_L(\omega) = 0. \end{cases} \tag{2.6}$$

In other oscillators, R_{out} becomes more negative with increasing amplitude [3, p. 563]. In this case, the startup conditions are given as the admittance formulation [5, p. 52]

$$\begin{cases} G_{out}(\hat{v} \approx 0, \omega) + G_L(\omega) < 0 \\ B_{out}(\hat{v} \approx 0, \omega) + B_L(\omega) = 0. \end{cases} \tag{2.7}$$

The steady-state conditions (2.3) and (2.5) are equivalent, which can be seen as follows:

$$\begin{aligned} & Z_{out} + Z_L = 0 \\ \iff & Z_{out} = -Z_L \\ \iff & \frac{1}{Z_{out}} = -\frac{1}{Z_L} \\ \iff & Y_{out} = -Y_L \\ \iff & Y_{out} + Y_L = 0. \end{aligned}$$

However, the startup conditions (2.6) and (2.7) are not necessarily fulfilled simultaneously [1, p. 25]. This can be shown by considering that the impedances

$$Z_{out} = -150\,\Omega - j5\,\Omega, \tag{2.8}$$

$$Z_L = 5\,\Omega + j5\,\Omega \tag{2.9}$$

fulfill (2.6) whereas the admittances

$$Y_{out} = \frac{1}{Z_{out}} = -6.659\,27\,\text{mS} + j0.221\,98\,\text{mS} \tag{2.10}$$

$$Y_L = \frac{1}{Z_L} = 100\,\text{mS} - j100\,\text{mS} \tag{2.11}$$

do not fulfill (2.7).

2.3 Amplitude dependence of negative resistance

The negative resistance or conductance of a practical device or circuit normally depends on both the oscillation amplitude and frequency. This characteristic is significant when designing an oscillator for maximum output power.

Gewartowski determined [4] that the magnitude of negative conductance $|G_N|$ of an IMPATT diode decreases with increasing RF voltage amplitude $\hat{v}$ according to the equation of a straight line as

$$|G_N(\hat{v})| = |G_m|(1 - \frac{\hat{v}}{\hat{v}_m}), \tag{2.12}$$

where $G_m < 0$ is the negative conductance in small-signal conditions and $\hat{v}_m$ is the RF voltage amplitude at which $|G_N| = 0$. This approximation was suggested by computations based on a large-signal model of the IMPATT diode.

An oscillator can be constructed by connecting an IMPATT diode having the negative-conductance characteristic of (2.12) to a load. The oscillator usually also involves a resonator which mainly determines the oscillation frequency. The power delivered to the load depends on the load conductance, G_L. The optimum value which maximizes the output power is [4]

$$G_L = -G_N = -\frac{G_m}{3}. \tag{2.13}$$

This optimum G_L can be found with the expression of power delivered to the load. Assuming that the load voltage is sinusoidal, the load power can be written as

$$P_L = \frac{1}{2} G_L \hat{v}^2, \tag{2.14}$$

where $\hat{v}$ is the load voltage amplitude. Since the circuit is oscillating in steady state, condition $G_L + G_N = 0$ holds. The load power can be expressed as

$$P_L = \frac{1}{2}|G_N|\hat{v}^2 = \frac{1}{2}|G_m|(1 - \frac{\hat{v}}{\hat{v}_m})\hat{v}^2. \tag{2.15}$$

This function can be maximized by computing the derivative, which results in

$$P_L'(\hat{v}) = \frac{1}{2}|G_m|(2\hat{v} - \frac{3\hat{v}^2}{\hat{v}_m}). \tag{2.16}$$

The derivative is zero at $\hat{v} = \frac{2}{3}\hat{v}_m$, which maximizes the output power.

From (2.12) it follows that $|G_N| = \frac{|G_m|}{3}$, which implies that the maximum power is

delivered to a load with conductance

$$G_L = -G_N = -\frac{G_m}{3}. \tag{2.17}$$

The RF amplitude dependence of the negative conductance of two-terminal semiconductor devices has been analytically determined or measured also in other papers than [4]. For example, the negative conductance of Gunn diodes has been measured as a function of input power [7]. The paper also provides an analytical model for the conductance as a function of the fundamental-frequency terminal voltage. Another paper [8] presents the measured admittance of Gunn and IMPATT diodes as a function of RF voltage amplitude, and [9] presents theoretical results of the IMPATT diode admittance.

The rule for the optimum load conductance of equation (2.13) and the assumption about the linear dependence of negative conductance have been applied to also transistor oscillators in textbooks and papers although originally derived for the IMPATT diode. In [10], it is assumed that the magnitude of negative resistance, in contrast to negative conductance, decreases linearly in the same fashion that negative conductance was assumed to decrease. In that paper, the oscillator is designed such that the magnitude of the small-signal negative output resistance, $|R_m|$, is maximized and the load resistance is chosen as $R_L = -\frac{1}{3}R_m$. A textbook [3, p. 563] suggests the relation $R_L = -\frac{1}{3}R_m$ for circuits with a decreasing negative resistance magnitude and the relation $G_L = -\frac{1}{3}G_m$ for circuits with a decreasing negative conductance magnitude. Another book [6, p. 253] suggests that in some cases, the negative input resistance of the active device can be approximated by an equation of a straight line, which leads to the same conclusion of selecting the optimum load resistance as $R_L = -\frac{1}{3}R_m$. A book [1, p. 451] states that $G_L = -\frac{1}{3}G_m$ is an empirical criterion to maximize the output power.

However, no studies have been published that would have validated the common assumption that the straight-line approximation of the negative output resistance or conductance is useful in transistor oscillator design. Therefore, the optimum load values may differ from $G_L = -\frac{1}{3}G_m$ or $R_L = -\frac{1}{3}R_m$.

Some research exists on the amplitude dependence of negative resistance in transistor oscillators. In [11], a formula was derived for the negative resistance in a Colpitts crystal oscillator. The negative resistance is the resistance "seen" by the resonator circuit consisting of the series combination of a crystal and a variable capacitor. The

obtained negative resistance magnitude is proportional to

$$\frac{2}{x}\frac{I_1(x)}{I_0(x)}, \tag{2.18}$$

where x is proportional to the resonator current amplitude and $I_1(x)$ and $I_0(x)$ are the modified Bessel functions of the first kind of orders 1 and 0. When x is large, the formula can be approximated as $\frac{2}{x}$. In other words, at large resonator current amplitudes, the negative resistance magnitude is inversely proportional to the resonator current amplitude.

In [3, p. 566], the input impedance of an oscillator was simulated as a function of the input current amplitude. The textbook also derives a formula which approximates the input impedance at high input current amplitudes. In this approximation, the negative input resistance is inversely proportional to the input current amplitude [3, p. 565]. Simulation results of the output admittance of an oscillator are presented in [1, p. 455]. Measurement method and results of a FET (field-effect transistor) oscillator output admittance are presented in [12].

In the above-discussed previous research on transistor oscillators, the accuracy of neither simulations nor analytical methods of determining the amplitude dependence of negative conductance or resistance was verified by measuring the amplitude dependence. The range of oscillator feedback element values was also limited. The paper with amplitude dependence measurements [12] does not discuss the straight-line approximation.

This thesis aims to determine the validity of the straight-line approximation in a Clapp oscillator which operates at frequencies near 100 MHz. The relation between the output voltage amplitude and the negative conductance is studied by simulations, measurements and analytical methods. This relation is determined for 16 combinations of feedback capacitance values. The simulations and analytical results are compared to measurements and their agreement is assessed. The validity of the rule $G_L = -\frac{1}{3}G_m$ for maximizing the load power is assessed by measurement results. As discussed above, this rule has been applied to transistor oscillators although no studies supporting its validity have been published.

3. SIMULATIONS

The negative conductance behavior of the Clapp oscillator was simulated with Keysight Advanced Design System 2015.01 circuit simulator. Two simulation methods were used: *a variable load method* and *a variable test voltage method*. Both methods involve finding the steady-state solution of the voltages and currents of the circuit with the harmonic balance technique. Harmonic balance does not capture the transient behavior which occurs when the circuit is switched on and the output voltage amplitude gradually increases as it reaches the steady-state value.

3.1 Variable load method

Figure 3.1 shows the simulation circuit of the variable load method.

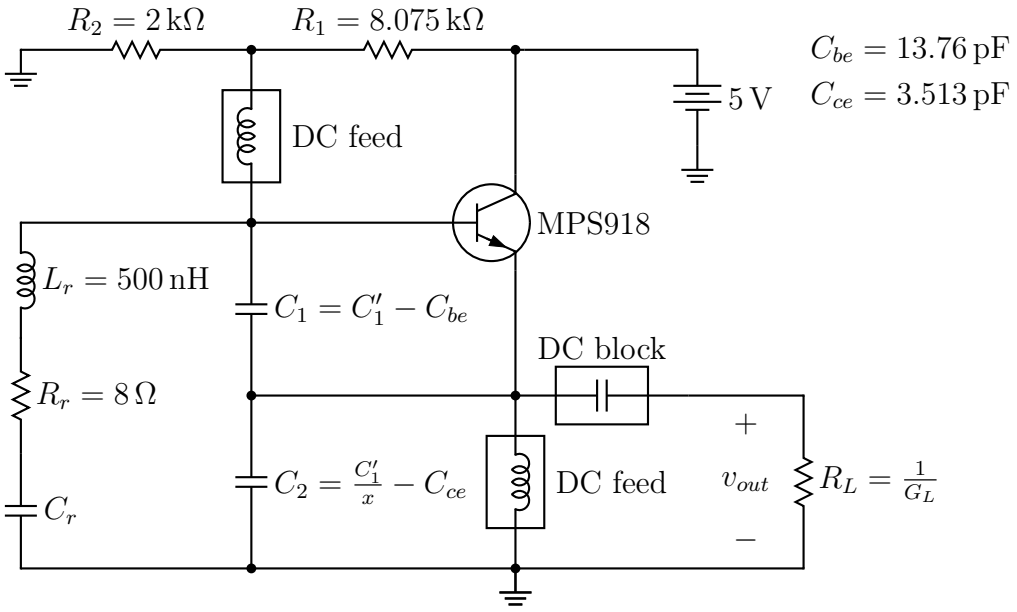

Figure 3.1. *The simulation circuit of the variable load method.*

The bipolar transistor MPS918 was selected in the simulation circuit because of its similarity with the PN3563 transistor which was used in the measurements. Resistors R_1 and R_2 set the collector-emitter bias voltage to $V_{CEQ} = 5\,\mathrm{V}$ and the collector bias current to $I_{CQ} = 20\,\mathrm{mA}$. The ideal RF chokes, denoted by "DC Feed",

pass DC currents and block currents of other frequencies. The DC block is an open circuit at DC and a short circuit at other frequencies.

Inductor L_r models an airwound inductor of 500 nH, and R_r models its losses. The quality factor is assumed 40, which implies a series resistance of $R_r = 8\,\Omega$ at 100 MHz [13].

The capacitance of C_1 is defined as $C_1 = C_1' - C_{be}$, where C_{be} is the small-signal base-emitter capacitance of the MPS918 transistor. The adjustable parameter C_1' is the total capacitance between the base and emitter nodes. Similarly, defining C_2 as $C_2 = C_1'/x - C_{ce}$ allows adjusting the ratio of total base-emitter and collector-emitter capacitances with parameter x. The amplitude dependence of the negative output conductance was simulated for 15 combinations of C_1' and x. The values of parameters C_{be} and C_{ce} were determined as described in Section 5.2.

The variable load method involves simulating the circuit with several load conductance values. For each load conductance G_L, the simulator attempts to find an oscillatory steady-state solution. If a solution is found, it satisfies the oscillation conditions of (2.5). Therefore, for a given G_L, the output admittance $Y_{out} = G_{out} + jB_{out}$ can be obtained as

$$\begin{aligned} G_{out} &= -G_L, \\ B_{out} &= 0. \end{aligned} \tag{3.1}$$

Equivalently, from the impedance conditions (2.3) it follows that

$$\begin{aligned} R_{out} &= -R_L, \\ X_{out} &= 0, \end{aligned} \tag{3.2}$$

where R_{out} is the output and R_L the load resistance. A similar measurement method based on varying the load is presented in [12].

For each (x, C_1')-combination, the value of C_r was first selected with a separate simulation procedure. A load resistor of $50\,\Omega$ was placed at the output port and C_r was varied until the simulated oscillation frequency was approximately 100 MHz. Next, C_r was fixed to this value, and the load conductance was swept. For each load conductance, a harmonic balance simulation was performed, and the resulting output voltage spectrum was recorded. The magnitude of the fundamental component of the resulting output voltage spectrum is treated as the output voltage amplitude. For this amplitude, the output conductance is $G_{out} = -G_L$.

The output negative conductance was obtained for 101 load conductances varying from 2 mS to 200 mS. Table 3.1 shows the values of C_r used for each (C_1', x)-

combination. Also shown are the frequencies obtained from the load conductance sweep simulation with the load conductance of 20 mS, a value which corresponds to a resistance of 50 Ω. As can be seen, the selected C_r values yield approximately the desired frequency of 100 MHz.

Table 3.1. *The C_r values used in the variable load simulations. Also shown are the oscillation frequencies obtained with $G_L = 20\,\text{mS}$.*

x	C_1' (pF)	C_r (pF)	f (MHz)
4	30	15.00	100.06
4	40	9.05	100.05
4	80	6.46	100.03
4	160	5.70	100.03
2	30	11.30	99.95
2	40	8.00	99.94
2	80	6.08	99.91
2	160	5.47	100.00
1	30	9.10	100.04
1	40	7.15	99.97
1	80	5.75	100.05
1	160	5.30	100.01
0.5	30	8.00	99.94
0.5	40	6.55	100.41
0.5	80	5.60	99.56

The variable load method is summarized as follows:

1. Select C_1' and x.
2. Select $G_L = 20\,\text{mS}$.
3. Select a value for C_r.
4. Simulate the circuit and record the oscillation frequency.
5. If the frequency is not approximately 100 MHz, go back to step 3. Otherwise, go to step 6.
6. Now G_L is varied. For all 101 G_L values from 2 mS to 200 mS, simulate the circuit and record the output voltage spectrum.
7. Go back to step 1.

3.2 Variable test voltage method

In the variable test voltage method, the load resistor at the output is replaced with a voltage source as shown in Figure 3.2. The voltage source provides a sinusoidal waveform at the fixed frequency of 100 MHz, and its amplitude is swept from 0 V to 8 V in intervals of 0.05 V. For each amplitude, the simulator finds the spectrum of the output current, i_{out}. At the fundamental frequency, the output admittance is calculated from

$$Y_{out} = \frac{i_{out,1}}{v_{out,1}}, \tag{3.3}$$

where $v_{out,1}$ is the fundamental frequency phasor of the voltage at the output port and $i_{out,1}$ the fundamental frequency phasor of the current flowing into the output port. The output conductance is obtained as the real part of (3.3). Similarly, the output resistance can be obtained as the real part of

$$Z_{out} = \frac{v_{out,1}}{i_{out,1}}. \tag{3.4}$$

Phasor $v_{out,1}$ equals the amplitude setting of the voltage source. A similar simulation method of obtaining the transistor oscillator output admittance with a test voltage source is presented in [1, p. 453–456].

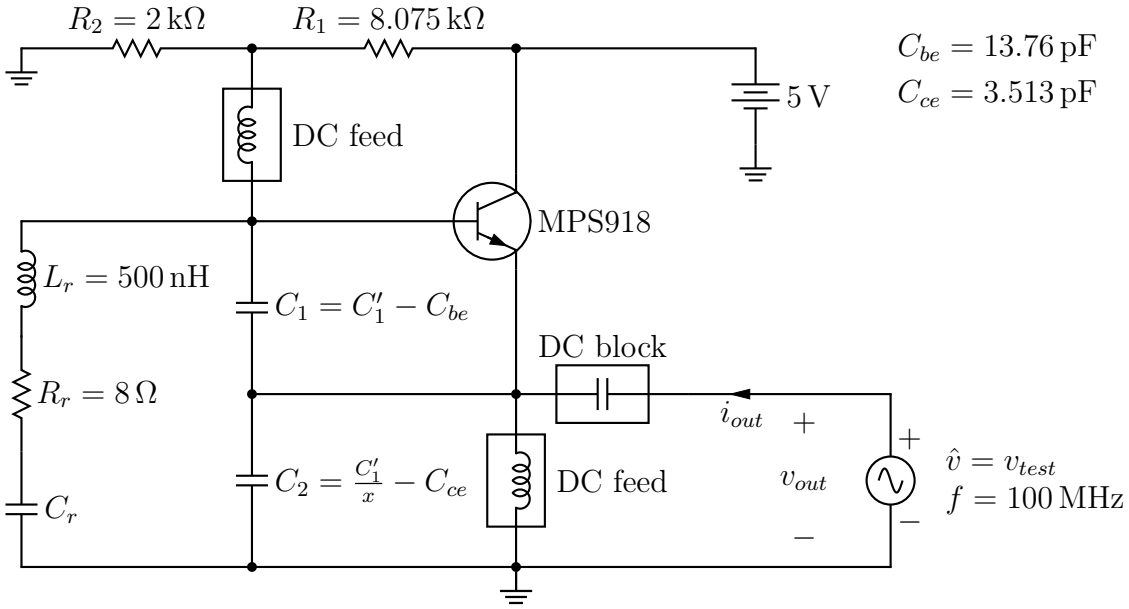

Figure 3.2. *The simulation circuit of the variable test voltage method.*

For each (C_1', x)-combination, the value of C_r was selected from Table 3.1. The variable test voltage method is summarized as follows:

1. Select C_1' and x.

2. Select C_r for this combination of C_1' and x from Table 3.1.
3. Simulate the circuit and record the output current spectrum for all test voltage amplitudes (from 0 V to 8 V in intervals of 0.05 V).
4. For each test voltage amplitude, calculate the output conductance $\mathrm{Re}\left\{\frac{i_{out,1}}{v_{out,1}}\right\}$.

Appendix C shows more detailed versions of the simulation circuits including the simulation settings. The simulation results are shown in Appendix A and discussed in Chapter 6.

4. MEASUREMENTS

This chapter presents the measurement method used to determine the output conductance of a Clapp oscillator. The output port of the oscillator is terminated with load conductance G_L, and output RF power is measured with a spectrum analyzer. The output conductance is obtained from $G_{out} = -G_L$ according to (2.5). The output voltage is calculated by using the load conductance and the measured power. Essentially, the output conductance is set to $-G_L$, and then the output voltage amplitude is obtained from a measurement result. A similar method involving a varying load is described in [12]. The paper determined the output admittance of a FET oscillator by measurements where the load admittance was varied.

When G_L is varied, the output voltage amplitude varies. The measurement is repeated with varying values of G_L to obtain a wide range of output voltage amplitudes. To vary G_L, resistors R_s and R_p were placed at the oscillator output as in Figure 4.1.

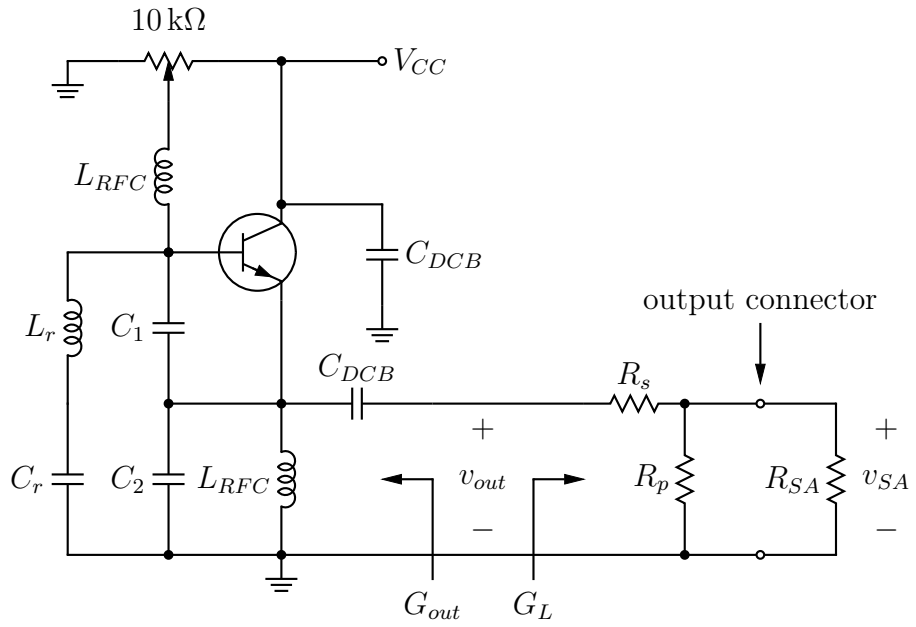

Figure 4.1. *The constructed Clapp oscillator is terminated with the variable load conductance. The spectrum analyzer input impedance $R_{SA} = 50\,\Omega$ is a part of the load.*

The spectrum analyzer was connected to the SMA output connector with a 50-Ω

cable. Therefore, the load conductance of the oscillator consists of the combination of R_s, R_p and the spectrum analyzer input impedance $R_{SA} = 50\,\Omega$ which parallels R_p:

$$G_L = \frac{1}{R_s + R_p \| R_{SA}}. \tag{4.1}$$

When the circuit is oscillating, the output conductance is $G_{out} = -G_L$. The spectrum analyzer input power P_{SA} can be expressed in terms of the spectrum analyzer input voltage amplitude $\hat{v}_{SA}$ as

$$P_{SA} = \frac{1}{2}\frac{\hat{v}_{SA}^2}{R_{SA}}, \tag{4.2}$$

which is equivalent to

$$\hat{v}_{SA} = \sqrt{2 R_{SA} P_{SA}}. \tag{4.3}$$

The spectrum analyzer input voltage is

$$\hat{v}_{SA} = \frac{R_p \| R_{SA}}{R_s + R_p \| R_{SA}} \hat{v}_{out}, \tag{4.4}$$

where $\hat{v}_{out}$ is the desired oscillator output voltage

$$\hat{v}_{out} = \frac{R_s + R_p \| R_{SA}}{R_p \| R_{SA}} \hat{v}_{SA} = \frac{R_s + R_p \| R_{SA}}{R_p \| R_{SA}} \sqrt{2 R_{SA} P_{SA}}. \tag{4.5}$$

4.1 Measurement circuit

The oscillator was constructed on a printed circuit board with through-hole and surface-mount components. The transistor is a bipolar, NPN, through-hole type PN3563 in TO-92 package.

The layout was designed to minimize the lengths of the RF current carrying paths. These include the paths between the transistor, feedback capacitors, resonator components, the DC blocks, R_s, R_p and the output connector.

Ceramic radial disc capacitors are used as C_1, C_2 and C_r and leaded axial resistors as R_s and R_p. Since the measurement procedure requires changing these components many times, 1-pin sockets are used as connectors. As shown in Figure 4.2, the 1-pin sockets were soldered on the bottom side of the board to minimize the path lengths from the components to the board. Two pairs of 1-pin sockets are used for each of C_1, C_2 and C_r to allow connecting two capacitors in parallel for a fine capacitance adjustment.

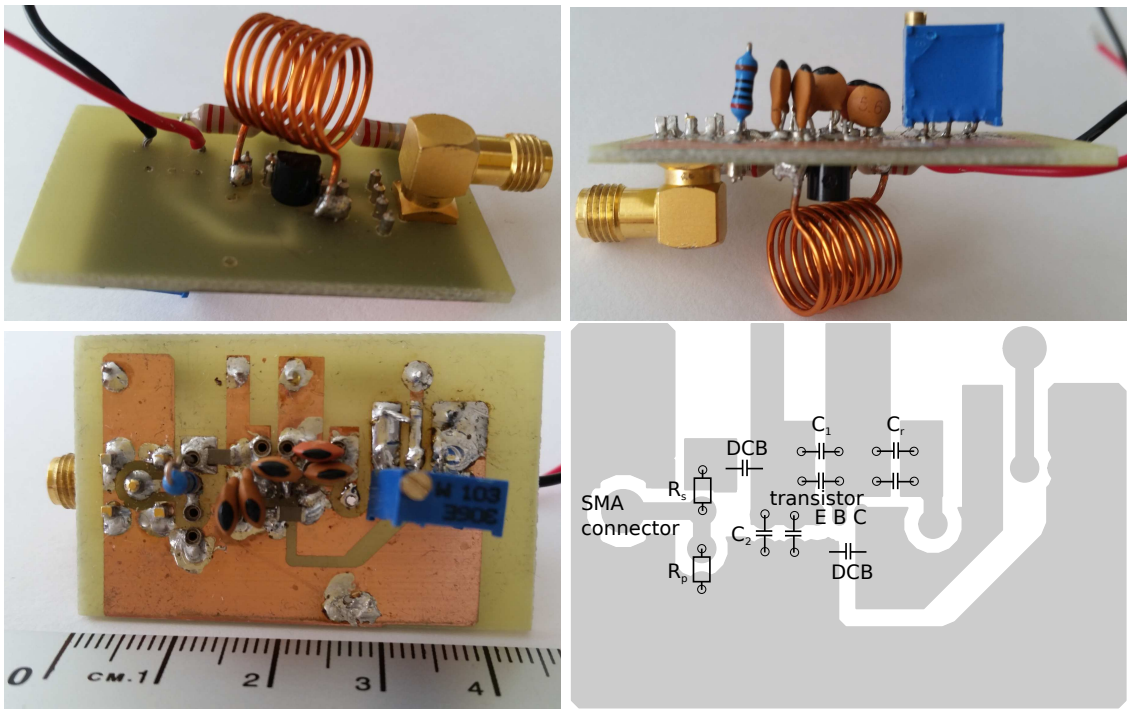

Figure 4.2. *The measured oscillator and the layout viewed from the bottom. The circles denote connectors for capacitors C_1, C_2, C_r and resistors R_p and R_s.*

The top side of the board includes the resonator coil, the RF chokes, the SMA output connector and the PN3563 transistor which is located below the resonator coil. The coil is soldered to the terminals of C_r and C_2. The 10-kΩ trimmer is placed on the bottom side to avoid a possible interference with the resonator coil.

Surface-mount 1206-sized 1-nF capacitors are used as the DC blocks. The RF chokes are leaded inductors of 2.2 µH.

The resonator coil is an air-core inductor designed using the approximate inductance formula [3, p. 24]

$$L = \frac{10\pi r^2 \mu_0 N^2}{9r + 10l}, \tag{4.6}$$

where $\mu_0 = 4\pi \cdot 10^{-7}\,\mathrm{H/m}$ is the permeability of free space, r is the radius, N the number of turns and l the length of the coil. The coil was wound on a rod with the radius of 5 mm. The coil radius is taken as the distance from the coil axis to the center of the coil wire. Since the diameter of the coil wire is 0.8 mm, the coil radius is $r = 5.4\,\mathrm{mm}$. The length and the number of turns were chosen as $l = 10\,\mathrm{mm}$ and $N = 8$, which results in $L = 496\,\mathrm{nH}$. The impedance of the coil was measured with a vector network analyzer. At $f = 100\,\mathrm{MHz}$ the measured reactance was $X = 321\,\Omega$ which results in the effective inductance of $X/(2\pi f) = 511\,\mathrm{nH}$.

4.2 Measurement procedure

The bias point of the circuit was set before the output conductance measurements. The collector-emitter bias voltage V_{CEQ} equals the 5-V supply voltage. The collector current was adjusted with the trimmer to 20 mA, and it was approximated as the measured total current drawn by the circuit. When setting the bias point, C_r was removed to prevent the circuit from oscillating.

The amplitude dependence of the output conductance was measured for 16 combinations of x and C_1'. The corresponding C_1 and C_2 were obtained by using the measured base-emitter and collector-emitter capacitances of the PN3563 in Table 5.1:

$$C_1 = C_1' - C_{be} = C_1' - 7.7\,\text{pF} \tag{4.7}$$

$$C_2 = \frac{C_1'}{x} - C_{ce} = \frac{C_1'}{x}. \tag{4.8}$$

For each (x, C_1') case, the output power was measured with approximately 20–40 combinations of R_s and R_p, each combination corresponding to a load conductance value. Low values of load conductances are obtained with combinations where R_p is omitted and R_s is high. High values are obtained with combinations where $R_s = 0\,\Omega$ and R_p is low.

First, the load conductance is set to 20 mS (corresponding to 50 Ω). The value of C_r is adjusted until the measured oscillation frequency is approximately 100 MHz. Then the load conductance is set to an initial value which was chosen as 1.04 mS with R_s = 910 Ω, R_p = open. The spectrum analyzer input power and oscillation frequency are measured. The load conductance is gradually increased and the power and frequency are measured. The measurement is terminated either when no oscillation is observed or when the measured oscillator output power decreases to a value close to the spectrum analyzer noise floor.

The measurement procedure for one (x, C_1') case is summarized as follows:

1. Capacitors C_1 and C_2 are inserted. Realization of certain capacitance values required two capacitors in parallel.
2. Load resistance value of 50 Ω was realized using a short jumper wire in the place of R_s and leaving R_p open.
3. An initial C_r is inserted.
4. The oscillation frequency is measured with the spectrum analyzer, and C_r is varied until the frequency is approximately 100 MHz. The frequency and the spectrum analyzer input power are recorded.

5. The oscillation frequency and the spectrum analyzer input power P_{SA} are recorded for the remaining combinations of R_s and R_p. The measurement is terminated when no oscillation exists or the measured power is close to the noise floor.

6. For each combination of R_s, R_p and measured P_{SA}, the output voltage is obtained with (4.5) and the output conductance with (4.1) and $G_{out} = -G_L$.

Tables in Appendix B show the results for each (x, C_1') case. The omission of a resistor is denoted with "–" and a jumper wire with "0". The last line of each table shows the load conductance for which no oscillation was observed or the measured power was close to the noise floor.

4.3 Observations

As discussed in the previous section, the measurement of an (x, C_1') case is terminated when no oscillation is observed or the measured power is close to the noise floor. This occurs when G_L exceeds a threshold value which may depend on x and C_1'.

In some (x, C_1') cases with G_L exceeding the corresponding threshold value, the output power is close to the noise floor. Additionally, the power at frequencies near the fundamental frequency is slightly elevated from the noise floor. In other words, the output signal spectrum is broad. In contrast, when the spectrum measured with load conductances equal or lower than the threshold value, the spectrum has a sharp peak at the fundamental frequency, and the power is significantly higher.

Figure 4.3 shows the effect when G_L exceeds the threshold value in case $x = 4$, $C_1' = 40\,\text{pF}$. The spectra were measured with varying collector-emitter bias voltages to distinguish the output spectrum from external interference. When the bias voltage is altered, the oscillation frequency shifts whereas the frequencies of the external interference remain constant.

The top figure shows the spectra measured with $V_{CEQ} = 4\,\text{V}$, 5 V and 6 V when $G_L = 45.6\,\text{mS}$. When $V_{CEQ} = 5\,\text{V}$, the output spectrum has a sharp peak of 1.45 dBm at 98.31 MHz. The output frequency of the oscillator is lower when $V_{CEQ} = 4\,\text{V}$ and higher when $V_{CEQ} = 6\,\text{V}$. The power of the external interference is small, and it is not visible because of the scaling of the figure.

When G_L is increased to 50.3 mS, the output power decreases significantly, having a maximum of −68.5 dBm at 99.67 MHz with $V_{CEQ} = 5\,\text{V}$. This output power is

close to the noise floor, and the output spectrum is wide. Therefore, this G_L exceeds the threshold value. Two major external interference peaks exist at 99.8 MHz and 102.1 MHz.

When G_L is increased to 53.3 mS, the output spectrum widens and lowers. Increasing G_L more widens and decreases the output spectrum.

The threshold value of G_L is apparently between 45.6 mS and 50.3 mS in case $x = 4$, $C_1' = 40$ pF. It should be noted that the threshold value may differ when the measurement is repeated. For example, the measurement results of case $x = 4$, $C_1' = 40$ pF in Appendix B show that clear oscillation existed at $G_L = 50.3$ mS with $P_{SA} = -12.3$ dBm. According to that measurement, the threshold value is greater than 50.3 mS. However, when the measurement was repeated to obtain the spectra in Figure 4.3, the sudden decrease of the output power already occurred at $G_L = 50.3$ mS.

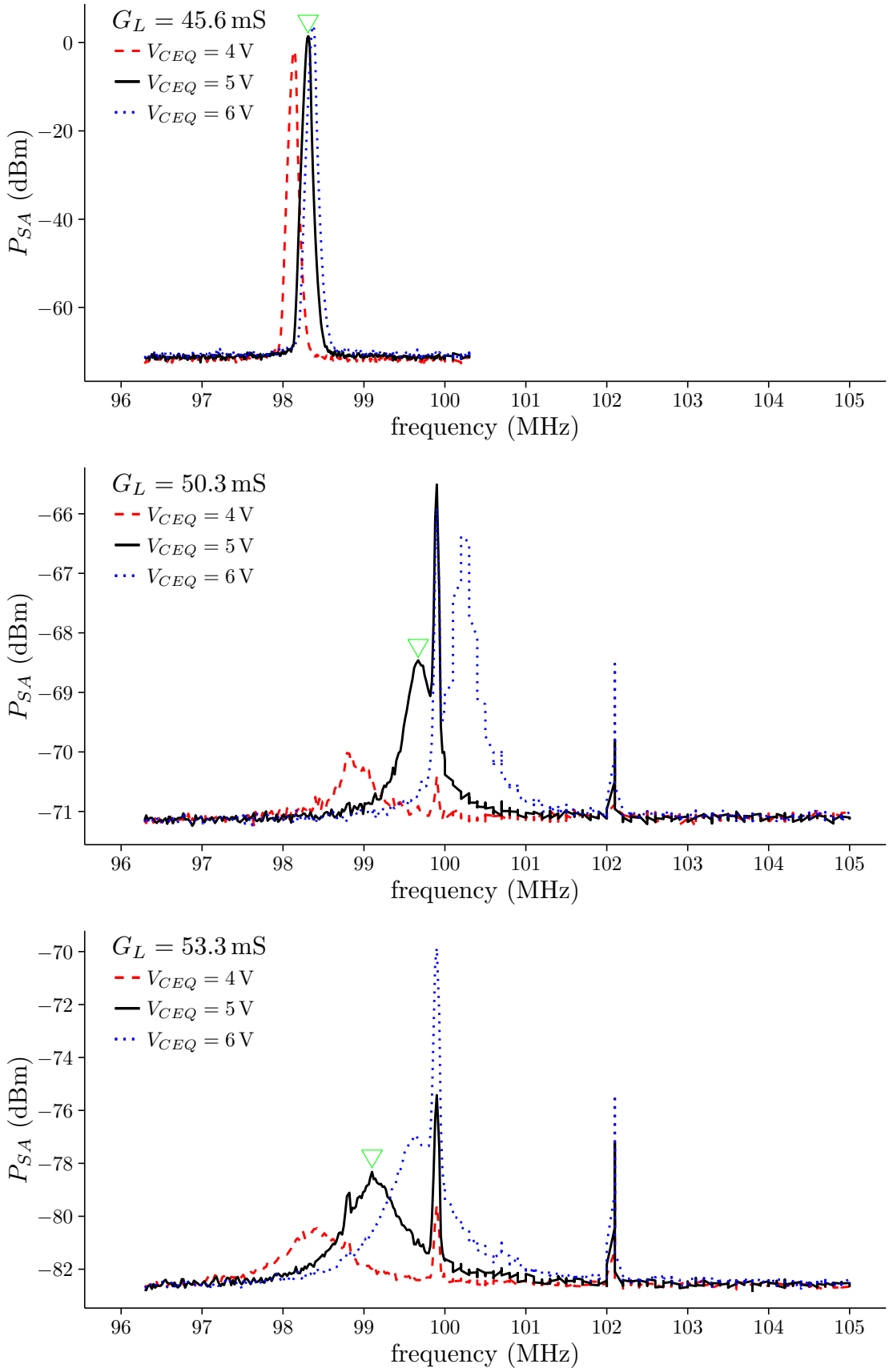

Figure 4.3. *The measured output spectra in case $x = 4$, $C_1' = 40\,\mathrm{pF}$ with varying load conductances and collector-emitter bias voltages. The triangular markers show the maxima of the oscillator output when $V_{CEQ} = 5\,\mathrm{V}$.*

5. ANALYTICAL METHODS

This chapter presents two analytical methods of predicting the amplitude dependence of the negative conductance in the Clapp oscillator. Both methods are based on the output admittance function derived in this chapter.

The output conductance G_{out} of the oscillator in Figure 5.1 is expressed as a function of the output voltage amplitude and the oscillation frequency. The analysis is based on a quasi-linear transistor model which is discussed in the following.

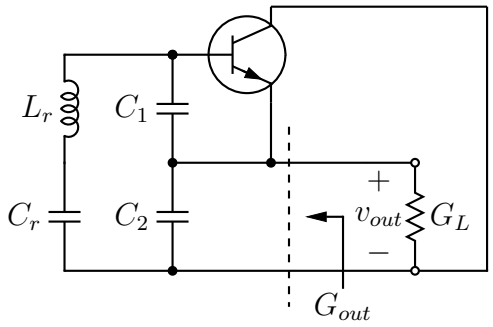

Figure 5.1. *Clapp oscillator with a load having conductance G_L. The biasing components are omitted.*

5.1 Quasi-linear transistor model

The conventional small-signal analysis involves the use of linear models for the active devices. These models are only applicable when the voltages and currents have small amplitudes. As the amplitudes increase, the nonlinear behavior of the active devices makes the analysis increasingly inaccurate. In particular, the output impedance of a linear network is independent of the test voltage amplitude. Therefore, linear models are inapplicable for predicting the amplitude variation of the output conductance.

A quasi-linear transistor model has been developed [14] to facilitate the large-signal analysis of transistor oscillators. The model has been previously used to successfully predict the output power of a Clapp oscillator [15]. In this thesis, the applicability of the model is evaluated in predicting the amplitude dependence of the output conductance of the Clapp oscillator.

The quasi-linear transistor model in Figure 5.2 is based on the traditional linear, lumped-element hybrid-π model which consists of resistors, capacitors and a voltage-controlled current source. In the traditional hybrid-π model, the current of the voltage-controlled current source is described as $i = g_m v_{be}$, where g_m is the constant transconductance and v_{be} the base-emitter small-signal voltage. However, as the base-emitter voltage amplitude $\hat{v}_{be}$ increases, the equation $i = g_m v_{be}$ becomes inaccurate since the nonlinearity of the transistor limits the increase of the current.

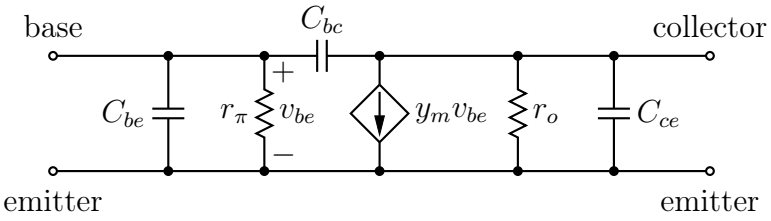

Figure 5.2. *The quasi-linear transistor model.*

The quasi-linear transistor model accounts for this limitation, in essence, the saturation of collector RF current. In the quasi-linear model, the transconductance g_m is substituted with the transadmittance phasor y_m. The magnitude of y_m is a decreasing function $f_{|y_m|}(\hat{v}_{be})$, and the phase of y_m is assumed constant and denoted as ϕ. The transadmittance is now written as

$$y_m = f_{|y_m|}(\hat{v}_{be})e^{j\phi}. \tag{5.1}$$

The magnitude function has been formulated [14] as

$$f_{|y_m|}(\hat{v}_{be}) = \frac{|y_{m_0}|}{\left(1 + \left(\frac{\hat{v}_{be}|y_{m_0}|}{\hat{i}_{c,max}}\right)^r\right)^{1/r}}. \tag{5.2}$$

When $\hat{v}_{be}$ is small, the value of the function is approximately $|y_{m_0}|$. At large values of $\hat{v}_{be}$,

$$f_{|y_m|}(\hat{v}_{be}) \approx \frac{|y_{m_0}|}{\left(\left(\frac{\hat{v}_{be}|y_{m_0}|}{\hat{i}_{c,max}}\right)^r\right)^{1/r}} = \frac{\hat{i}_{c,max}}{\hat{v}_{be}} \tag{5.3}$$

and the current of the voltage-controlled current source in this case is $f_{|y_m|}(\hat{v}_{be})\hat{v}_{be} = \hat{i}_{c,max}$, which is a constant. As shown in Figure 5.3, parameter r controls the steepness of the transition from the region of $f_{|y_m|}(\hat{v}_{be}) \approx |y_{m_0}|$ at small values of $\hat{v}_{be}$ to the region $f_{|y_m|}(\hat{v}_{be}) \approx \frac{\hat{i}_{c,max}}{\hat{v}_{be}}$ at large values of $\hat{v}_{be}$.

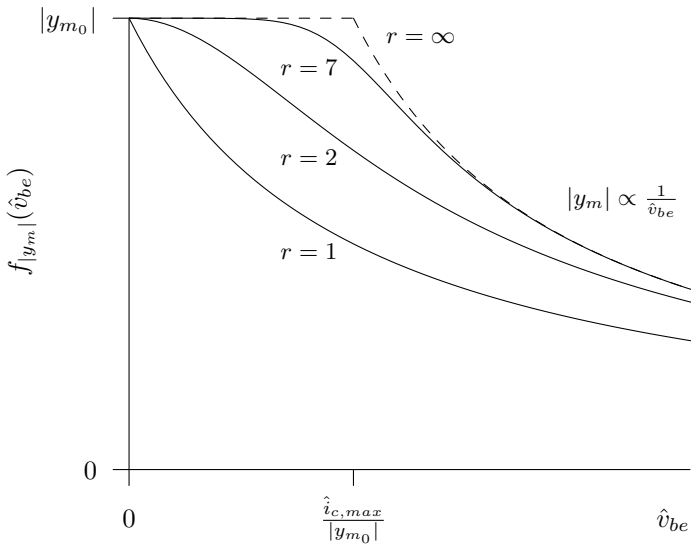

Figure 5.3. *The transadmittance magnitude function $f_{|y_m|}(\hat{v}_{be})$ with varying r.*

5.2 Quasi-linear models of PN3563 and MPS918

Table 5.1 shows the quasi-linear transistor model parameters of the PN3563 used in measurements. These parameters have been obtained from measurement results in [14].

Table 5.1. *The measured quasi-linear transistor model parameters of PN3563.*

Parameter	Value
C_{be}	7.7 pF
r_π	141 Ω
C_{bc}	3.3 pF
C_{ce}	0 pF
r_o	1232 Ω
$\lvert y_{m_0}\rvert$	105 mS
ϕ	−64°
$\hat{i}_{c,max}$	30.6 mA
r	2

To compare the analytical methods with the simulation methods, the parameters of the quasi-linear transistor model in Figure 5.2 were determined for the MPS918 transistor simulation model.

Characterizing the transistor simulation model is similar to characterizing a physical transistor with measurements which is described in [14], [15] and [16]. When characterizing a transistor with measurements, the S-parameters of the transistor are measured as a function of input power, and the transistor parameters are calculated from the results. When characterizing a transistor simulation model, the transistor

parameters are calculated from the simulated large-signal S-parameters [17].

The characterization of the simulation model involves simulating the small-signal and large-signal S-parameters of MPS918 at 100 MHz. The transadmittance function parameters y_{m_0}, ϕ, $\hat{i}_{c,max}$ and r are obtained from the power-dependent large-signal S-parameters. The large-signal S-parameters were simulated at input power levels from $-30\,\mathrm{dBm}$ to $0\,\mathrm{dBm}$ at the bias point $V_{CEQ} = 5\,\mathrm{V}$, $I_{CQ} = 20\,\mathrm{mA}$ as shown in the simulation circuit in Figure 5.4.

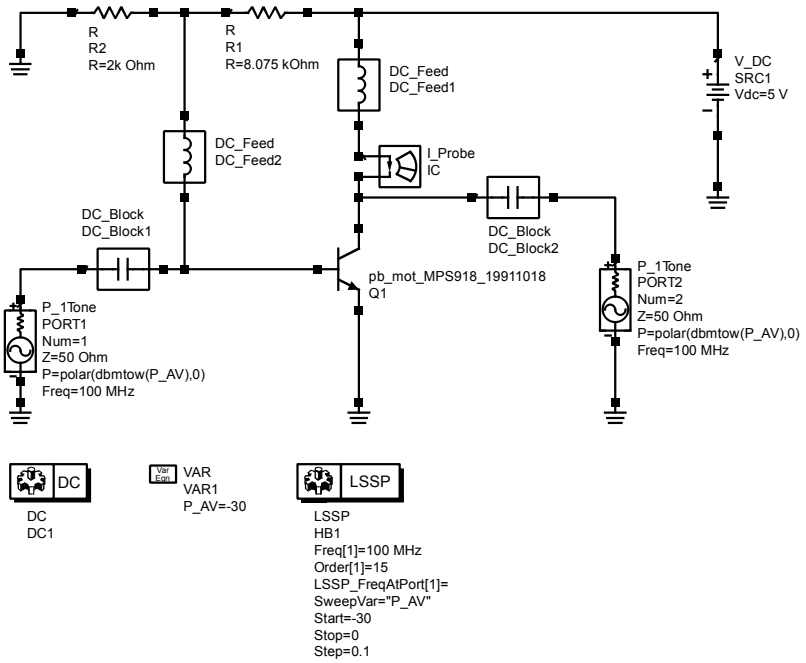

Figure 5.4. *The large-signal S-parameters of the MPS918 transistor were simulated with Agilent ADS.*

At each power level, the S-parameters were converted to Y-parameters and the value of the transadmittance was calculated from

$$y_m = Y_{21} - Y_{12}. \tag{5.4}$$

The base-emitter voltage amplitude was obtained from

$$\hat{v}_{be} = 2\sqrt{2}\left|\frac{Z_{in}}{Z_{in} + Z_0}\right|\sqrt{Z_0 P_{av}}, \tag{5.5}$$

where P_{av} is the available power of the generator, $Z_0 = 50\,\Omega$ and the input impedance is

$$Z_{in} = Z_0\frac{1 + S_{11}}{1 - S_{11}}. \tag{5.6}$$

The transadmittance function parameters r and $\hat{i}_{c,max}$ are obtained by fitting the values of the simulated $|y_m|$ and $\hat{v}_{be}$ into equation (5.2) with the method of least

squares. The value of $|y_{m_0}|$ is taken as the value of $|y_m|$ at the power level of $-30\,\text{dBm}$ and ϕ as the phase angle of this y_m. As seen in Figure 5.5, the fitted transadmittance function agrees with the simulated transadmittance values. The resulting quasi-linear transistor model parameter values are shown in Table 5.2.

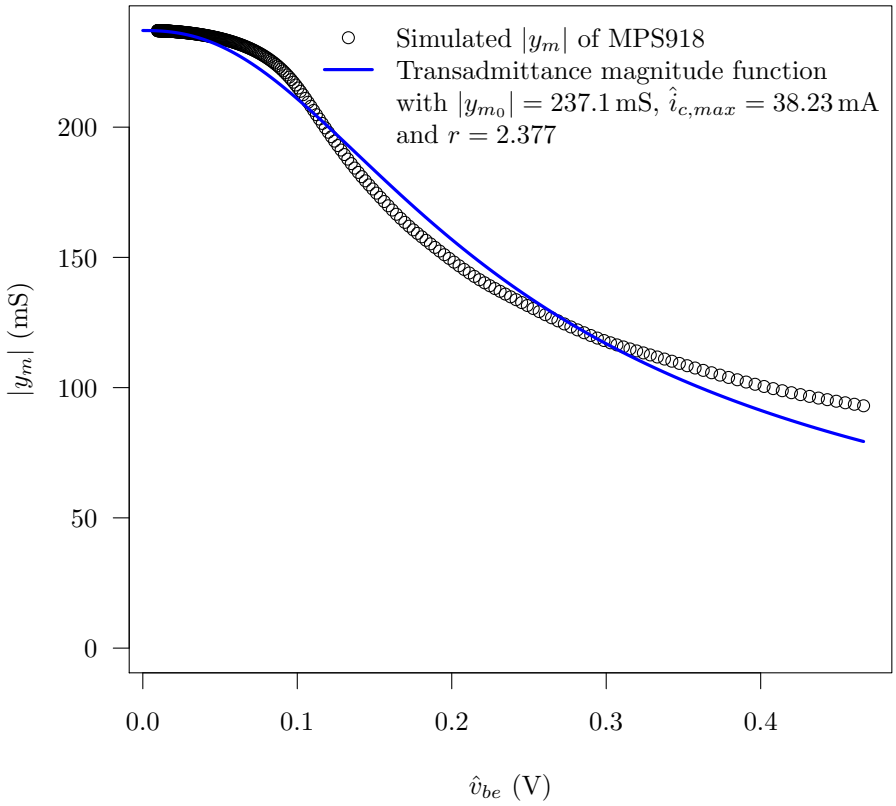

Figure 5.5. *The simulated transadmittance magnitude of the MPS918 transistor and the fitted transadmittance function* (5.2).

The small-signal S-parameters are used to extract the values of C_{be}, C_{bc}, C_{ce}, r_π and r_o. These S-parameters are converted to Y-parameters, and the values of C_{be}, C_{bc}, C_{ce}, r_π and r_o are extracted with the following formulae [14]

$$C_{be} = \frac{\text{Im}\{Y_{11}\} + \text{Im}\{Y_{12}\}}{\omega} \tag{5.7}$$

$$r_\pi = \frac{1}{\text{Re}\{Y_{11}\}} \tag{5.8}$$

$$C_{bc} = -\frac{\text{Im}\{Y_{12}\}}{\omega} \tag{5.9}$$

$$C_{ce} = \frac{\text{Im}\{Y_{22}\} + \text{Im}\{Y_{12}\}}{\omega} \tag{5.10}$$

$$r_o = \frac{1}{\text{Re}\{Y_{22}\}}, \tag{5.11}$$

where $\omega = 2\pi \cdot 100\,\text{MHz}$.

Table 5.2. *The simulated quasi-linear transistor model parameters of MPS918.*

Parameter	Value
C_{be}	13.76 pF
r_π	57.93 Ω
C_{bc}	0.5617 pF
C_{ce}	3.513 pF
r_o	332.1 Ω
$\lvert y_{m_0}\rvert$	237.1 mS
ϕ	−58.40°
$\hat{i}_{c,max}$	38.23 mA
r	2.377

5.3 Deriving the output admittance function

In Figure 5.6, the transistor has been replaced with the quasi-linear model, and the load, with conductance G_L, has been replaced with a voltage source v_{test} having amplitude $\hat{v}_{test}$ and frequency $\omega = 2\pi f$. The voltage source makes current i_{out} flow into the emitter terminal. The output admittance is given by $Y_{out} = i_{out}/v_{test}$.

The parallel connection of capacitances C_1 and C_{be} is denoted as $C_1' = C_1 + C_{be}$ which represents the total capacitance between the base and the emitter nodes. Similarly, the total capacitance between the collector and the emitter nodes is defined as $C_2' = C_2 + C_{ce}$. The behavior of the output admittance will be analyzed in terms of C_1' and C_2'.

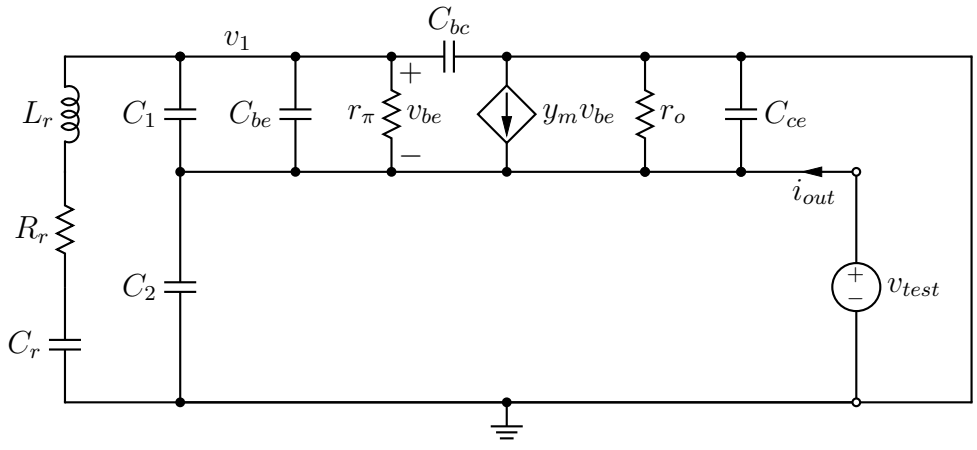

Figure 5.6. *The output admittance of the Clapp oscillator is analyzed with the quasi-linear transistor model.*

To simplify the expressions, Figure 5.7 shows the circuit in Figure 5.6 redrawn with

the substitutions

$$Y_1 = j\omega C_1' + 1/r_\pi \tag{5.12}$$
$$Y_2 = j\omega C_2' + 1/r_o \tag{5.13}$$
$$Y_3 = j\omega C_{bc} + 1/\left(j\omega L_r + 1/(j\omega C_r) + R_r\right). \tag{5.14}$$

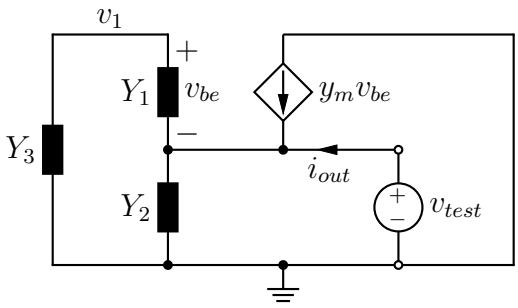

Figure 5.7. *The simplified form of the circuit in Figure 5.6.*

Current i_{out} is obtained by solving the nodal equations

$$\begin{cases} v_1(Y_1 + Y_3) - v_{test}Y_1 = 0 & (5.15) \\ v_{test}(Y_2 + Y_1) - v_1 Y_1 = y_m(v_1 - v_{test}) + i_{out}. & (5.16) \end{cases}$$

Simplifying and solving (5.15) for v_1 yields

$$\begin{cases} v_1 = v_{test}\dfrac{Y_1}{Y_1 + Y_3} & (5.17) \\ v_{test}(Y_2 + Y_1 + y_m) + v_1(-Y_1 - y_m) = i_{out}. & (5.18) \end{cases}$$

Substituting (5.17) into (5.18) yields

$$v_{test}\left((Y_2 + Y_1 + y_m) + \frac{Y_1}{Y_1 + Y_3}(-Y_1 - y_m)\right) = i_{out}. \tag{5.19}$$

The output admittance is obtained as

$$Y_{out} = \frac{i_{out}}{v_{test}} \tag{5.20}$$
$$= Y_2 + Y_1 + y_m + \frac{Y_1}{Y_1 + Y_3}(-Y_1 - y_m) \tag{5.21}$$
$$= Y_1 + Y_2 + y_m\frac{Y_3}{Y_1 + Y_3} - \frac{{Y_1}^2}{Y_1 + Y_3}. \tag{5.22}$$

The value of y_m depends on the base-emitter voltage v_{be} which is obtained as

$$v_{be} = v_1 - v_{test} = v_{test}\frac{Y_1}{Y_1 + Y_3} - v_{test} = v_{test}\frac{-Y_3}{Y_1 + Y_3}. \tag{5.23}$$

Therefore, y_m can be written as

$$y_m = f_{|y_m|}(\hat{v}_{be})e^{j\phi} = f_{|y_m|}\left(\left|v_{test}\left(\frac{-Y_3}{Y_1 + Y_3}\right)\right|\right)e^{j\phi} = f_{|y_m|}\left(\hat{v}_{test}\left|\frac{Y_3}{Y_1 + Y_3}\right|\right)e^{j\phi}. \tag{5.24}$$

Substituting this into equation (5.22) yields the output admittance as a function of the test voltage amplitude $\hat{v}_{test}$ and frequency:

$$Y_{out}(\hat{v}_{test}, \omega) = Y_1 + Y_2 + f_{|y_m|}\left(\hat{v}_{test}\left|\frac{Y_3}{Y_1 + Y_3}\right|\right)e^{j\phi}\left(\frac{Y_3}{Y_1 + Y_3}\right) - \frac{{Y_1}^2}{Y_1 + Y_3}. \tag{5.25}$$

The output conductance and susceptance are the real and imaginary parts of the output admittance:

$$G_{out}(\hat{v}_{test}, \omega) = \mathrm{Re}\{Y_{out}(\hat{v}_{test}, \omega)\} \tag{5.26}$$

$$B_{out}(\hat{v}_{test}, \omega) = \mathrm{Im}\{Y_{out}(\hat{v}_{test}, \omega)\}. \tag{5.27}$$

5.4 Using the output admittance function

The output admittance function, equation (5.25), predicts the output conductance amplitude dependence of the Clapp oscillator. The output admittance is expressed as a function of the output voltage amplitude and the oscillation frequency. The evaluation of its real part yields the predicted output conductance. However, the evaluation of the function requires specifying an appropriate frequency. This frequency should be close to the oscillation frequency which would be obtained with the chosen set of other parameters Y_1, Y_2 and Y_3. The value of Y_3 depends on capacitance C_r which was determined in measurements.

The frequency can be specified in two methods. The first method is simple. Since the oscillation frequency in the measurements was adjusted to be near 100 MHz by choosing a proper value for C_r, the value of 100 MHz is used as the frequency when evaluating the function. That is, the output conductance at an output voltage amplitude $\hat{v}_{out}$ is obtained from

$$G_{out} = \mathrm{Re}\left\{Y_{out}(\hat{v}_{out}, 2\pi \cdot 100\,\mathrm{MHz})\right\}. \tag{5.28}$$

A problem with this approach is that the measured oscillation frequency varies with the load conductance. Hence, the predicted output conductance at 100 MHz may

differ from the measured output conductance because of the frequency difference.

The second method is related to the oscillation conditions (2.5) which are fulfilled during steady-state oscillation. The output conductance was measured with load admittances which are assumed to have a negligibly small susceptance: $B_L = 0$. Therefore, the output conductance and susceptance fulfill

$$\begin{aligned} G_{out} &= -G_L \\ B_{out} &= 0 \end{aligned} \tag{5.29}$$

when steady-state oscillation exists. However, condition $B_{out} = 0$ may not be satisfied if the output admittance function is evaluated at the frequency of 100 MHz. In other words, the imaginary part of $Y_{out}(\hat{v}_{out}, 2\pi \cdot 100\,\text{MHz})$ is nonzero. The frequency at which the output admittance function is evaluated should therefore be selected such that the imaginary part is zero. For a given $\hat{v}_{out}$, this frequency f_s is obtained by solving

$$\operatorname{Im}\{Y_{out}(\hat{v}_{out}, 2\pi f_s)\} = 0 \tag{5.30}$$

for f_s. Then the predicted output conductance is obtained by evaluating the real part of the output admittance function using the solved f_s as

$$G_{out} = \operatorname{Re}\{Y_{out}(\hat{v}_{out}, 2\pi f_s)\}\,. \tag{5.31}$$

The effect of using f_s instead of 100 MHz is the following: the analytical model predicts that if the load conductance is set to $G_L = -G_{out} = -\operatorname{Re}\{Y_{out}(\hat{v}_{out}, 2\pi f_s)\}$ and the load susceptance is set to zero, then the output voltage amplitude will be $\hat{v}_{out}$ and the oscillation frequency will be f_s. The results obtained with this method correspond to the results obtained with measurements since in both, this method and in measurements, conditions (5.29) are fulfilled.

Multiple values of f_s which solve (5.30) may exist. In this case, those values of f_s which do not correspond to steady-state oscillation are discarded. To qualify as a solution which corresponds to steady-state oscillation, f_s must fulfill two conditions. First, the output conductance should be negative, $\operatorname{Re}\{Y_{out}(\hat{v}_{out}, 2\pi f_s)\} < 0$. As the load conductance is positive, a negative output conductance is required.

Second, it is required that the solution corresponds to stable oscillation. That is, if the oscillation amplitude or frequency is perturbed slightly, it returns to its original value [2, p. 586]. The stability of the solution can be determined by evaluating a stability condition. The condition [18] [1, p. 18] involves the amplitude and frequency

derivatives of the total admittance $Y_T = Y_{out} + Y_L$, where Y_L is the load admittance:

$$S = \frac{\partial \operatorname{Re}\{Y_T\}}{\partial \hat{v}_{out}} \frac{\partial \operatorname{Im}\{Y_T\}}{\partial \omega} - \frac{\partial \operatorname{Im}\{Y_T\}}{\partial \hat{v}_{out}} \frac{\partial \operatorname{Re}\{Y_T\}}{\partial \omega} > 0. \tag{5.32}$$

The measured loads consisted of resistors and the spectrum analyzer input impedance as described in Chapter 4. The resistors have parasitic inductance because of their terminal wires, which causes a nonzero load susceptance and nonzero derivatives $\frac{\partial \operatorname{Re}\{Y_L\}}{\partial \omega}$ and $\frac{\partial \operatorname{Im}\{Y_L\}}{\partial \omega}$. For simplicity, it is assumed that these frequency derivatives and the amplitude derivatives $\frac{\partial \operatorname{Re}\{Y_L\}}{\partial \hat{v}_{out}}$ and $\frac{\partial \operatorname{Im}\{Y_L\}}{\partial \hat{v}_{out}}$ can be neglected:

$$\frac{\partial \operatorname{Re}\{Y_T\}}{\partial \omega} = \frac{\partial \operatorname{Re}\{Y_{out}\}}{\partial \omega} + \frac{\partial \operatorname{Re}\{Y_L\}}{\partial \omega} \approx \frac{\partial \operatorname{Re}\{Y_{out}\}}{\partial \omega} \tag{5.33}$$

$$\frac{\partial \operatorname{Im}\{Y_T\}}{\partial \omega} = \frac{\partial \operatorname{Im}\{Y_{out}\}}{\partial \omega} + \frac{\partial \operatorname{Im}\{Y_L\}}{\partial \omega} \approx \frac{\partial \operatorname{Im}\{Y_{out}\}}{\partial \omega} \tag{5.34}$$

$$\frac{\partial \operatorname{Re}\{Y_T\}}{\partial \hat{v}_{out}} = \frac{\partial \operatorname{Re}\{Y_{out}\}}{\partial \hat{v}_{out}} + \frac{\partial \operatorname{Re}\{Y_L\}}{\partial \hat{v}_{out}} \approx \frac{\partial \operatorname{Re}\{Y_{out}\}}{\partial \hat{v}_{out}} \tag{5.35}$$

$$\frac{\partial \operatorname{Im}\{Y_T\}}{\partial \hat{v}_{out}} = \frac{\partial \operatorname{Im}\{Y_{out}\}}{\partial \hat{v}_{out}} + \frac{\partial \operatorname{Im}\{Y_L\}}{\partial \hat{v}_{out}} \approx \frac{\partial \operatorname{Im}\{Y_{out}\}}{\partial \hat{v}_{out}}. \tag{5.36}$$

Hence, the stability condition can be written in terms of the output admittance as

$$S = \frac{\partial \operatorname{Re}\{Y_{out}\}}{\partial \hat{v}_{out}} \frac{\partial \operatorname{Im}\{Y_{out}\}}{\partial \omega} - \frac{\partial \operatorname{Im}\{Y_{out}\}}{\partial \hat{v}_{out}} \frac{\partial \operatorname{Re}\{Y_{out}\}}{\partial \omega} > 0. \tag{5.37}$$

The condition is evaluated at the given $\hat{v}_{out}$ and the solved $\omega = 2\pi f_s$. In practice, this is done numerically. To summarize, those values of f_s which do not correspond to a negative output conductance or which do not fulfill the stability condition are discarded.

In conclusion, two methods exist for obtaining the output conductance with the analytical output admittance function:

1. $G_{out} = \operatorname{Re}\{Y_{out}(\hat{v}_{out}, 2\pi \cdot 100\,\mathrm{MHz})\}$
2. $G_{out} = \operatorname{Re}\{Y_{out}(\hat{v}_{out}, 2\pi f_s)\}$ such that $\operatorname{Im}\{Y_{out}(\hat{v}_{out}, 2\pi f_s)\} = 0$, $G_{out} < 0$ and f_s corresponds to stable oscillation.

The first method uses a constant frequency to predict the output conductance. The second method predicts both the output conductance and oscillation frequency by assuming that the conditions in (5.29) are fulfilled.

Analytical method 2 has similarities to a simulation method described in [1, p. 27–32]. The simulation method involves finding the total admittance $Y_T(\hat{v}_{out}, \omega) = Y_L + Y_{out}$

of a FET-oscillator. The values of $\hat{v}_{out}$ and ω are optimized such that the steady-state oscillation condition $Y_T(\hat{v}_{out}, \omega) = 0$ is satisfied in the simulation. Finally, the stability parameter S is evaluated by computing the derivatives numerically.

5.5 Calculation examples

Graphs in Appendix A compare the output voltage amplitude dependence of the output conductance obtained with measurements, analytical methods and simulation methods. Case $x = 4$, $C_1' = 30\,\mathrm{pF}$ is shown in Figure 5.8 as an example.

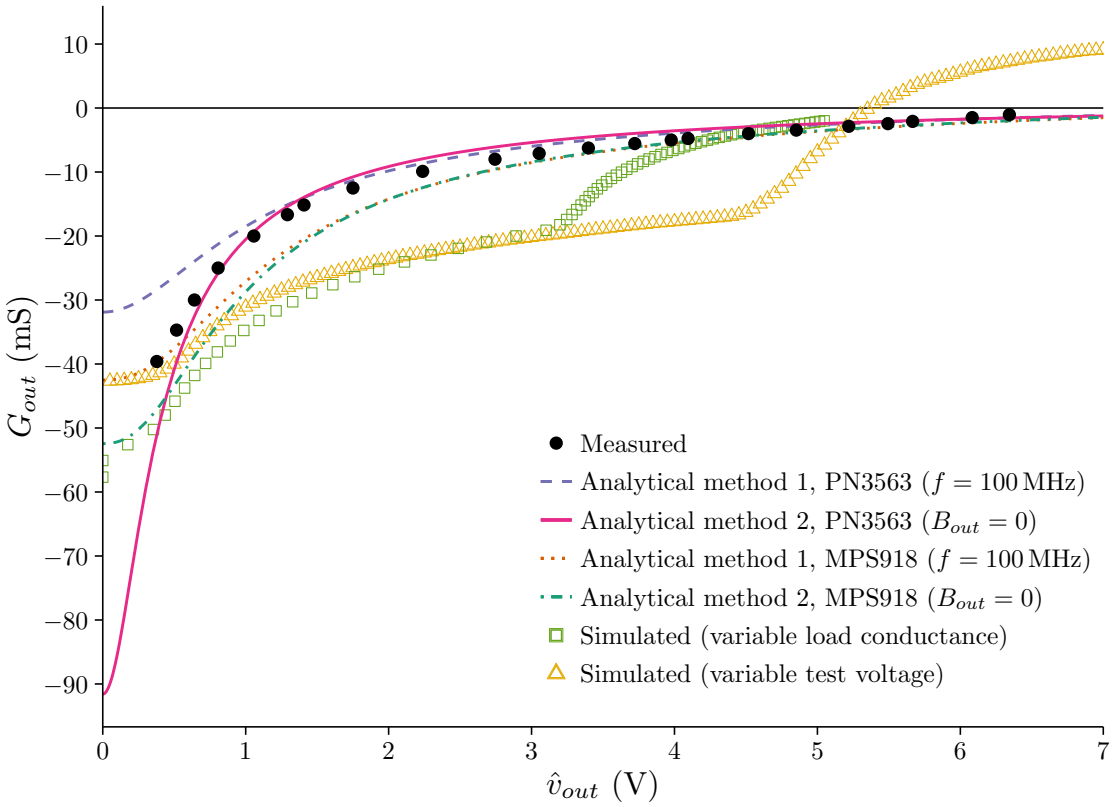

Figure 5.8. *The measured, simulated and analytically determined output conductance in case* $x = 4$, $C_1' = 30\,\mathrm{pF}$.

Each (x, C_1') combination has 4 curves obtained with analytical methods. Curves 1 and 2 are results of the analytical methods 1 and 2 obtained using the component values of the measurement circuit and the quasi-linear parameters of the PN3563 transistor extracted from actual measurements [14]. Curves 3 and 4 are results of the analytical methods 1 and 2 obtained using the component values of the simulation circuit and the quasi-linear parameters extracted for MPS918 from the ADS model of MPS918. The calculations involved in obtaining the curves were done with R [19].

The next example illustrates obtaining curve "Analytical method 1, PN3563 ($f = 100\,\mathrm{MHz}$)". As can be seen from (5.25), the output admittance depends on Y_1, Y_2 and Y_3. The values of these admittances are evaluated by using the component values of the measurement circuit and the measured quasi-linear model of the PN3563 transistor. Component values C_r, C_1 and C_2 used in the measurements are shown in Appendix B. As an example, the output conductance at $\hat{v}_{out} = 0.8\,\mathrm{V}$ is calculated with analytical method 1 and PN3563 transistor in case $x = 4, C_1' = 30\,\mathrm{pF}$ as follows:

$$\omega = 2\pi \cdot 100\,\mathrm{MHz} \tag{5.38}$$
$$\hat{v}_{out} = 0.8\,\mathrm{V} \tag{5.39}$$
$$L_r = 500\,\mathrm{nH} \tag{5.40}$$
$$R_r = 8\,\Omega \tag{5.41}$$
$$C_r = 8.6\,\mathrm{pF} \tag{5.42}$$
$$C_1' = C_1 + C_{be} = 22\,\mathrm{pF} + 7.7\,\mathrm{pF} = 29.7\,\mathrm{pF} \tag{5.43}$$
$$C_2' = C_2 + C_{ce} = 7.8\,\mathrm{pF} + 0\,\mathrm{pF} = 7.8\,\mathrm{pF} \tag{5.44}$$
$$Y_1 = j\omega C_1' + 1/r_\pi = (0.0070922 + j0.0186611)\mathrm{S} \tag{5.45}$$
$$Y_2 = j\omega C_2' + 1/r_o = (8.1169 \cdot 10^{-4} + j4.9009 \cdot 10^{-3})\mathrm{S} \tag{5.46}$$
$$Y_3 = j\omega C_{bc} + 1/(j\omega L_r + 1/(j\omega C_r) + R_r) \tag{5.47}$$
$$= (4.7819 \cdot 10^{-4} - j5.6431 \cdot 10^{-3})\mathrm{S} \tag{5.48}$$

$$Y_{out}(\omega, \hat{v}_{out}) = (-0.02137957 + j0.01093298)\mathrm{S} \tag{5.49}$$
$$G_{out} = -21.4\,\mathrm{mS}. \tag{5.50}$$

Curve "Analytical method 2, PN3563 ($B_{out} = 0$)" is obtained according to the following example. At $\hat{v}_{out} = 0.8\,\mathrm{V}$, the output conductance is found by first solving frequency f_s numerically from

$$\mathrm{Im}\,\{Y_{out}(0.8\,\mathrm{V}, 2\pi f_s)\} = 0, \tag{5.51}$$

which yields two solutions: $f_{s1} = 92.628\,892\,\mathrm{MHz}$ and $f_{s2} = 17.779\,359\,\mathrm{MHz}$. The output conductance and the stability parameter S are calculated for both solutions,

which results in

$$S_{f_{s1}} = 1.571\,264 \cdot 10^{-11}\,\frac{\mathrm{S^2s}}{\mathrm{V}} > 0 \tag{5.52}$$

$$G_{out,f_{s1}} = \mathrm{Re}\left\{Y_{out}(0.8\,\mathrm{V}, 2\pi f_{s1})\right\} = -26.0\,\mathrm{mS} \tag{5.53}$$

$$S_{f_{s2}} = 1.549\,385 \cdot 10^{-13}\,\frac{\mathrm{S^2s}}{\mathrm{V}} > 0 \tag{5.54}$$

$$G_{out,f_{s2}} = \mathrm{Re}\left\{Y_{out}(0.8\,\mathrm{V}, 2\pi f_{s2})\right\} = 16.4\,\mathrm{mS} > 0. \tag{5.55}$$

The stability conditions indicate that both solutions are stable. However, f_{s2} is discarded since the corresponding output conductance is positive.

Obtaining curve "Analytical method 1, MPS918 ($f = 100\,\mathrm{MHz}$)" involves using the component values of the simulation circuit and the quasi-linear model of the MPS918 transistor to calculate Y_1, Y_2 and Y_3. The value of C_r was obtained from Table 3.1. As an example, the output conductance at $\hat{v}_{out} = 0.8\,\mathrm{V}$ is calculated in case $x = 4, C_1' = 30\,\mathrm{pF}$ as follows:

$$\omega = 2\pi \cdot 100\,\mathrm{MHz} \tag{5.56}$$

$$\hat{v}_{out} = 0.8\,\mathrm{V} \tag{5.57}$$

$$L_r = 500\,\mathrm{nH} \tag{5.58}$$

$$R_r = 8\,\Omega \tag{5.59}$$

$$C_r = 15\,\mathrm{pF} \tag{5.60}$$

$$C_1' = 30\,\mathrm{pF} \tag{5.61}$$

$$C_2' = C_1'/x = 7.5\,\mathrm{pF} \tag{5.62}$$

$$Y_1 = j\omega C_1' + 1/r_\pi = (0.017\,262\,21 + j0.018\,849\,56)\mathrm{S} \tag{5.63}$$

$$Y_2 = j\omega C_2' + 1/r_o = (0.003\,011\,141 + j0.004\,712\,389)\mathrm{S} \tag{5.64}$$

$$Y_3 = j\omega C_{bc} + 1/(j\omega L_r + 1/(j\omega C_r) + R_r) \tag{5.65}$$

$$= (0.000\,184\,539 - j0.004\,446\,377)\mathrm{S} \tag{5.66}$$

$$Y_{out}(\omega, \hat{v}_{out}) = (-0.031\,181\,47 + j0.003\,186\,01)\mathrm{S} \tag{5.67}$$

$$G_{out} = -31.2\,\mathrm{mS}. \tag{5.68}$$

6. RESULTS

This chapter is organized as follows. Section 6.1 uses the measurement results to determine the validity of the output power maximization rule which follows from the straight-line approximation of output conductance. Section 6.2 compares the analytically obtained and simulated output conductance to measurement results. Section 6.3 discusses the differences between analytical method 1 and the simulation methods. Section 6.4 discusses the differences between the simulation methods.

6.1 Examining the validity of the straight-line approximation

As discussed in Section 2.3, the straight-line approximation of the output conductance amplitude dependence implies that the condition $G_L = -G_m/3$ maximizes the output power. Table 6.1 evaluates the assumption $G_L = -G_m/3$ for maximum output power based on the measurement results of Appendix B. Each row corresponds to a combination of x and C_1'. The small-signal output conductance, G_m, is assumed to be the maximally negative output conductance obtained from the measurement results. This output conductance was obtained with the highest value of load conductance for which clear oscillation existed. Column $G_{L,1/3}$ is the load conductance used in the measurement closest to $-G_m/3$. Column $P_{L,1/3}$ is the output power obtained with this load conductance: $P_{L,1/3} = \frac{1}{2}G_{L,1/3}\hat{v}_{out}^2$. The assumption $G_L = -G_m/3$ for maximum output power implies that $P_{L,1/3}$ should be the maximum output power. Column $G_{L,Pmax}$ is the load conductance which yields the maximum measured output power, column $P_{L,max}$. Ratios $\frac{-G_m/3}{G_{L,Pmax}}$ and $\frac{P_{L,max}}{P_{L,1/3}}$ evaluate the validity of the assumption $G_L = -G_m/3$ for maximum output power. If the assumption is true, the values in both columns should be approximately 1.

Table 6.1. *Determining the validity of the load conductance assumption $G_L = -G_m/3$ for maximum output power for the measured combinations of x and C_1'.*

x	C_1' (pF)	G_m (mS)	$G_{L,1/3}$ (mS)	$P_{L,1/3}$ (mW)	$G_{L,Pmax}$ (mS)	$P_{L,max}$ (mW)	$\frac{-G_m/3}{G_{L,Pmax}}$	$\frac{P_{L,max}}{P_{L,1/3}}$
0.5	30	−86.7	30.0	4.1	7.09	12.0	4.1	2.9
0.5	40	−103.3	34.7	4.1	12.50	7.0	2.8	1.7
0.5	80	−323.0	103.3	1.3	323.03	2.8	0.3	2.1
0.5	160	−120.0	39.6	0.02	75.56	0.03	0.5	1.2
1.0	30	−65.5	20.0	15.9	5.56	48.0	3.9	3.0
1.0	40	−70.0	25.0	6.8	4.76	35.4	4.9	5.2
1.0	80	−120.0	39.6	3.3	4.76	8.2	8.4	2.5
1.0	160	−120.0	39.6	0.4	50.30	0.4	0.8	1.1
2.0	30	−53.3	16.7	17.3	4.76	47.2	3.7	2.7
2.0	40	−61.7	20.0	10.1	4.00	37.0	5.1	3.7
2.0	80	−86.7	30.0	5.2	4.00	23.1	7.2	4.5
2.0	160	−61.7	20.0	2.9	7.09	5.1	2.9	1.8
4.0	30	−39.6	12.5	19.1	4.00	40.8	3.3	2.1
4.0	40	−50.3	16.7	11.7	4.00	37.8	4.2	3.2
4.0	80	−70.0	25.0	6.1	2.86	31.7	8.2	5.2
4.0	160	−45.6	15.2	6.4	3.45	19.8	4.4	3.1

In 13 out of 16 cases, $\frac{-G_m/3}{G_{L,Pmax}}$ is at least 2.8. That is, the load conductance selected according to $G_L = -G_m/3$ is several times greater than the load conductance which yields the maximum output power. Additionally, the maximum output power is in almost all cases significantly higher than the power obtained with $G_L = -G_m/3$.

The data shows that choosing $G_L = -G_m/3$ yields output powers that are not even close to the maximum values in many cases. Since this condition follows from the straight-line approximation, the usefulness of the straight-line approximation is questionable in predicting the maximum oscillator output power.

Cases $(0.5, 80\,\text{pF})$, $(0.5, 160\,\text{pF})$, $(1, 160\,\text{pF})$ are exceptions (the lines shown in grey). In these cases, $\frac{-G_m/3}{G_{L,Pmax}}$ is less than 1 and $G_{L,Pmax}$ is high. The measured output voltage amplitude is small, less than 0.5 V, for all measured load conductances in these cases. The small output voltage amplitude may indicate that the oscillation is not stable. Instead, the circuit is on the verge of oscillation. This may contribute to the difference of these 3 cases compared to the 13 other cases.

6.2 Comparison of the measurements and predictions

Table 6.2 shows maximum and average percentage differences of the output conductance obtained with analytical methods and simulations compared to the mea-

surement results. The selected cases are those in which the analytical methods best agree with the measurement results.

A percentage difference between the predicted and measured G_{out} was calculated for each measured output voltage amplitude. The difference is relative to the measured output conductance:

$$\%\text{-difference} = 100\,\% \cdot \frac{G_{out,predicted} - G_{out,measured}}{G_{out,measured}}. \tag{6.1}$$

The maximum percentage difference is defined as the value which has the largest absolute value. The average percentage difference is defined as the average of the absolute values of the percentage differences.

The results of the analytical methods were obtained with the component values of the measurement circuit and the quasi-linear model of the PN3563 transistor. As discussed in Section 5.4, analytical method 1 evaluates the real part of the output admittance function at the frequency of 100 MHz. In analytical method 2, the frequency at which the output admittance function is evaluated, is solved from $\mathrm{Im}\,\{Y_{out}(\hat{v}_{out}, 2\pi f_s)\} = 0$.

In case $x = 4, C_1' = 30\,\mathrm{pF}$, both analytical methods yield similar results: the average difference from the measured values is less than 20 % and the maximum difference is less than 50 %. In this case, the analytical methods have the best agreement. The capacitance ratio $x = C_1'/C_2'$ affects the accuracy of the analytical methods. In cases of Table 6.2, the accuracy decreases with decreasing x when C_1' is constant. In other words, at low values of C_2' the accuracy is better than at high values. The same is true for C_1': low values of C_1' yield a better accuracy than high values.

Simulation methods tend to overestimate the negative output conductance. One reason for this may be that the simulation model of the MPS918 transistor does not accurately represent the PN3563 of the measurement circuit.

In other cases than those in Table 6.2, analytical methods are less applicable. Analytical method 1 tends to predict a positive output conductance at all output voltage amplitudes, or it predicts that the output conductance becomes zero at a lower value than measured. Analytical method 2 tends to predict that no oscillation exists for output voltage amplitudes greater than a limit value which is approximately 1 V or less.

Table 6.2. *Maximum and average relative difference of the predictions compared to measurement results. VL: variable load simulation method, VTV: variable test voltage simulation method.*

x	C_1' (pF)	method	max %-difference (%)	average |%-difference| (%)
4	30	Analytical 1, PN3563	+47	17
4	30	Analytical 2, PN3563	+49	19
4	30	VL	+172	73
4	30	VTV	−793	184
4	40	Analytical 1, PN3563	−300	74
4	40	Analytical 2, PN3563	+94	28
4	40	VL	+192	99
4	40	VTV	−877	192
4	80	Analytical 1, PN3563	−974	297
4	80	Analytical 2, PN3563	−96	48
4	80	VL	+218	103
4	80	VTV	+239	88
2	30	Analytical 1, PN3563	−183	68
2	30	Analytical 2, PN3563	−91	44
2	30	VL	+207	75
2	30	VTV	+306	132
2	40	Analytical 1, PN3563	−353	112
2	40	Analytical 2, PN3563	−99	39
2	40	VL	+252	137
2	40	VTV	+287	120

6.3 Comparison of the output conductance function and simulations

Figure 6.1 compares the results obtained with the output conductance function and the simulation methods in case $x = 4$, $C_1' = 40\,\text{pF}$. The figure has two curves obtained with the output conductance function. One curve corresponds to analytical method 1. In other words, the output conductance was obtained by evaluating $\text{Re}\,\{Y_{out}(\hat{v}_{out}, 2\pi f)\}$ at the frequency of 100 MHz. The other curve was obtained with a frequency-adjusted analysis which is described in this section. Both curves were obtained using the quasi-linear model of the MPS918 transistor and the component values of the simulation circuit.

At output voltage amplitudes of less than 0.1 V, the variable test voltage simulation method and analytical method 1 predict a negative conductance of approximately −58 mS at 100 MHz. This agreement is expected as is shown in the following. At output voltage amplitudes close to zero, the transadmittance of the quasi-linear

transistor model is approximately its small-signal value, $|y_{m_0}|e^{j\phi}$. The other component values of the quasi-linear model were obtained with the S-parameter simulation at a low power level. Therefore, the quasi-linear model is approximately the same as a linear small-signal model. In this case, the analytical method corresponds to a linear analysis. When the output voltage amplitude is low in the variable test voltage method, the circuit voltages and currents are small, which makes linear analysis agree with the simulation.

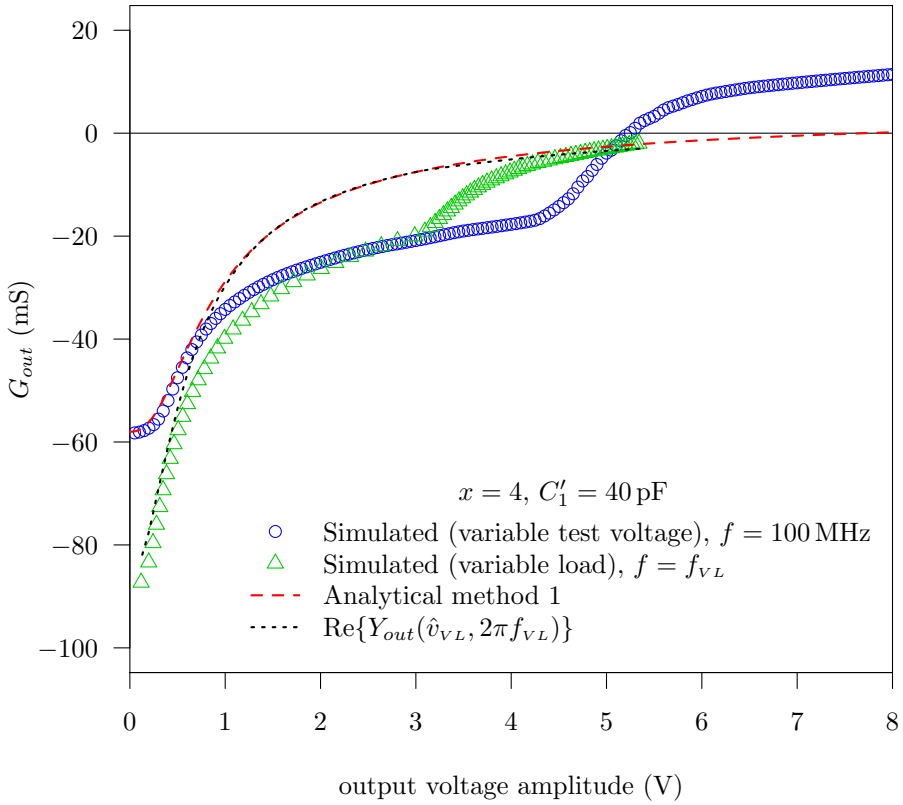

Figure 6.1. *The amplitude dependence of the output conductance obtained with the variable test voltage method, variable load method, and the output conductance function with MPS918 in case $x = 4$, $C_1' = 40\,\mathrm{pF}$. Symbols $\hat{v}_{VL}$ and f_{VL} denote the output voltage amplitude and oscillation frequency obtained with the variable load method.*

At low output voltage amplitudes, a discrepancy exists between analytical method 1 and the variable load method. With $\hat{v}_{out} = 0.1183\,\mathrm{V}$, analytical method 1 predicts a negative conductance of $-57.45\,\mathrm{mS}$ at 100 MHz. The variable load method yields a more negative output conductance, $-87.30\,\mathrm{mS}$. However, the oscillation frequency in this case is 93.89 MHz instead of 100 MHz. As can be seen from Figure 6.2, the oscillation frequency depends on the load conductance with the variable load method.

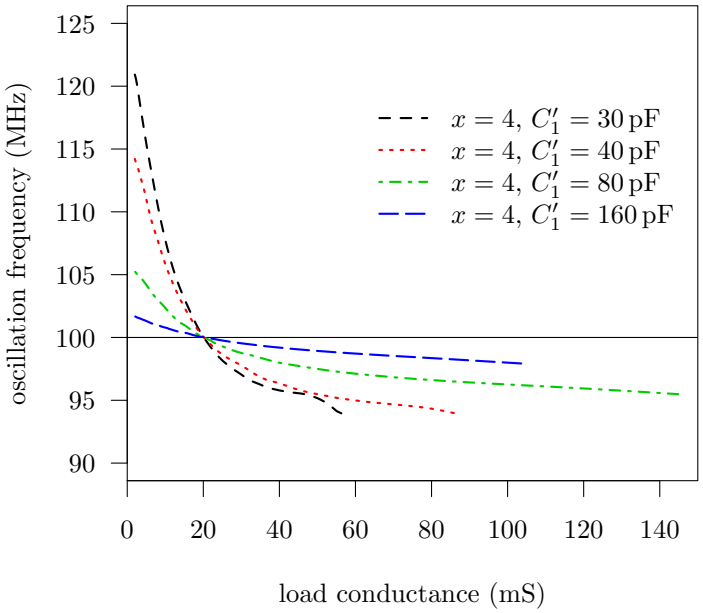

Figure 6.2. *The oscillation frequency of the variable load method as a function of the load conductance in cases where* $x = 4$.

To investigate the effect of this frequency difference on the discrepancy between the variable load method and analytical method 1, a frequency-adjusted analysis was performed. In this analysis, the output conductance was calculated with the frequencies and amplitudes obtained with the variable load method. That is, G_{out} was calculated using the output admittance function according to

$$\mathrm{Re}\left\{Y_{out}(\hat{v}_{VL}, 2\pi f_{VL})\right\}, \tag{6.2}$$

where $\hat{v}_{VL}$ and f_{VL} are the output voltage amplitude and frequency obtained for each load conductance value using the variable load simulation method. For example, when G_L is set as 87.30 mS, the variable load method yields the oscillation frequency of $f_{VL} = 93.89\,\mathrm{MHz}$ and the output voltage amplitude of $\hat{v}_{VL} = 0.1183\,\mathrm{V}$. Since $G_{out} = -G_L$, the output conductance according to the variable load method is $G_{out} = -87.3\,\mathrm{mS}$ at the output voltage amplitude 0.1183 V. At this output voltage amplitude, the frequency-adjusted analysis predicts

$$\mathrm{Re}\left\{Y_{out}(0.1183\,\mathrm{V}, 2\pi \cdot 93.89\,\mathrm{MHz})\right\} = -83\,\mathrm{mS}. \tag{6.3}$$

This value is close to the value obtained with the variable load method.

At output voltage amplitudes of less than 0.6 V, the frequency-adjusted analysis agrees better with the variable load method than analytical results obtained at 100 MHz. Therefore, the discrepancy between analytical method 1 and the variable load method at low amplitudes can be largely attributed to frequency differences.

However, at higher amplitudes, both curves obtained with the output conductance function disagree with the simulation results. The accuracy of the quasi-linear transistor model deteriorates as the base-emitter and collector-emitter voltages increase, which probably contributes to the discrepancy between the methods.

6.4 Comparison of the simulation methods

At low output voltage amplitudes, the variable test voltage method yields a less negative output conductance than the variable load method. The simulated oscillation frequency varies in the variable load method as shown in Figure 6.2. In contrast, the frequency in the variable test voltage method is kept at 100 MHz. To determine if the frequency difference causes the difference between the results, the output conductance was simulated with the variable test voltage method using some of the oscillation voltage amplitudes and frequencies obtained with the variable load method. The results are shown in Table 6.3.

Table 6.3. *The negative output conductance obtained with simulation methods in case* $x = 4$, $C_1' = 40\,\mathrm{pF}$.

Method	$\hat{v}_{out}$ (V)	f (MHz)	G_{out} (mS)
Variable load	0.1183	93.89	−87.30
Variable test voltage	0.1183	93.89	−87.31
Variable test voltage	0.1183	100.00	−57.99
Variable load	0.9937	96.37	−39.91
Variable test voltage	0.9937	96.37	−40.25
Variable test voltage	0.9937	100.00	−34.34
Variable load	2.9883	100.05	−20.00
Variable test voltage	2.9883	100.05	−20.85
Variable test voltage	2.9883	100.00	−20.89
Variable load	4.0329	108.43	−7.26
Variable test voltage	4.0329	108.43	−13.22
Variable test voltage	4.0329	100.00	−17.62

At $\hat{v}_{out}$ of 0.1183 V, 0.9937 V and 2.9883 V, the variable test voltage method yields similar results to the variable load method when the frequencies are equal. However, at 4.0329 V, the variable load method yields a negative output conductance which is approximately half that of the variable test voltage method. Therefore, the frequency difference is insufficient to explain the discrepancy.

A possible reason for the discrepancy at 4.0329 V can be found by considering the spectra of the output voltage and current. As shown in Figure 6.3, the output voltage

spectrum of the variable load method consists of multiple frequency components. Table 6.4 shows the values of the voltage and current phasors.

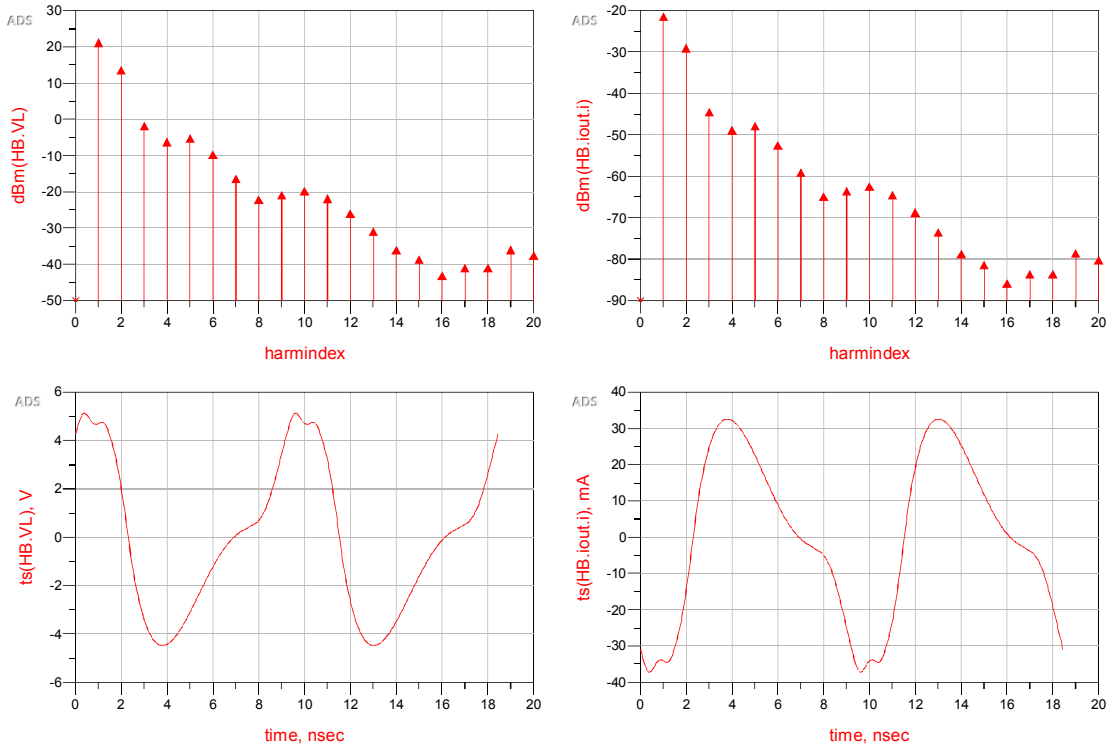

Figure 6.3. *The output voltage and current spectra and the time-domain forms of the variable load method with* $x = 4$, $C_1' = 40\,\mathrm{pF}$, $G_L = 7.26\,\mathrm{mS}$, $\hat{v}_{out} = 4.0329\,\mathrm{V}$, $f = 108.43\,\mathrm{MHz}$.

Table 6.4. *The output voltage and current frequency components of the variable load method with* $x = 4$, $C_1' = 40\,\mathrm{pF}$, $G_L = 7.26\,\mathrm{mS}$, $\hat{v}_{out} = 4.0329\,\mathrm{V}$, $f = 108.43\,\mathrm{MHz}$.

k	f_k (MHz)	$\hat{v}_{out,k}$ (V)	Arg$\{v_{out,k}\}$ (°)	$\hat{i}_{out,k}$ (mA)	Arg$\{i_{out,k}\}$ (°)
1	108.4	4.033	−3.4	29.285	176.6
2	216.9	1.696	−88.0	12.314	92.0
3	325.3	0.285	−130.9	2.071	49.1
4	433.7	0.172	42.4	1.247	−137.6
5	542.2	0.193	2.5	1.403	−177.5
6	650.6	0.114	−38.0	0.827	142.0
7	759.0	0.053	−76.7	0.386	103.3
8	867.5	0.027	−86.7	0.198	93.3
9	975.9	0.032	−88.4	0.230	91.6
10	1084.3	0.036	−115.7	0.261	64.3
11	1192.8	0.028	−153.1	0.207	26.9
12	1301.2	0.017	160.1	0.127	−19.9
13	1409.6	0.010	119.8	0.073	−60.2
14	1518.1	0.006	115.3	0.040	−64.7
15	1626.5	0.004	108.0	0.030	−72.0
16	1734.9	0.002	30.7	0.018	−149.3
17	1843.4	0.003	−72.7	0.023	107.3
18	1951.8	0.003	−164.6	0.023	15.4
19	2060.2	0.006	100.5	0.041	−79.5
20	2168.7	0.005	106.7	0.034	−73.3

Figure 6.4 and Table 6.5 show the output voltage and current spectra when the circuit is simulated with the variable test voltage method. The test voltage source is set equal to the fundamental frequency component of the load voltage obtained with the variable load method. As a result, the output voltage spectrum of the variable test voltage method consists of a single component at the fundamental frequency. This is because the voltage source is a short circuit at other frequencies.

The resulting output current component at the fundamental frequency, $54.9\,\mathrm{mA}\angle 163°$, differs from the value obtained with the variable load method, $29.3\,\mathrm{mA}\angle 177°$. Consequently, also the resulting output admittance ($-13.2\,\mathrm{mS}$) differs from the value obtained with the variable load method ($-7.26\,\mathrm{mS}$).

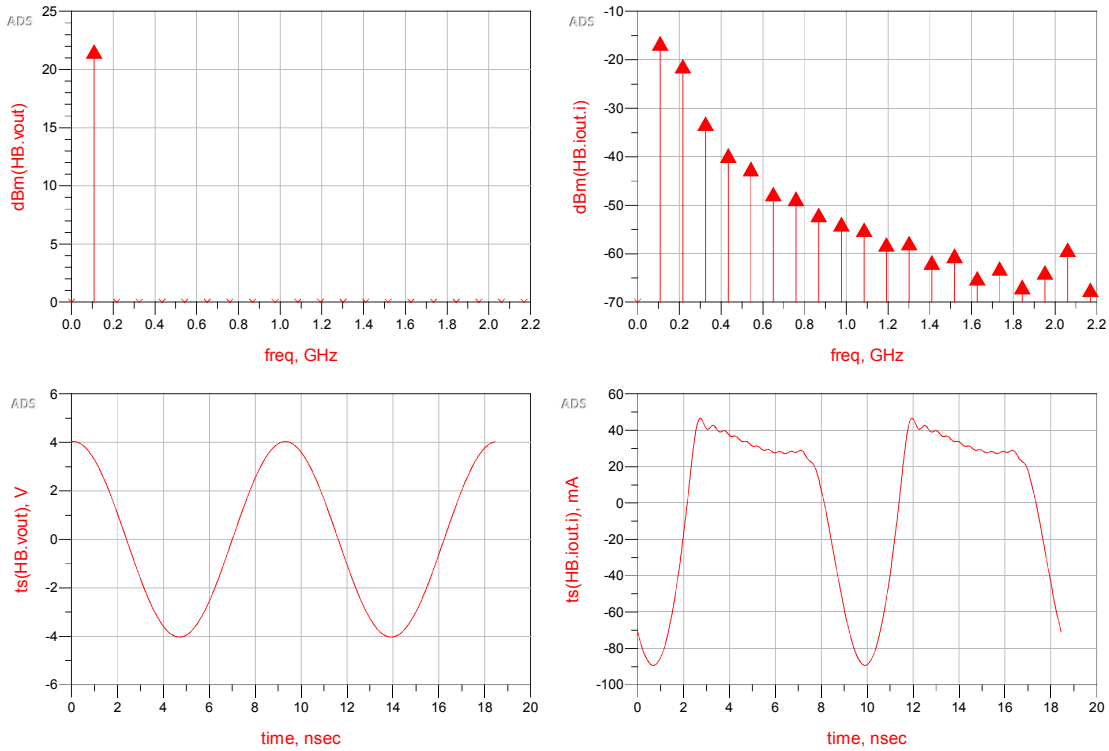

Figure 6.4. *The output voltage and current spectra and the time-domain forms of the variable test voltage method with* $x = 4$, $C_1' = 40\,\mathrm{pF}$, $\hat{v}_{test} = 4.033\,\mathrm{V}$, $f = 108.4\,\mathrm{MHz}$.

Table 6.5. *The output voltage and current frequency components of the variable test voltage method with* $x = 4$, $C_1' = 40\,\mathrm{pF}$, $\hat{v}_{test} = 4.033\,\mathrm{V}$, $f = 108.4\,\mathrm{MHz}$.

k	f_k (MHz)	$\hat{v}_{out,k}$ (V)	Arg$\{v_{out,k}\}$ (°)	$\hat{i}_{out,k}$ (mA)	Arg$\{i_{out,k}\}$ (°)
1	108.4	4.033	−3.4	54.877	163.4
2	216.9	0.000	0.0	31.807	129.1
3	325.3	0.000	0.0	8.133	82.0
4	433.7	0.000	0.0	3.818	−56.3
5	542.2	0.000	0.0	2.782	−131.7
6	650.6	0.000	0.0	1.528	120.1
7	759.0	0.000	0.0	1.372	19.7
8	867.5	0.000	0.0	0.928	−68.9
9	975.9	0.000	0.0	0.747	171.6
10	1084.3	0.000	0.0	0.655	90.7
11	1192.8	0.000	0.0	0.461	−36.8
12	1301.2	0.000	0.0	0.477	−115.0
13	1409.6	0.000	0.0	0.302	108.7
14	1518.1	0.000	0.0	0.353	30.7
15	1626.5	0.000	0.0	0.207	−116.4
16	1734.9	0.000	0.0	0.261	162.8
17	1843.4	0.000	0.0	0.169	−14.7
18	1951.8	0.000	0.0	0.238	−82.1
19	2060.2	0.000	0.0	0.408	74.0
20	2168.7	0.000	0.0	0.157	−109.4

The difference between the fundamental components of the output current may be caused by the difference in the output voltage spectra. To test this, the output conductance was simulated with the variable test voltage method such that the test voltage source has a spectrum consisting of the first 10 frequency components of the spectrum in Table 6.4. The resulting output voltage and current waveforms in Figure 6.5 are more similar to those obtained with the variable load method in Figure 6.3 than the waveforms obtained with a single frequency component in Figure 6.4. Table 6.6 shows the resulting fundamental component of the output current, 29.1 mA$\angle$177°. This value is closer to that of the variable load method, 29.3 mA$\angle$177° than the fundamental output current of the single-frequency case, 54.9 mA$\angle$163°.

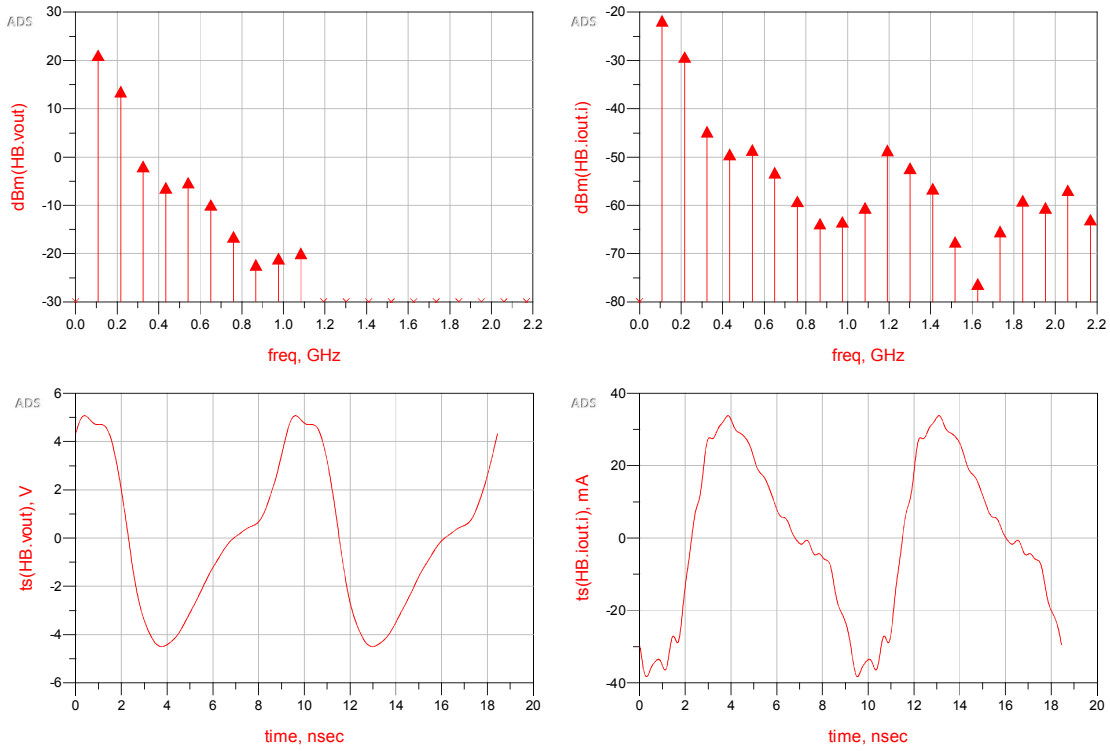

Figure 6.5. *The output voltage and current spectra and the time-domain forms of the variable test voltage method when the test voltage consists of the first 10 frequency components of the spectrum obtained with the variable load method.*

From this analysis, it can be concluded that at low output voltage amplitudes, the disagreement between the variable load method and the variable test voltage method can be explained by the frequency differences. Secondly, if the output voltage amplitude is sufficiently high, the frequency difference is insufficient to explain the disagreement. Instead, the disagreement can be attributed to harmonic components of the output voltage and current.

Table 6.6. *The output voltage and current frequency components of the variable test voltage method when the test voltage consists of the first 10 frequency components of the spectrum obtained with the variable load method.*

k	f_k (MHz)	$\hat{v}_{out,k}$ (V)	Arg$\{v_{out,k}\}$ (°)	$\hat{i}_{out,k}$ (mA)	Arg$\{i_{out,k}\}$ (°)
1	108.4	4.033	−3.4	29.096	176.8
2	216.9	1.696	−88.0	12.242	91.8
3	325.3	0.285	−130.9	2.057	49.9
4	433.7	0.172	42.4	1.203	−140.1
5	542.2	0.193	2.5	1.341	179.8
6	650.6	0.114	−38.0	0.777	135.5
7	759.0	0.053	−76.7	0.392	85.9
8	867.5	0.027	−86.7	0.231	51.9
9	975.9	0.032	−88.4	0.240	37.0
10	1084.3	0.036	−115.7	0.336	12.2
11	1192.8	0.000	0.0	1.325	104.0
12	1301.2	0.000	0.0	0.863	47.8
13	1409.6	0.000	0.0	0.531	−9.6
14	1518.1	0.000	0.0	0.149	−51.2
15	1626.5	0.000	0.0	0.055	147.0
16	1734.9	0.000	0.0	0.191	−168.5
17	1843.4	0.000	0.0	0.399	160.9
18	1951.8	0.000	0.0	0.335	96.2
19	2060.2	0.000	0.0	0.509	−18.0
20	2168.7	0.000	0.0	0.254	−54.1

7. CONCLUSIONS

This thesis investigated the amplitude dependence of the negative output conductance in a Clapp oscillator by measurements, simulations and analytical methods. One aim was to determine the validity of the straight-line assumption of the output conductance. The straight-line assumption implies that the output power is maximized when the load conductance G_L is selected as $G_L = -G_m/3$, where G_m is the small-signal negative output conductance. With 13 out of 16 measured feedback capacitor combination cases, the load conductance which maximizes the output power was significantly less than $-G_m/3$. Additionally, the output power obtained with the selection $G_L = -G_m/3$ was significantly less than the output power obtained with the actual optimum G_L. According to these results, the straight-line assumption is invalid for the Clapp oscillator.

An output admittance function based on a quasi-linear transistor model was derived. The output admittance of the Clapp oscillator is expressed as a function of the output voltage amplitude and oscillation frequency. This function was used to predict the negative conductance by two methods. Analytical method 1 uses a constant frequency of 100 MHz which approximates the oscillation frequency in the measurements. Analytical method 2 predicts both the output conductance and the oscillation frequency by accounting for the steady-state oscillation conditions. The analytical methods agree best with measurement results in cases where the feedback capacitors have low values. In other cases, the analytical methods are less applicable.

The simulation methods generally overestimated the magnitude of negative output conductance compared to measurements. This may be attributed to the differences between the transistor model of the simulator and the transistor used in the measurements.

Further research could develop analytical methods based on the quasi-linear transistor model to other oscillator topologies. Measurements could be extended to include reactive loads for a more complete understanding of output power maximization.

REFERENCES

[1] A. Suárez, *Analysis and Design of Autonomous Microwave Circuits*. Wiley, 2009.

[2] D. M. Pozar, *Microwave Engineering*. Wiley, third ed., 2005.

[3] R. Ludwig and G. Bogdanov, *RF Circuit Design: Theory and Applications*. Pearson Prentice Hall, second ed., 2009.

[4] J. Gewartowski, "The effect of series resistance on avalanche diode (IMPATT) oscillator efficiency," *Proceedings of the IEEE*, vol. 56, no. 6, pp. 1139–1140, 1968.

[5] A. Grebennikov, *RF and Microwave Transistor Oscillator Design*. Wiley, 2007.

[6] G. Gonzalez, *Foundations of Oscillator Circuit Design*. Artech House, 2006.

[7] B. Perlman, C. Upadhyayula, and W. Siekanowicz, "Microwave properties and applications of negative conductance transferred electron devices," *Proceedings of the IEEE*, vol. 59, pp. 1229–1237, Aug. 1971.

[8] M. J. Howes and M. Jeremy, "Large signal circuit characterization of solid-state microwave oscillator devices," *IEEE Transactions on Electron Devices*, vol. 21, pp. 488–499, Aug. 1974.

[9] J. Blue, "Approximate large-signal analysis of IMPATT oscillators," *The Bell System Technical Journal*, vol. 48, pp. 383–396, Feb. 1969.

[10] M. Maeda, K. Kimura, and H. Kodera, "Design and Performance of X-Band Oscillators with GaAs Schottky-Gate Field-Effect Transistors," *IEEE Transactions on Microwave Theory and Techniques*, vol. 23, no. 8, pp. 661–667, 1975.

[11] Y. Tsuzuki, T. Adachi, and J. W. Zhang, "Formulation of nonlinear negative resistance for calculation of start-up characteristics of crystal oscillators," in *Frequency Control Symposium, 1996. 50th., Proceedings of the 1996 IEEE International.*, pp. 710–713, June 1996.

[12] C. M. Snowden, M. J. Howes, and D. V. Morgan, "Microwave FET Oscillator Design Based on Large-Signal Characterisation," in *Microwave Conference, 1983. 13th European*, pp. 325–329, Sept. 1983.

[13] J. Jokinen, *Kelan hyvyysluvun mittaaminen radiotaajuuksilla*. Bachelor's thesis, Tampere University of Technology, 2012, 27 p.

[14] K. Konttinen, *Bipolaaritransistorin siirtokonduktanssin epälineaarinen mallintaminen*. Bachelor's thesis, Tampere University of Technology, 2012, 26 p.

[15] O.-P. Lunden, K. Konttinen, and M. Hasani, "A Simple Closed-Form Analysis of Clapp Oscillator Output Power Using a Novel Quasi-Linear Transistor Model," *2014 IEEE Radio and Wireless Symposium (RWS)*, pp. 88–90, 2014.

[16] K. Rykov, *Quasi-Linear Modeling of Power Saturation in Bipolar Junction Transistors*. Master's thesis, Tampere University of Technology, 2013, 57 p.

[17] "LSSP Simulation Description," Available (accessed on 9.5.2016): `http://edadocs.software.keysight.com/display/ads2009/LSSP+Simulation+Description`.

[18] K. Kurokawa, "Some Basic Characteristics of Broadband Negative Resistance Oscillator Circuits," *The Bell System Technical Journal*, vol. 48, pp. 1937–1955, July 1969.

[19] R Core Team, *R: A Language and Environment for Statistical Computing*. R Foundation for Statistical Computing, Vienna, Austria, 2015. `https://www.R-project.org/`.

APPENDIX A. NEGATIVE CONDUCTANCE CURVES

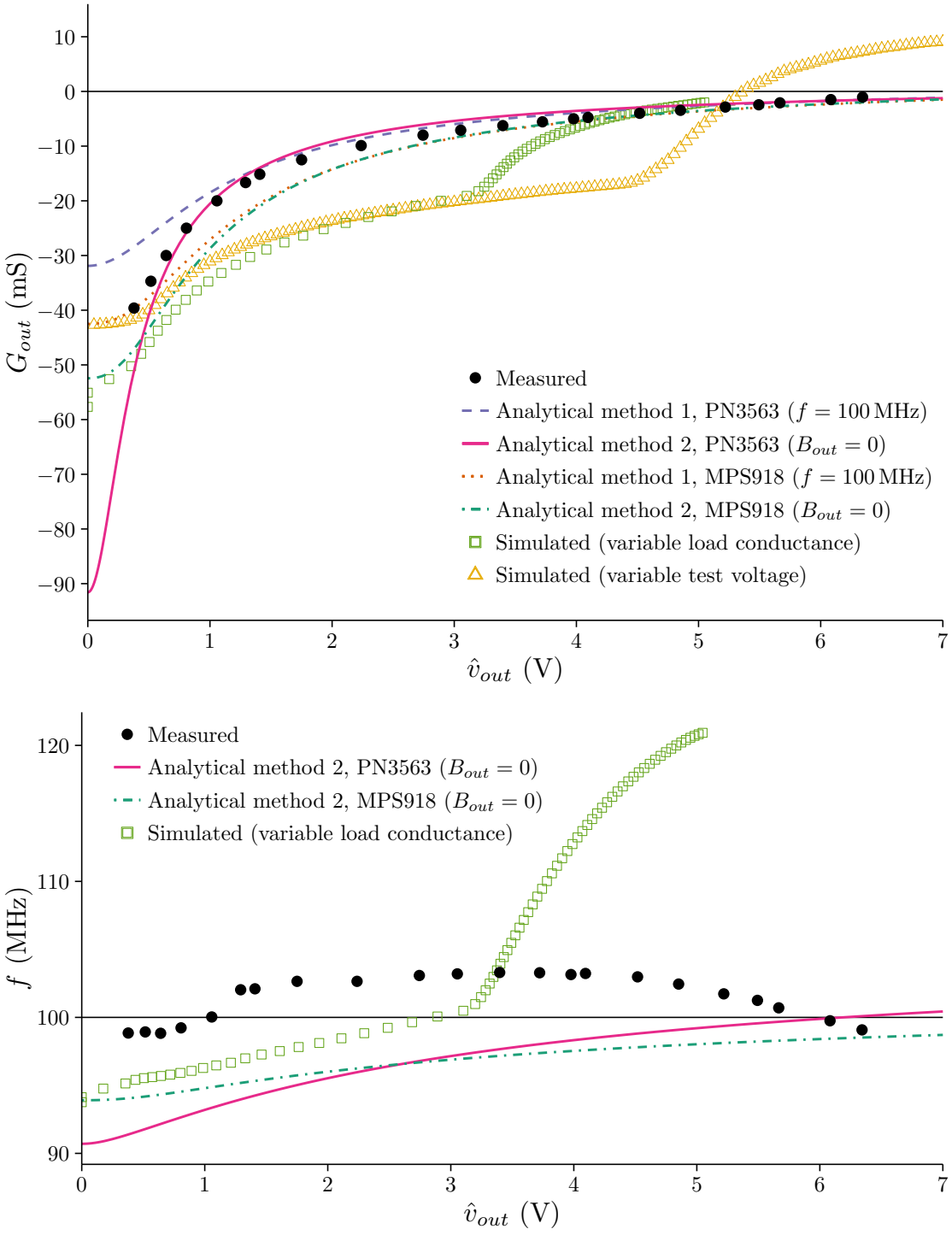

Figure 1. *The measured, simulated and analytically determined output conductance and oscillation frequency in case $x = 4$, $C_1' = 30\,\mathrm{pF}$.*

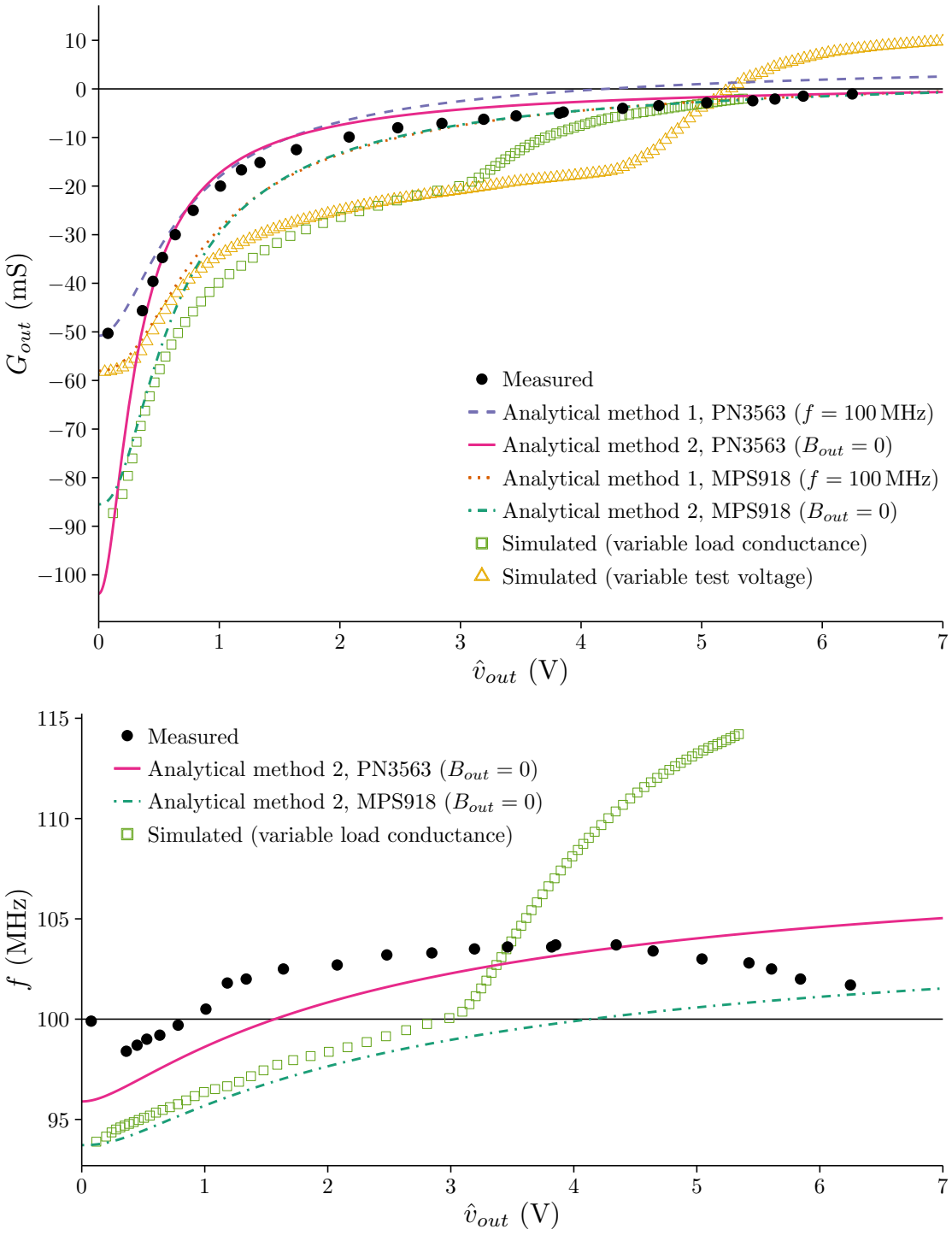

Figure 2. *The measured, simulated and analytically determined output conductance and oscillation frequency in case $x = 4$, $C_1' = 40\,\mathrm{pF}$.*

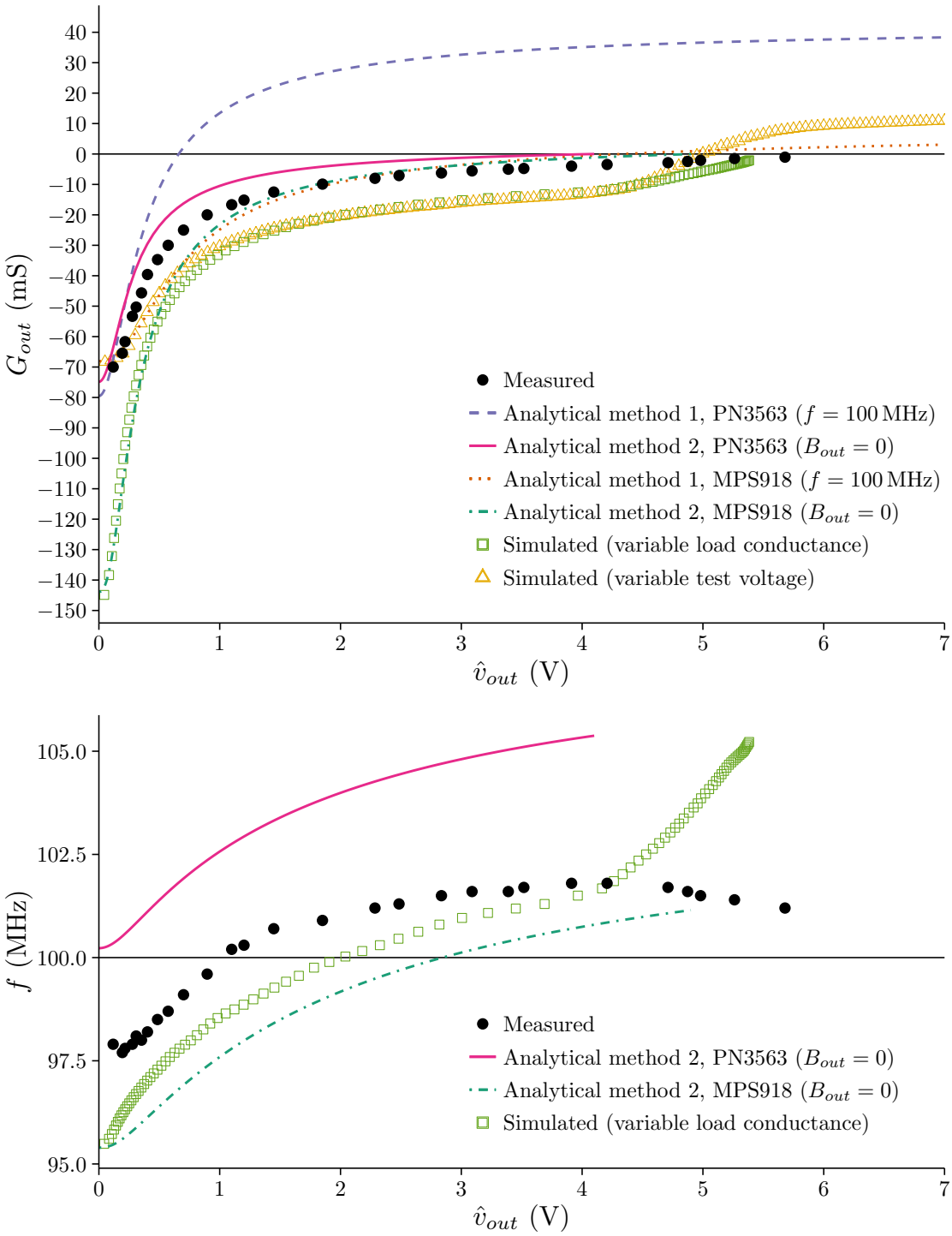

Figure 3. *The measured, simulated and analytically determined output conductance and oscillation frequency in case $x = 4$, $C_1' = 80\,\mathrm{pF}$.*

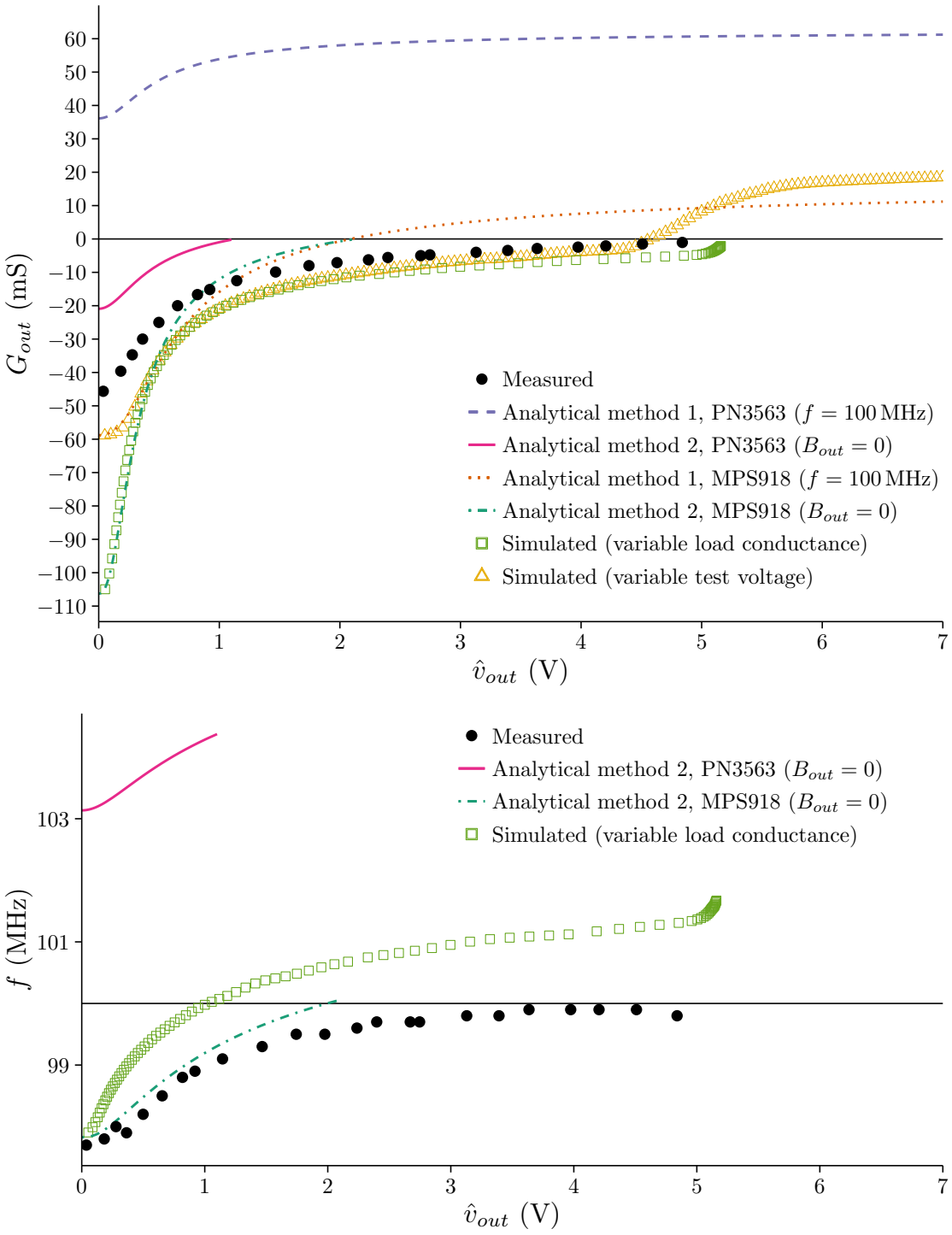

Figure 4. *The measured, simulated and analytically determined output conductance and oscillation frequency in case* $x = 4$, $C_1' = 160\,\mathrm{pF}$.

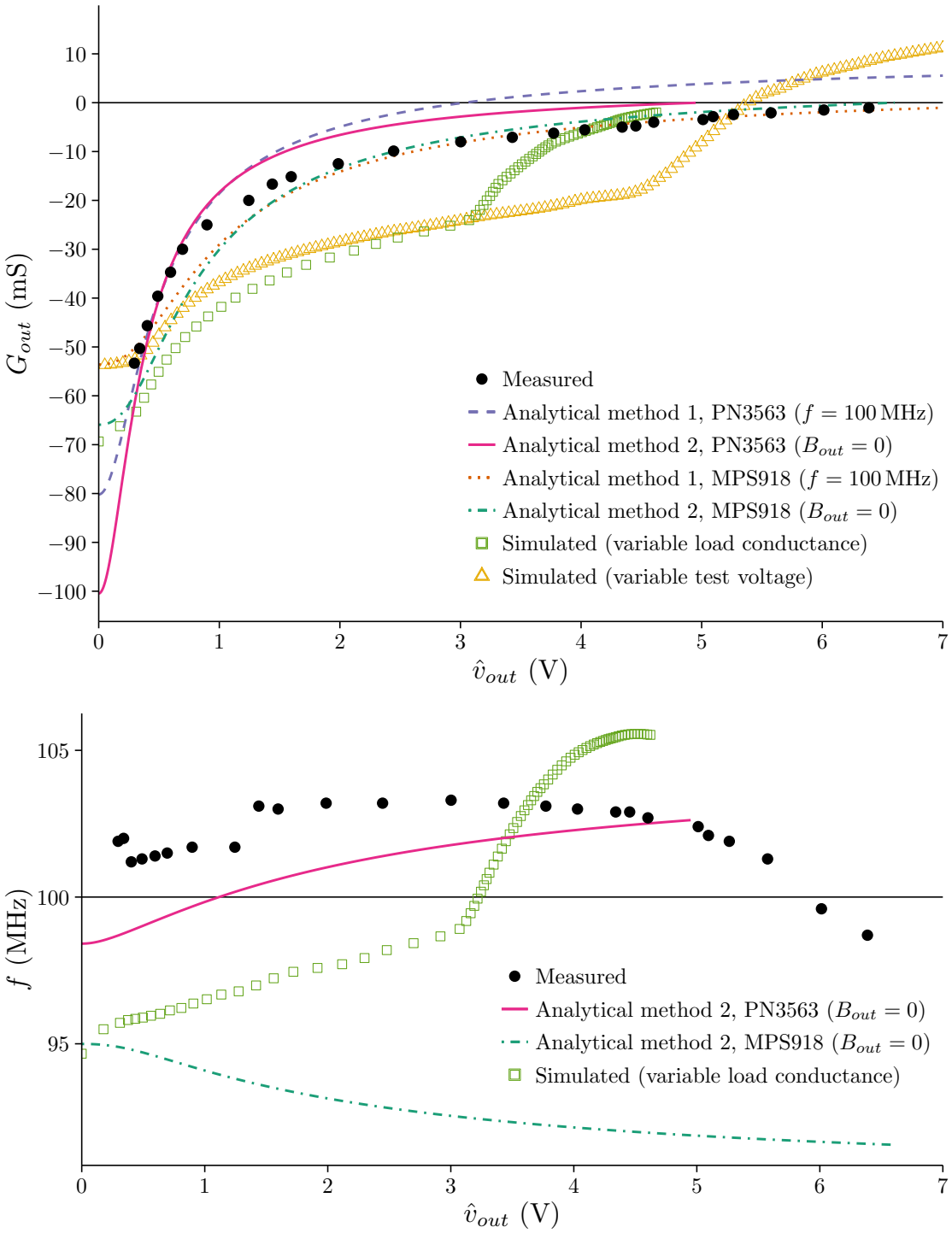

Figure 5. *The measured, simulated and analytically determined output conductance and oscillation frequency in case* $x = 2$, $C_1' = 30\,\mathrm{pF}$.

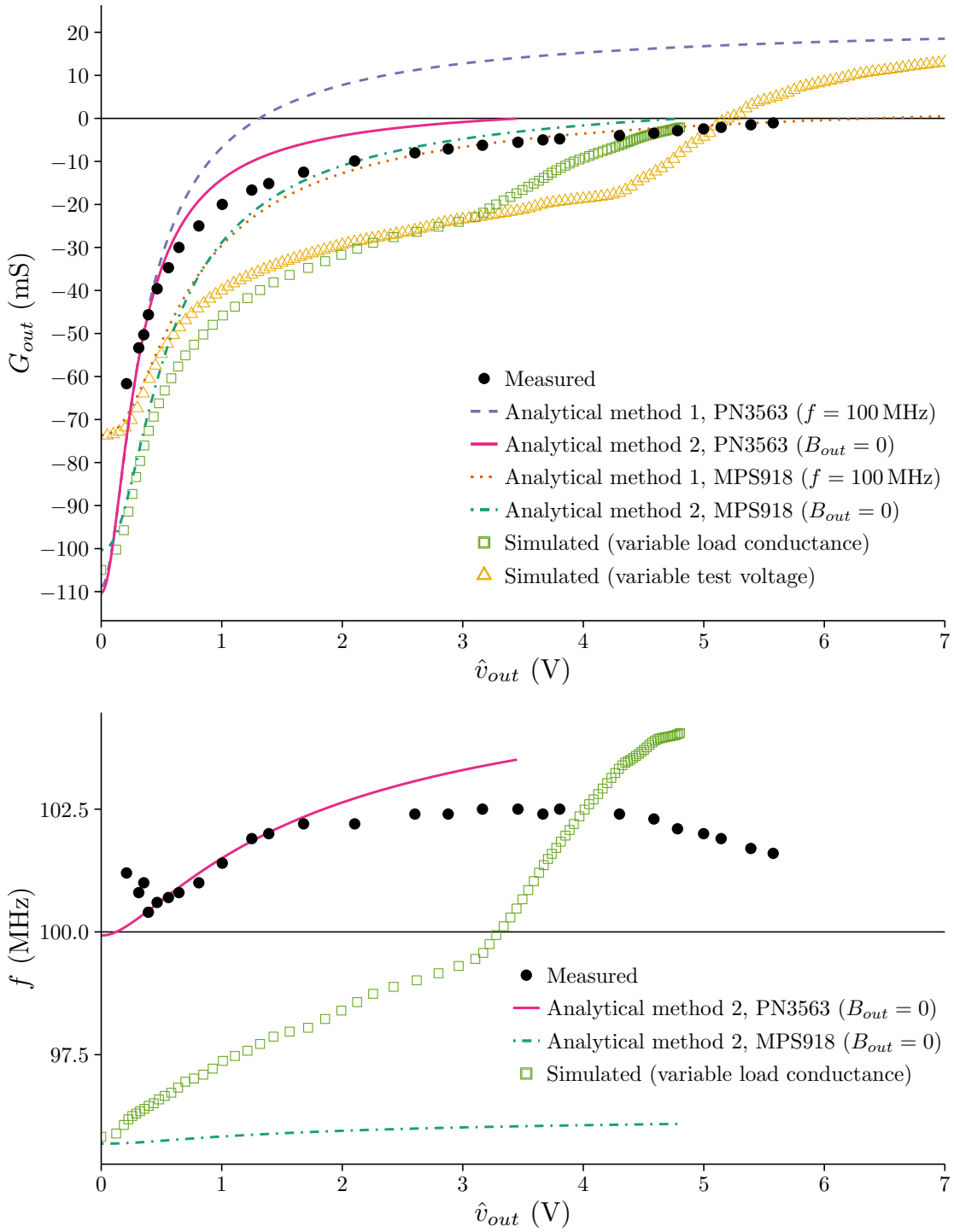

Figure 6. *The measured, simulated and analytically determined output conductance and oscillation frequency in case $x = 2$, $C_1' = 40\,\mathrm{pF}$. In the variable load method, the simulator found that oscillation exists for 14 load conductances between 110 mS and 200 mS. For these load conductances, the fundamental frequency is 22.1 MHz and the amplitudes of all the frequency components are less than $3.1 \cdot 10^{-15}\,\mathrm{V}$. These solutions have been omitted from the figures.*

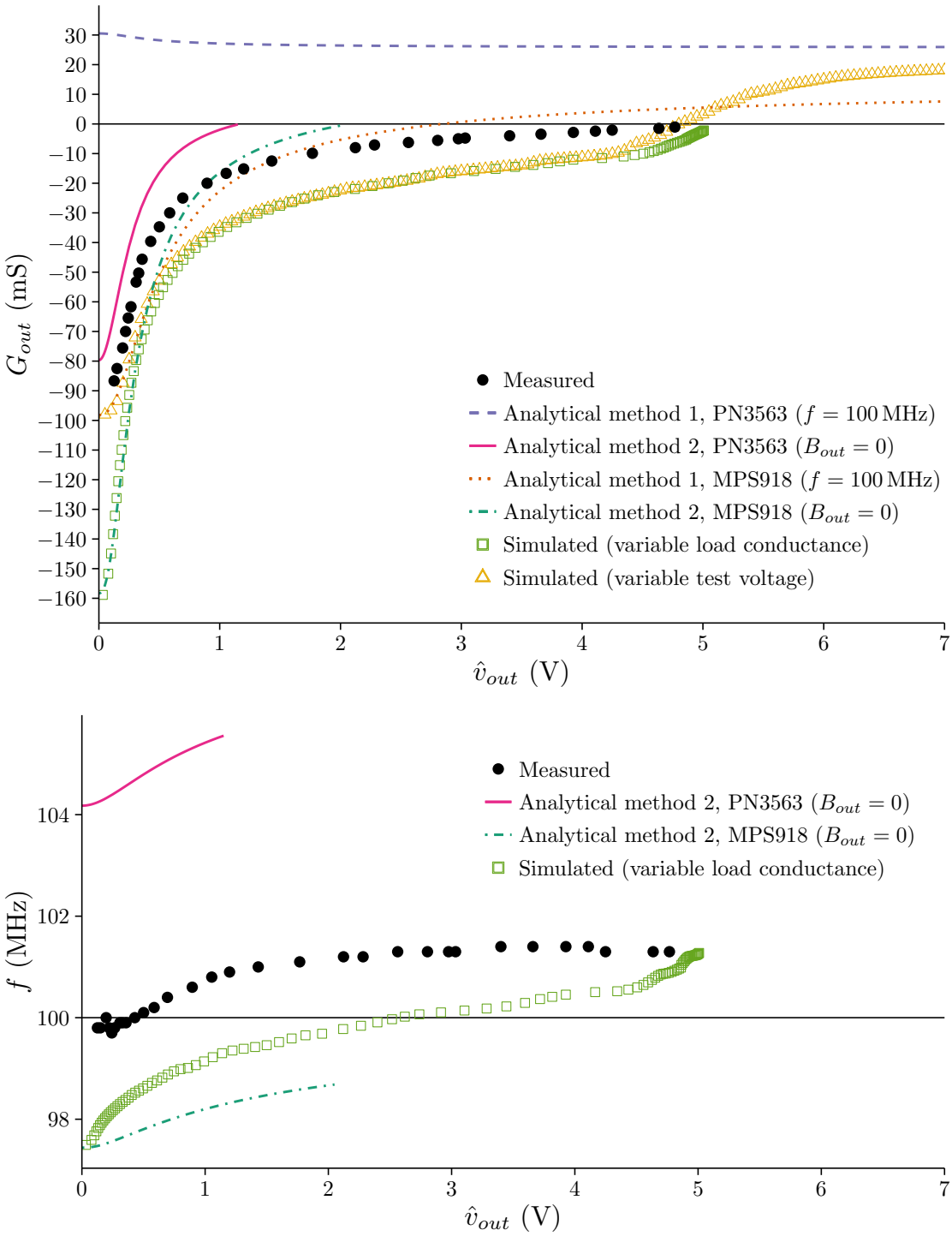

Figure 7. *The measured, simulated and analytically determined output conductance and oscillation frequency in case $x = 2$, $C_1' = 80\,\mathrm{pF}$.*

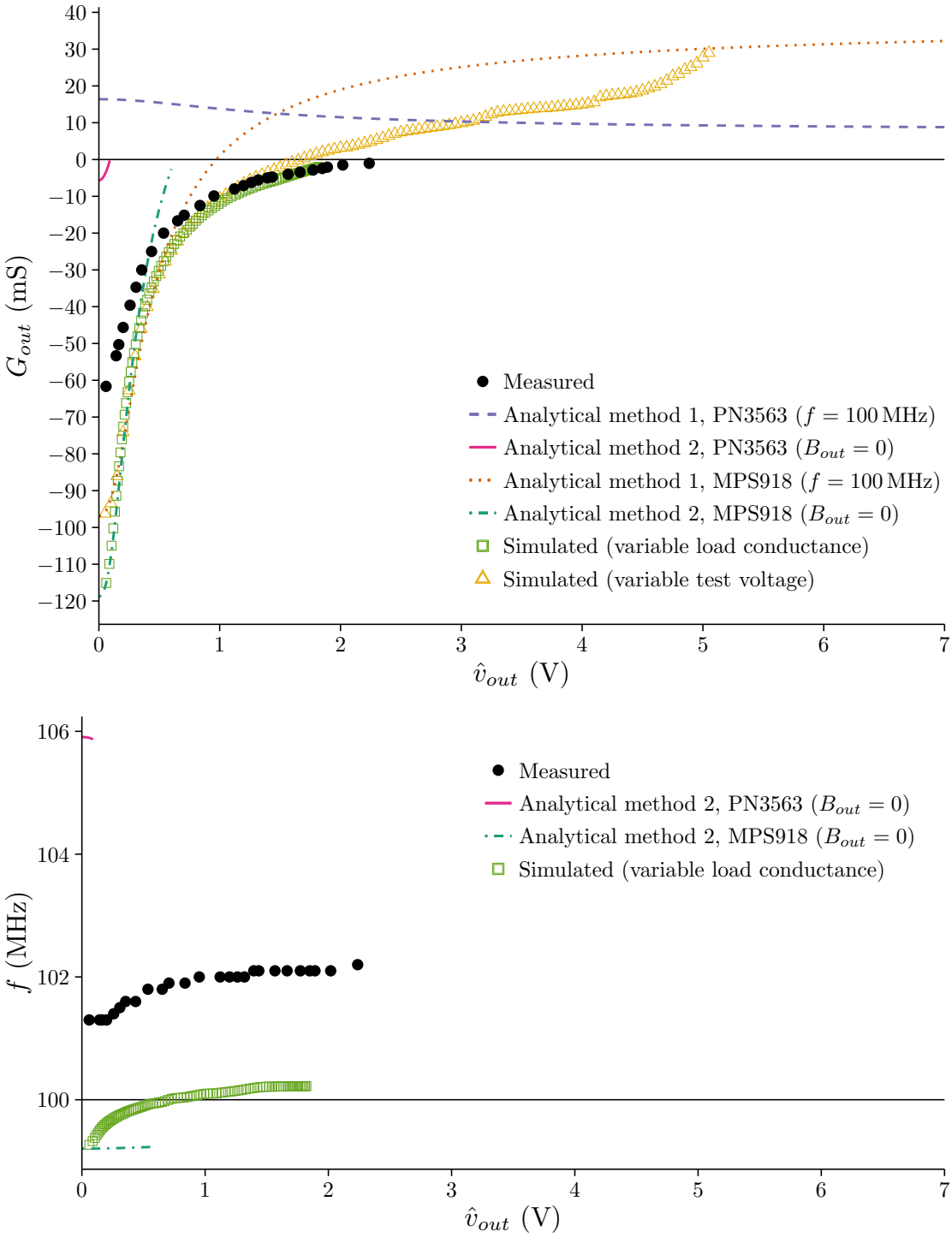

Figure 8. *The measured, simulated and analytically determined output conductance and oscillation frequency in case $x = 2$, $C_1' = 160\,\mathrm{pF}$.*

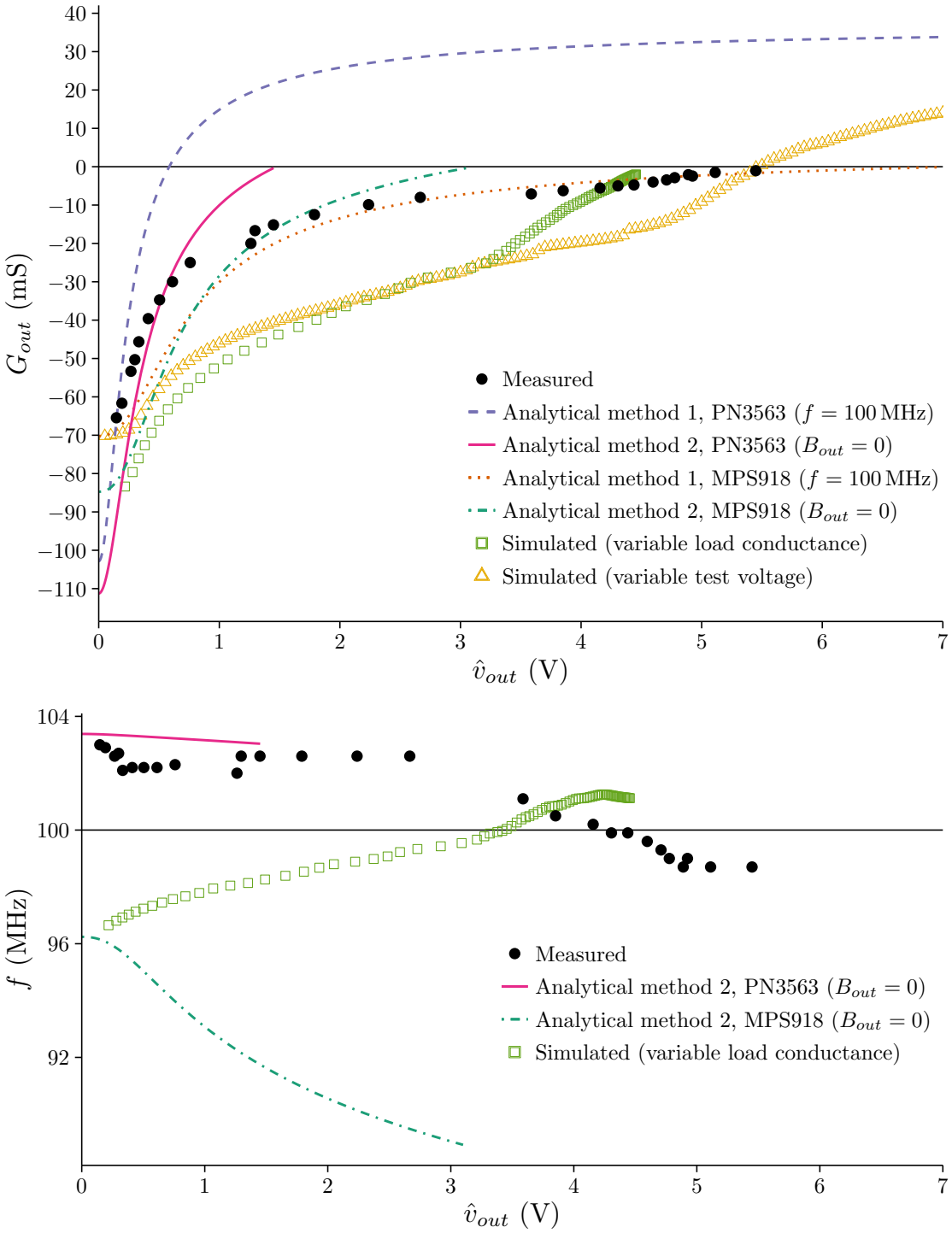

Figure 9. *The measured, simulated and analytically determined output conductance and oscillation frequency in case* $x = 1$, $C_1' = 30\,\mathrm{pF}$.

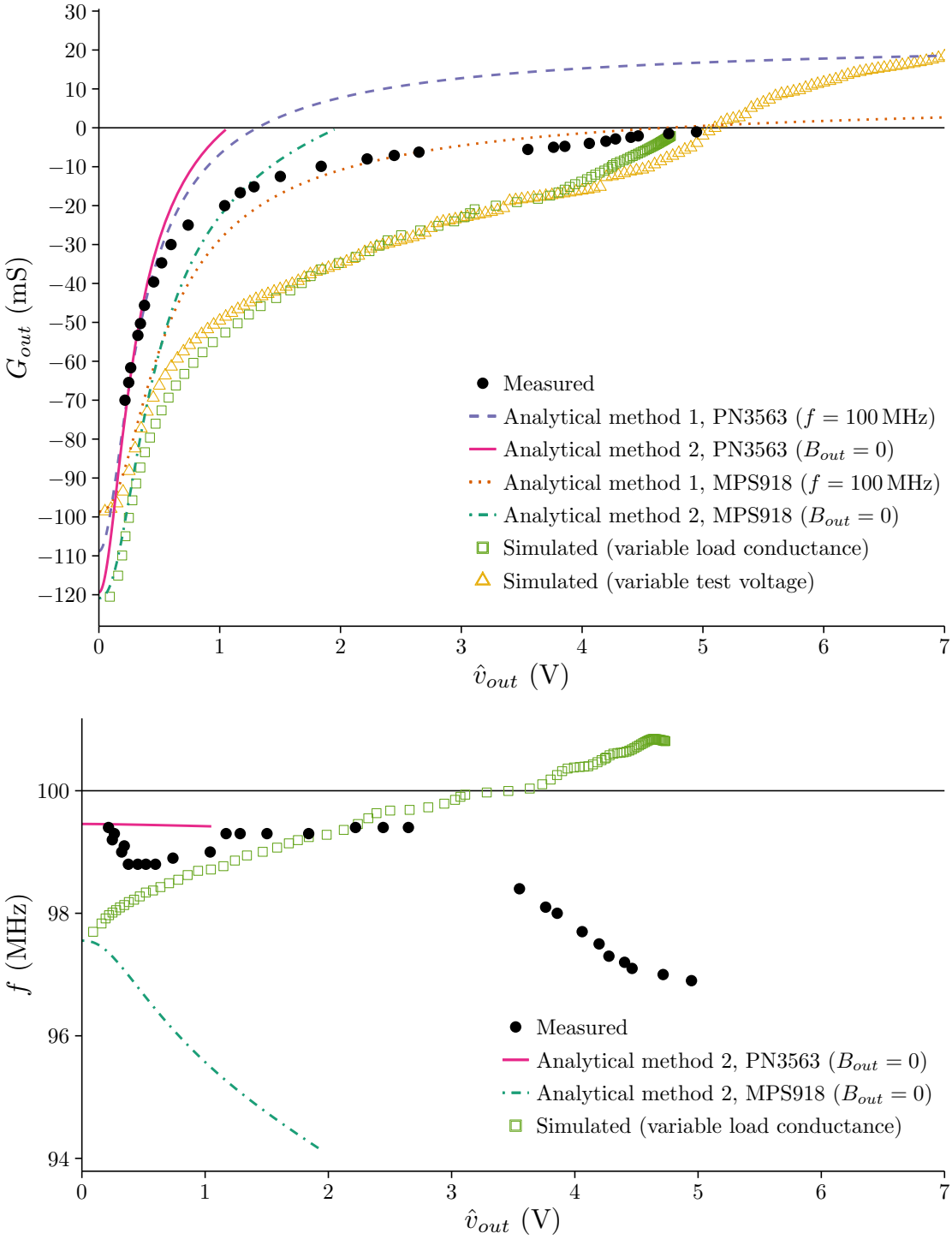

Figure 10. *The measured, simulated and analytically determined output conductance and oscillation frequency in case $x = 1$, $C_1' = 40\,\mathrm{pF}$.*

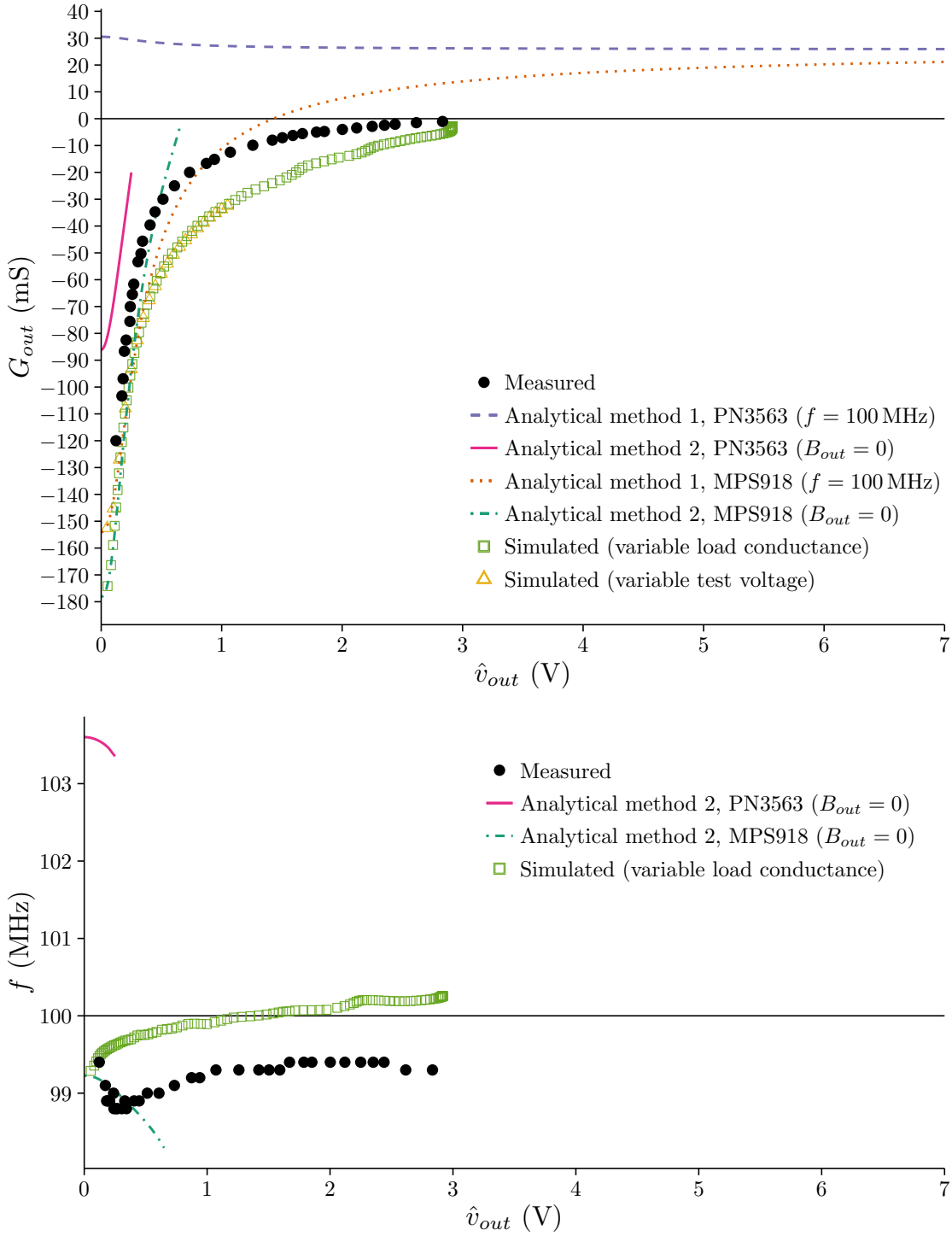

Figure 11. *The measured, simulated and analytically determined output conductance and oscillation frequency in case $x = 1$, $C_1' = 80\,\mathrm{pF}$.*

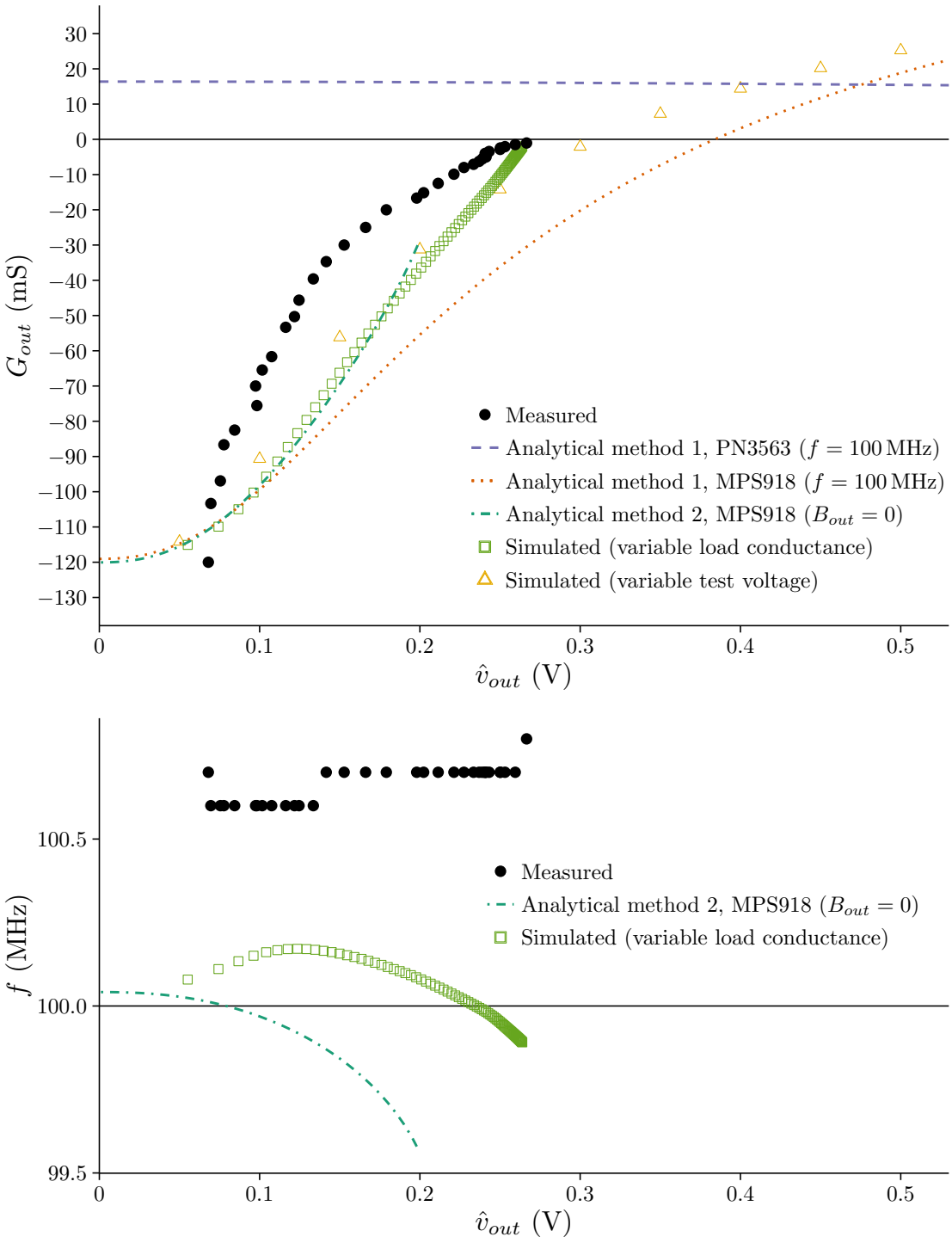

Figure 12. *The measured, simulated and analytically determined output conductance and oscillation frequency in case* $x = 1$, $C_1' = 160\,\mathrm{pF}$.

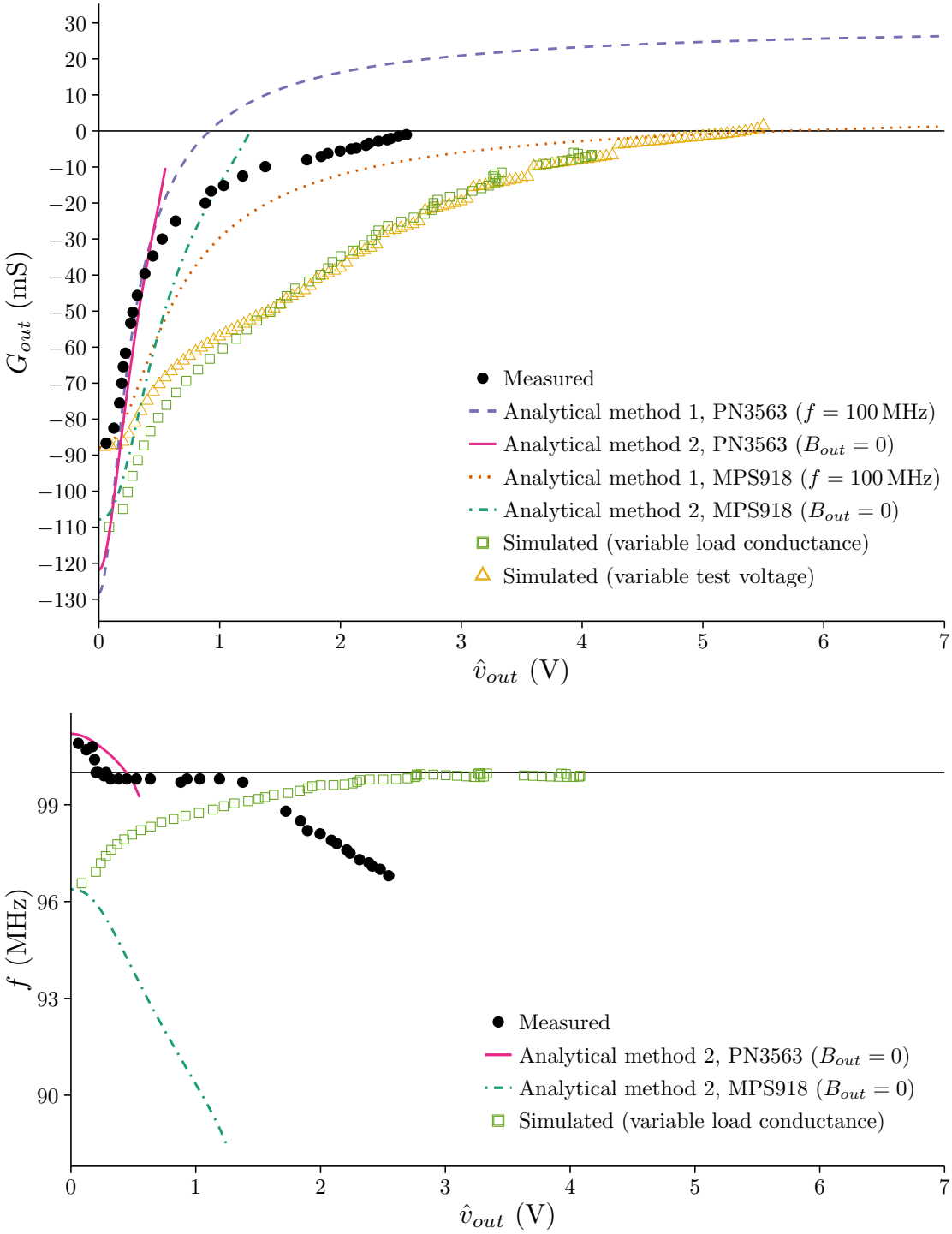

Figure 13. *The measured, simulated and analytically determined output conductance and oscillation frequency in case* $x = 0.5$, $C_1' = 30\,\mathrm{pF}$.

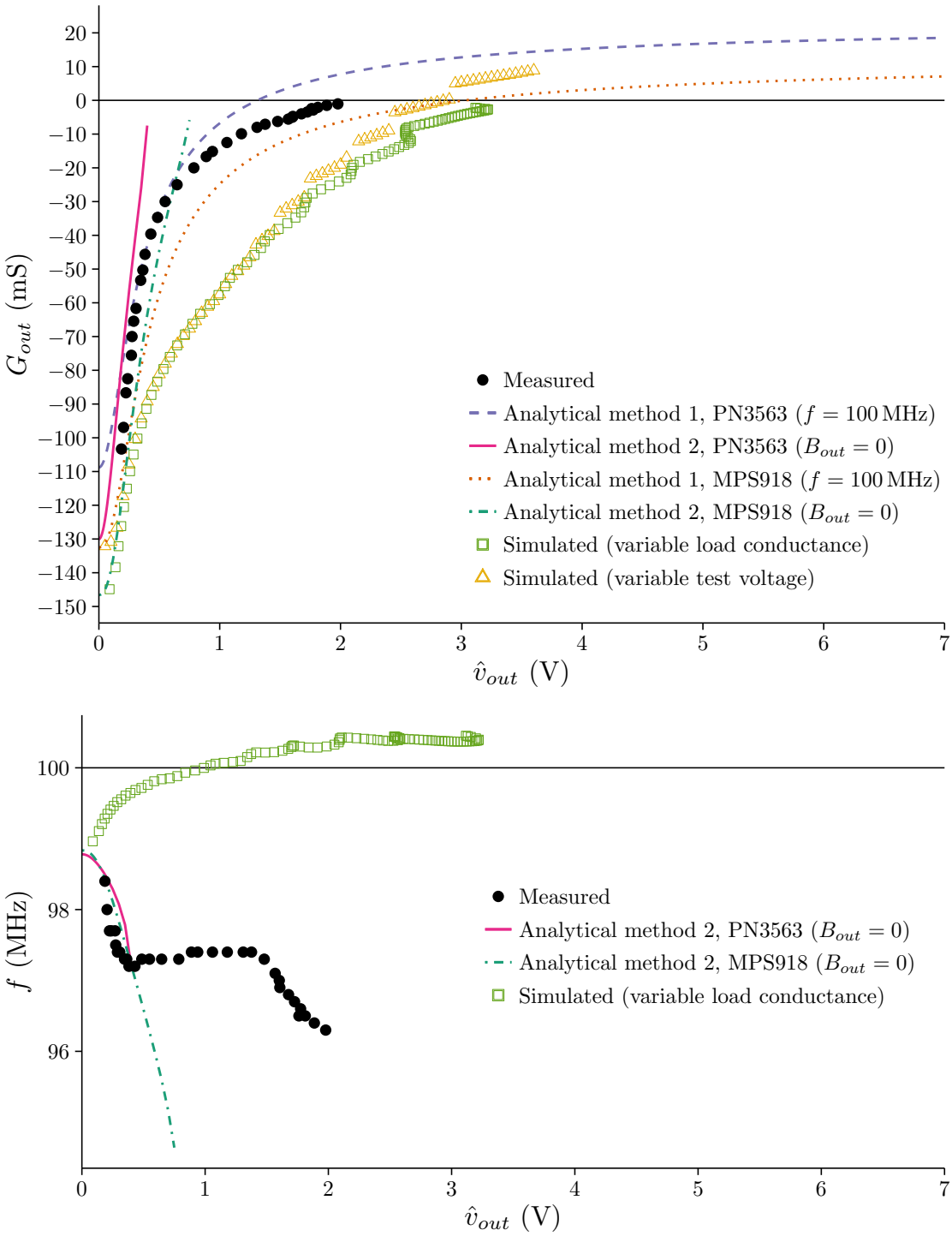

Figure 14. *The measured, simulated and analytically determined output conductance and oscillation frequency in case* $x = 0.5$, $C_1' = 40\,\mathrm{pF}$.

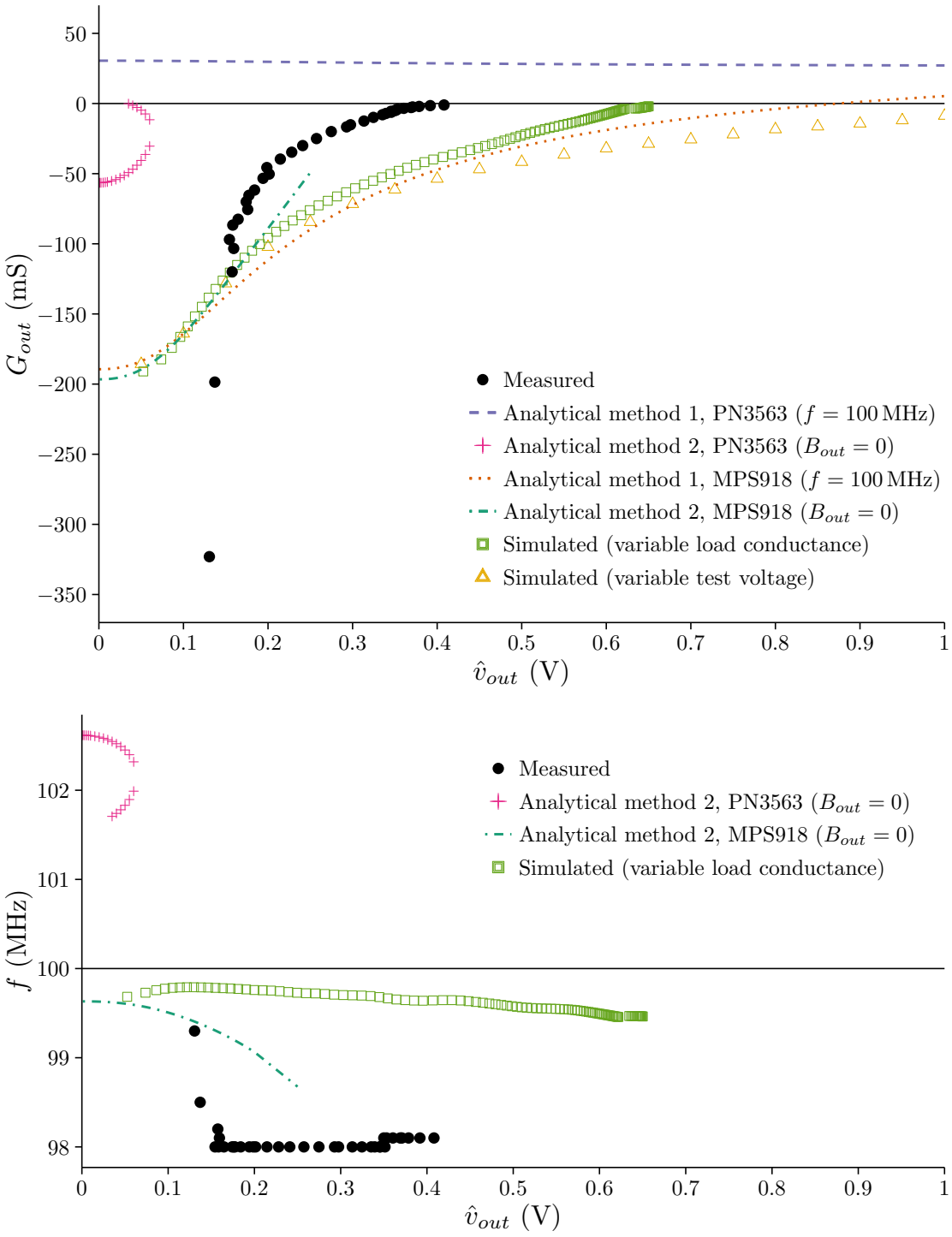

Figure 15. *The measured, simulated and analytically determined output conductance and oscillation frequency in case $x = 0.5$, $C_1' = 80\,\mathrm{pF}$. Multiple solutions exist for some $\hat{v}_{out}$ values with "Analytical method 2, PN3563 ($B_{out} = 0$)".*

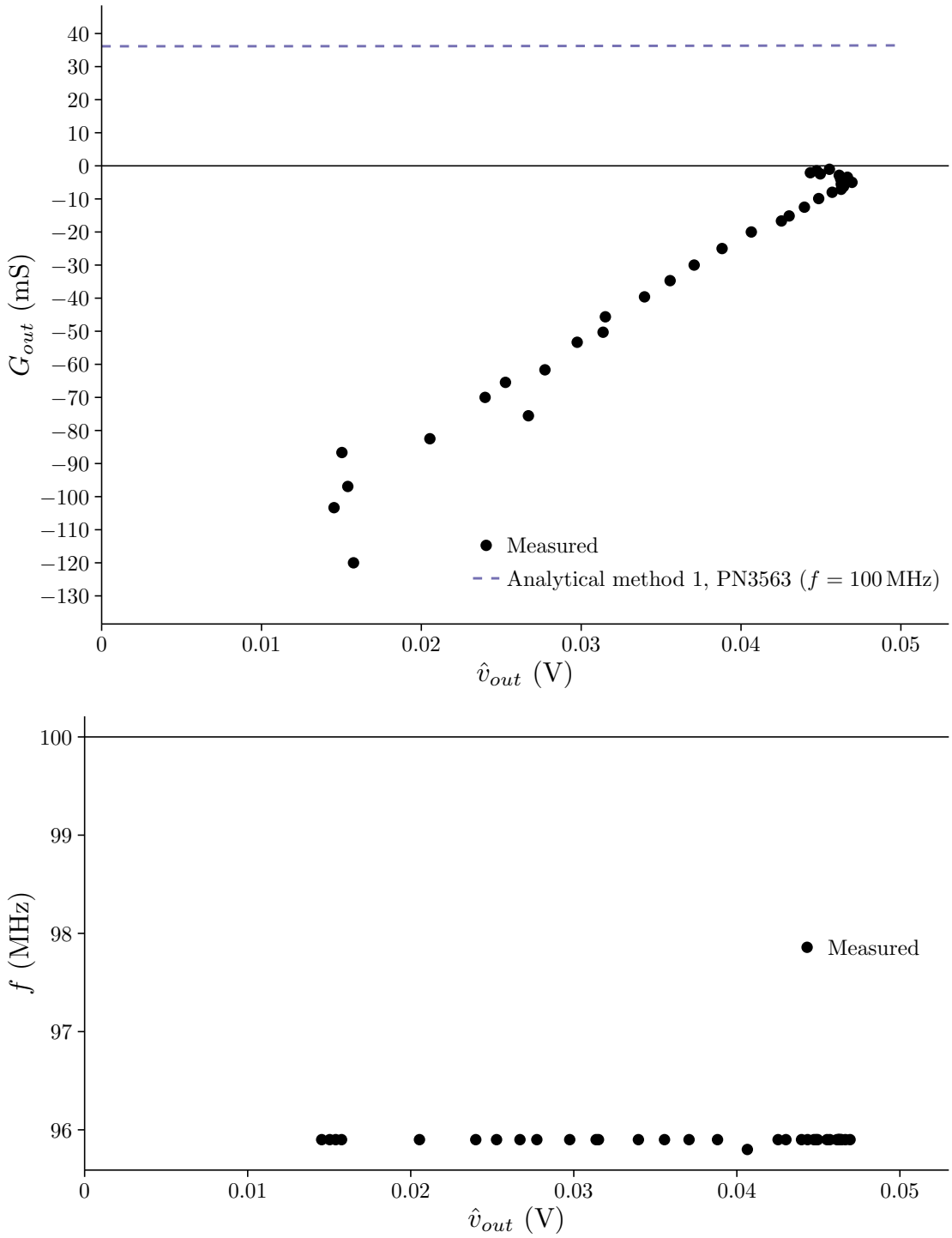

Figure 16. *The measured, simulated and analytically determined output conductance and oscillation frequency in case* $x = 0.5$, $C_1' = 160\,\mathrm{pF}$.

APPENDIX B. MEASUREMENT RESULTS

Table 1. *Measurement results in case* $x \approx 4$, $C_1' \approx 30\,\mathrm{pF}$ *:* $C_r = 8.6\,\mathrm{pF}$, $C_1 = 22\,\mathrm{pF}$, $C_2 = 7.8\,\mathrm{pF} \implies C_1' = 29.7\,\mathrm{pF}$, $C_2' = 7.8\,\mathrm{pF}$.

R_s (Ω)	R_p (Ω)	P_{SA} (dBm)	f (MHz)	G_L (mS)	$\hat{v}_{out}$ (V)
0	–	10.48	100.0	20.00	1.06
910	–	0.38	99.1	1.04	6.34
620	–	3.14	99.8	1.49	6.08
430	–	5.42	100.7	2.08	5.67
360	–	6.52	101.2	2.44	5.49
300	–	7.45	101.7	2.86	5.22
240	–	8.45	102.5	3.45	4.85
200	–	9.12	103.0	4.00	4.52
160	–	9.78	103.2	4.76	4.09
150	–	9.95	103.2	5.00	3.98
130	–	10.29	103.3	5.56	3.72
110	–	10.52	103.3	6.25	3.40
91	–	10.69	103.2	7.09	3.05
75	–	10.81	103.1	8.00	2.74
51	–	10.89	102.7	9.90	2.24
30	–	10.78	102.7	12.50	1.75
16	–	10.56	102.1	15.15	1.41
10	–	10.64	102.0	16.67	1.29
0	200	8.14	99.2	25.00	0.81
0	100	6.14	98.8	30.00	0.64
0	68	4.26	98.9	34.71	0.52
0	51	1.55	98.8	39.61	0.38
0	39	–	–	45.64	–

Table 2. *Measurement results in case* $x \approx 4$, $C_1' \approx 40\,\mathrm{pF}$ *:* $C_r = 6.8\,\mathrm{pF}$, $C_1 = 32\,\mathrm{pF}$, $C_2 = 10\,\mathrm{pF} \implies C_1' = 39.7\,\mathrm{pF}$, $C_2' = 10\,\mathrm{pF}$.

R_s (Ω)	R_p (Ω)	P_{SA} (dBm)	f (MHz)	G_L (mS)	$\hat{v}_{out}$ (V)
0	–	10.08	100.5	20.00	1.01
910	–	0.25	101.7	1.04	6.25
620	–	2.79	102.0	1.49	5.84
430	–	5.33	102.5	2.08	5.61
360	–	6.41	102.8	2.44	5.42
300	–	7.15	103.0	2.86	5.04
240	–	8.07	103.4	3.45	4.64
200	–	8.78	103.7	4.00	4.34
160	–	9.25	103.7	4.76	3.85
150	–	9.60	103.6	5.00	3.82
130	–	9.66	103.6	5.56	3.46
110	–	9.98	103.5	6.25	3.19
91	–	10.08	103.3	7.09	2.85
75	–	9.93	103.2	8.00	2.48
51	–	10.24	102.7	9.90	2.08
30	–	10.21	102.5	12.50	1.64
16	–	10.11	102.0	15.15	1.34
10	–	9.88	101.8	16.67	1.18
0	200	7.88	99.7	25.00	0.78
0	100	6.05	99.2	30.00	0.63
0	68	4.46	99.0	34.71	0.53
0	51	3.06	98.7	39.61	0.45
0	39	1.18	98.4	45.64	0.36
0	33	−12.30	99.9	50.30	0.08
0	30	–	–	53.33	–

Table 3. *Measurement results in case* $x \approx 4$, $C_1' \approx 80\,\mathrm{pF}$ *:* $C_r = 5.6\,\mathrm{pF}$, $C_1 = 71\,\mathrm{pF}$, $C_2 = 20\,\mathrm{pF} \implies C_1' = 78.7\,\mathrm{pF}$, $C_2' = 20\,\mathrm{pF}$.

R_s (Ω)	R_p (Ω)	P_{SA} (dBm)	f (MHz)	G_L (mS)	$\hat{v}_{out}$ (V)
0	–	9.05	99.6	20.00	0.90
910	–	−0.58	101.2	1.04	5.68
620	–	1.88	101.4	1.49	5.26
430	–	4.30	101.5	2.08	4.98
360	–	5.48	101.6	2.44	4.87
300	–	6.56	101.7	2.86	4.71
240	–	7.21	101.8	3.45	4.21
200	–	7.87	101.8	4.00	3.91
160	–	8.46	101.7	4.76	3.52
150	–	8.56	101.6	5.00	3.39
130	–	8.67	101.6	5.56	3.09
110	–	8.95	101.5	6.25	2.84
91	–	8.90	101.3	7.09	2.48
75	–	9.22	101.2	8.00	2.29
51	–	9.24	100.9	9.90	1.85
30	–	9.13	100.7	12.50	1.45
16	–	9.18	100.3	15.15	1.20
10	–	9.24	100.2	16.67	1.10
0	200	6.91	99.1	25.00	0.70
0	100	5.17	98.7	30.00	0.57
0	68	3.72	98.5	34.71	0.49
0	51	2.09	98.2	39.61	0.40
0	39	0.95	98.0	45.64	0.35
0	33	−0.21	98.1	50.30	0.31
0	30	−1.15	97.9	53.33	0.28
0	24	−3.29	97.8	61.67	0.22
0	22	−4.24	97.7	65.45	0.19
0	20	−8.55	97.9	70.00	0.12
0	18	–	–	75.56	–

Table 4. *Measurement results in case* $x \approx 4$, $C_1' \approx 160\,\mathrm{pF}$ *:* $C_r = 5.1\,\mathrm{pF}$, $C_1 = 150\,\mathrm{pF}$, $C_2 = 39\,\mathrm{pF} \implies C_1' = 157.7\,\mathrm{pF}$, $C_2' = 39\,\mathrm{pF}$.

R_s (Ω)	R_p (Ω)	P_{SA} (dBm)	f (MHz)	G_L (mS)	$\hat{v}_{out}$ (V)
0	–	6.31	98.5	20.00	0.65
910	–	−1.97	99.8	1.04	4.84
620	–	0.54	99.9	1.49	4.51
430	–	2.83	99.9	2.08	4.21
360	–	3.71	99.9	2.44	3.97
300	–	4.31	99.9	2.86	3.64
240	–	5.34	99.8	3.45	3.39
200	–	5.93	99.8	4.00	3.13
160	–	6.31	99.7	4.76	2.75
150	–	6.49	99.7	5.00	2.67
130	–	6.47	99.7	5.56	2.40
110	–	6.89	99.6	6.25	2.24
91	–	6.91	99.5	7.09	1.98
75	–	6.87	99.5	8.00	1.74
51	–	7.22	99.3	9.90	1.47
30	–	7.09	99.1	12.50	1.14
16	–	6.87	98.9	15.15	0.92
10	–	6.68	98.8	16.67	0.82
0	200	3.96	98.2	25.00	0.50
0	100	1.22	97.9	30.00	0.36
0	68	−1.11	98.0	34.71	0.28
0	51	−4.75	97.8	39.61	0.18
0	39	−18.50	97.7	45.64	0.04
0	33	–	–	50.30	–

Table 5. *Measurement results in case* $x \approx 2$, $C_1' \approx 30\,\mathrm{pF}$ *:* $C_r = 6.8\,\mathrm{pF}$, $C_1 = 22\,\mathrm{pF}$, $C_2 = 15\,\mathrm{pF} \implies C_1' = 29.7\,\mathrm{pF}$, $C_2' = 15\,\mathrm{pF}$.

R_s (Ω)	R_p (Ω)	P_{SA} (dBm)	f (MHz)	G_L (mS)	$\hat{v}_{out}$ (V)
0	–	11.90	101.7	20.00	1.24
910	–	0.44	98.7	1.04	6.39
620	–	3.04	99.6	1.49	6.01
430	–	5.28	101.3	2.08	5.58
360	–	6.15	101.9	2.44	5.26
300	–	7.24	102.1	2.86	5.09
240	–	8.73	102.4	3.45	5.01
200	–	9.28	102.7	4.00	4.60
160	–	10.51	102.9	4.76	4.45
150	–	10.71	102.9	5.00	4.34
130	–	10.98	103.0	5.56	4.03
110	–	11.43	103.1	6.25	3.77
91	–	11.70	103.2	7.09	3.43
75	–	11.59	103.3	8.00	3.00
51	–	11.66	103.2	9.90	2.45
30	–	11.88	103.2	12.50	1.99
16	–	11.65	103.0	15.15	1.60
10	–	11.58	103.1	16.67	1.44
0	200	9.06	101.7	25.00	0.90
0	100	6.84	101.5	30.00	0.70
0	68	5.50	101.4	34.71	0.60
0	51	3.80	101.3	39.61	0.49
0	39	2.10	101.2	45.64	0.40
0	33	0.63	102.0	50.30	0.34
0	30	−0.59	101.9	53.33	0.30
0	24	–	–	61.67	–

Table 6. *Measurement results in case* $x \approx 2$, $C_1' \approx 40\,\mathrm{pF}$ *:* $C_r = 6.1\,\mathrm{pF}$, $C_1 = 32\,\mathrm{pF}$, $C_2 = 20\,\mathrm{pF} \implies C_1' = 39.7\,\mathrm{pF}$, $C_2' = 20\,\mathrm{pF}$.

R_s (Ω)	R_p (Ω)	P_{SA} (dBm)	f (MHz)	G_L (mS)	$\hat{v}_{out}$ (V)
0	–	10.04	101.4	20.00	1.00
910	–	−0.74	101.6	1.04	5.58
620	–	2.09	101.7	1.49	5.39
430	–	4.58	101.9	2.08	5.14
360	–	5.70	102.0	2.44	5.00
300	–	6.69	102.1	2.86	4.78
240	–	7.96	102.3	3.45	4.59
200	–	8.69	102.4	4.00	4.30
160	–	9.14	102.5	4.76	3.80
150	–	9.24	102.4	5.00	3.66
130	–	9.65	102.5	5.56	3.46
110	–	9.90	102.5	6.25	3.16
91	–	10.18	102.4	7.09	2.88
75	–	10.35	102.4	8.00	2.60
51	–	10.35	102.2	9.90	2.10
30	–	10.42	102.2	12.50	1.68
16	–	10.45	102.0	15.15	1.39
10	–	10.35	101.9	16.67	1.25
0	200	8.17	101.0	25.00	0.81
0	100	6.19	100.8	30.00	0.64
0	68	4.93	100.7	34.71	0.56
0	51	3.33	100.6	39.61	0.46
0	39	1.85	100.4	45.64	0.39
0	33	0.96	101.0	50.30	0.35
0	30	−0.13	100.8	53.33	0.31
0	24	−3.55	101.2	61.67	0.21
0	22	–	–	65.45	–

Table 7. *Measurement results in case* $x \approx 2$, $C_1' \approx 80\,\mathrm{pF}$ *:* $C_r = 5.1\,\mathrm{pF}$, $C_1 = 71\,\mathrm{pF}$, $C_2 = 39\,\mathrm{pF} \implies C_1' = 78.7\,\mathrm{pF}$, $C_2' = 39\,\mathrm{pF}$.

R_s (Ω)	R_p (Ω)	P_{SA} (dBm)	f (MHz)	G_L (mS)	$\hat{v}_{out}$ (V)
0	–	9.04	100.6	20.00	0.90
910	–	−2.10	101.3	1.04	4.77
620	–	0.78	101.3	1.49	4.64
430	–	2.92	101.3	2.08	4.25
360	–	4.00	101.4	2.44	4.11
300	–	4.98	101.4	2.86	3.93
240	–	6.00	101.4	3.45	3.66
200	–	6.65	101.4	4.00	3.40
160	–	7.17	101.3	4.76	3.03
150	–	7.43	101.3	5.00	2.98
130	–	7.83	101.3	5.56	2.80
110	–	8.07	101.3	6.25	2.56
91	–	8.16	101.2	7.09	2.28
75	–	8.58	101.2	8.00	2.12
51	–	8.84	101.1	9.90	1.77
30	–	9.03	101.0	12.50	1.43
16	–	9.16	100.9	15.15	1.20
10	–	8.87	100.8	16.67	1.05
0	200	6.83	100.4	25.00	0.69
0	100	5.36	100.2	30.00	0.59
0	68	3.99	100.1	34.71	0.50
0	51	2.65	100.0	39.61	0.43
0	39	1.08	99.9	45.64	0.36
0	33	0.36	99.9	50.30	0.33
0	30	−0.22	99.9	53.33	0.31
0	24	−1.51	99.8	61.67	0.27
0	22	−2.30	99.7	65.45	0.24
0	20	−3.11	99.8	70.00	0.22
0	18	−4.12	100.0	75.56	0.20
0	16	−6.47	99.8	82.50	0.15
0	15	−8.00	99.8	86.67	0.13
0	13	–	–	96.92	–

Table 8. *Measurement results in case* $x \approx 2$, $C_1' \approx 160\,\mathrm{pF}$ *:* $C_r = 4.7\,\mathrm{pF}$, $C_1 = 150\,\mathrm{pF}$, $C_2 = 78\,\mathrm{pF} \implies C_1' = 157.7\,\mathrm{pF}$, $C_2' = 78\,\mathrm{pF}$.

R_s (Ω)	R_p (Ω)	P_{SA} (dBm)	f (MHz)	G_L (mS)	$\hat{v}_{out}$ (V)
0	–	4.58	101.8	20.00	0.54
910	–	−8.67	102.2	1.04	2.24
620	–	−6.44	102.1	1.49	2.02
430	–	−4.11	102.1	2.08	1.89
360	–	−2.94	102.1	2.44	1.85
300	–	−1.93	102.1	2.86	1.77
240	–	−0.84	102.1	3.45	1.67
200	–	−0.08	102.1	4.00	1.57
160	–	0.68	102.1	4.76	1.44
150	–	0.85	102.1	5.00	1.39
130	–	1.28	102.0	5.56	1.32
110	–	1.92	102.0	6.25	1.26
91	–	2.56	102.0	7.09	1.20
75	–	3.04	102.0	8.00	1.12
51	–	3.47	102.0	9.90	0.95
30	–	4.37	101.9	12.50	0.84
16	–	4.57	101.9	15.15	0.71
10	–	4.70	101.8	16.67	0.65
0	200	2.79	101.6	25.00	0.44
0	100	1.00	101.6	30.00	0.35
0	68	−0.24	101.5	34.71	0.31
0	51	−1.77	101.4	39.61	0.26
0	39	−3.95	101.3	45.64	0.20
0	33	−5.68	101.3	50.30	0.16
0	30	−6.90	101.3	53.33	0.14
0	24	−14.55	101.3	61.67	0.06
0	22	–	–	65.45	–

Table 9. *Measurement results in case* $x \approx 1$, $C_1' \approx 30\,\mathrm{pF}$ *:* $C_r = 5.9\,\mathrm{pF}$, $C_1 = 22\,\mathrm{pF}$, $C_2 = 30\,\mathrm{pF} \implies C_1' = 29.7\,\mathrm{pF}$, $C_2' = 30\,\mathrm{pF}$.

R_s (Ω)	R_p (Ω)	P_{SA} (dBm)	f (MHz)	G_L (mS)	$\hat{v}_{out}$ (V)
0	–	12.02	102.0	20.00	1.26
910	–	−0.94	98.7	1.04	5.45
620	–	1.63	98.7	1.49	5.11
430	–	4.14	98.7	2.08	4.89
360	–	5.57	99.0	2.44	4.92
300	–	6.68	99.0	2.86	4.78
240	–	8.19	99.3	3.45	4.71
200	–	9.27	99.6	4.00	4.60
160	–	10.48	99.9	4.76	4.44
150	–	10.64	99.9	5.00	4.31
130	–	11.25	100.2	5.56	4.16
110	–	11.61	100.5	6.25	3.85
91	–	12.09	101.1	7.09	3.59
75	–	10.56	102.6	8.00	2.67
51	–	10.89	102.6	9.90	2.24
30	–	10.97	102.6	12.50	1.79
16	–	10.81	102.6	15.15	1.45
10	–	10.67	102.6	16.67	1.30
0	200	7.60	102.3	25.00	0.76
0	100	5.73	102.2	30.00	0.61
0	68	4.06	102.2	34.71	0.50
0	51	2.27	102.2	39.61	0.41
0	39	0.44	102.1	45.64	0.33
0	33	−0.47	102.7	50.30	0.30
0	30	−1.46	102.6	53.33	0.27
0	24	−4.33	102.9	61.67	0.19
0	22	−6.67	103.0	65.45	0.15
0	20	–	–	70.00	–

Table 10. *Measurement results in case* $x \approx 1$, $C_1' \approx 40\,\mathrm{pF}$ *:* $C_r = 6.1\,\mathrm{pF}$, $C_1 = 32\,\mathrm{pF}$, $C_2 = 39\,\mathrm{pF} \implies C_1' = 39.7\,\mathrm{pF}$, $C_2' = 39\,\mathrm{pF}$.

R_s (Ω)	R_p (Ω)	P_{SA} (dBm)	f (MHz)	G_L (mS)	$\hat{v}_{out}$ (V)
0	–	10.35	99.0	20.00	1.04
910	–	−1.78	96.9	1.04	4.95
620	–	0.93	97.0	1.49	4.72
430	–	3.35	97.1	2.08	4.46
360	–	4.60	97.2	2.44	4.40
300	–	5.72	97.3	2.86	4.28
240	–	7.19	97.5	3.45	4.20
200	–	8.19	97.7	4.00	4.06
160	–	9.26	98.0	4.76	3.86
150	–	9.47	98.1	5.00	3.76
130	–	9.88	98.4	5.56	3.55
110	–	8.36	99.4	6.25	2.65
91	–	8.76	99.4	7.09	2.44
75	–	8.97	99.4	8.00	2.22
51	–	9.19	99.3	9.90	1.84
30	–	9.45	99.3	12.50	1.50
16	–	9.76	99.3	15.15	1.28
10	–	9.78	99.3	16.67	1.17
0	200	7.37	98.9	25.00	0.74
0	100	5.52	98.8	30.00	0.60
0	68	4.31	98.8	34.71	0.52
0	51	3.13	98.8	39.61	0.45
0	39	1.53	98.8	45.64	0.38
0	33	0.73	99.1	50.30	0.34
0	30	0.18	99.0	53.33	0.32
0	24	−1.59	99.3	61.67	0.26
0	22	−2.15	99.2	65.45	0.25
0	20	−3.31	99.4	70.00	0.22
0	18	–	–	75.56	–

Table 11. *Measurement results in case* $x \approx 1$, $C_1' \approx 80\,\mathrm{pF}$ *:* $C_r = 5.1\,\mathrm{pF}$, $C_1 = 71\,\mathrm{pF}$, $C_2 = 78\,\mathrm{pF} \implies C_1' = 78.7\,\mathrm{pF}$, $C_2' = 78\,\mathrm{pF}$.

R_s (Ω)	R_p (Ω)	P_{SA} (dBm)	f (MHz)	G_L (mS)	$\hat{v}_{out}$ (V)
0	–	7.31	99.1	20.00	0.73
910	–	−6.62	99.3	1.04	2.83
620	–	−4.19	99.3	1.49	2.62
430	–	−1.90	99.4	2.08	2.44
360	–	−0.85	99.4	2.44	2.35
300	–	0.14	99.4	2.86	2.25
240	–	1.26	99.4	3.45	2.12
200	–	2.05	99.4	4.00	2.00
160	–	2.89	99.4	4.76	1.85
150	–	3.00	99.4	5.00	1.79
130	–	3.33	99.4	5.56	1.67
110	–	3.93	99.3	6.25	1.59
91	–	4.54	99.3	7.09	1.50
75	–	5.09	99.3	8.00	1.42
51	–	5.89	99.3	9.90	1.26
30	–	6.52	99.3	12.50	1.07
16	–	7.05	99.2	15.15	0.94
10	–	7.24	99.2	16.67	0.87
0	200	5.68	99.0	25.00	0.61
0	100	4.20	99.0	30.00	0.51
0	68	3.01	98.9	34.71	0.45
0	51	2.16	98.9	39.61	0.41
0	39	0.72	98.8	45.64	0.34
0	33	0.37	98.9	50.30	0.33
0	30	−0.30	98.8	53.33	0.31
0	24	−1.36	98.8	61.67	0.27
0	22	−1.74	98.8	65.45	0.26
0	20	−2.35	98.8	70.00	0.24
0	18	−2.45	99.0	75.56	0.24
0	16	−3.68	98.9	82.50	0.21
0	15	−4.33	98.9	86.67	0.19
0	13	−4.80	98.9	96.92	0.18
0	12	−5.30	99.1	103.33	0.17
0	10	−8.24	99.4	120.00	0.12
0	5.6	–	–	198.57	–

Table 12. *Measurement results in case* $x \approx 1$, $C_1' \approx 160\,\mathrm{pF}$ *:* $C_r = 4.7\,\mathrm{pF}$, $C_1 = 150\,\mathrm{pF}$, $C_2 = 160\,\mathrm{pF} \implies C_1' = 157.7\,\mathrm{pF}$, $C_2' = 160\,\mathrm{pF}$.

R_s (Ω)	R_p (Ω)	P_{SA} (dBm)	f (MHz)	G_L (mS)	$\hat{v}_{out}$ (V)
0	–	−4.94	100.7	20.00	0.18
910	–	−27.15	100.8	1.04	0.27
620	–	−24.26	100.7	1.49	0.26
430	–	−21.58	100.7	2.08	0.25
360	–	−20.31	100.7	2.44	0.25
300	–	−18.94	100.7	2.86	0.25
240	–	−17.55	100.7	3.45	0.24
200	–	−16.35	100.7	4.00	0.24
160	–	−14.84	100.7	4.76	0.24
150	–	−14.39	100.7	5.00	0.24
130	–	−13.56	100.7	5.56	0.24
110	–	−12.61	100.7	6.25	0.24
91	–	−11.64	100.7	7.09	0.23
75	–	−10.82	100.7	8.00	0.23
51	–	−9.21	100.7	9.90	0.22
30	–	−7.58	100.7	12.50	0.21
16	–	−6.29	100.7	15.15	0.20
10	–	−5.65	100.7	16.67	0.20
0	200	−5.59	100.7	25.00	0.17
0	100	−6.32	100.7	30.00	0.15
0	68	−6.98	100.7	34.71	0.14
0	51	−7.49	100.6	39.61	0.13
0	39	−8.09	100.6	45.64	0.12
0	33	−8.29	100.6	50.30	0.12
0	30	−8.69	100.6	53.33	0.12
0	24	−9.37	100.6	61.67	0.11
0	22	−9.86	100.6	65.45	0.10
0	20	−10.22	100.6	70.00	0.10
0	18	−10.15	100.6	75.56	0.10
0	16	−11.47	100.6	82.50	0.08
0	15	−12.19	100.6	86.67	0.08
0	13	−12.44	100.6	96.92	0.08
0	12	−13.15	100.6	103.33	0.07
0	10	−13.35	100.7	120.00	0.07
0	5.6	–	–	198.57	–

Table 13. *Measurement results in case* $x \approx 0.5$, $C_1' \approx 30\,\mathrm{pF}$ *:* $C_r = 6.1\,\mathrm{pF}$, $C_1 = 22\,\mathrm{pF}$, $C_2 = 59.9\,\mathrm{pF} \implies C_1' = 29.7\,\mathrm{pF}$, $C_2' = 59.9\,\mathrm{pF}$.

R_s (Ω)	R_p (Ω)	P_{SA} (dBm)	f (MHz)	G_L (mS)	$\hat{v}_{out}$ (V)
0	–	8.89	99.7	20.00	0.88
910	–	−7.55	96.8	1.04	2.55
620	–	−4.66	97.0	1.49	2.48
430	–	−1.99	97.1	2.08	2.41
360	–	−0.72	97.2	2.44	2.39
300	–	0.38	97.3	2.86	2.31
240	–	1.72	97.5	3.45	2.24
200	–	2.91	97.6	4.00	2.21
160	–	4.10	97.8	4.76	2.13
150	–	4.35	97.9	5.00	2.09
130	–	4.88	98.1	5.56	2.00
110	–	5.45	98.2	6.25	1.90
91	–	6.29	98.5	7.09	1.84
75	–	6.76	98.8	8.00	1.72
51	–	6.67	99.7	9.90	1.38
30	–	7.43	99.8	12.50	1.19
16	–	7.87	99.8	15.15	1.03
10	–	7.78	99.8	16.67	0.93
0	200	6.06	99.8	25.00	0.64
0	100	4.38	99.8	30.00	0.52
0	68	3.01	99.8	34.71	0.45
0	51	1.61	99.8	39.61	0.38
0	39	0.04	99.8	45.64	0.32
0	33	−1.02	100.0	50.30	0.28
0	30	−1.58	99.9	53.33	0.26
0	24	−3.16	100.0	61.67	0.22
0	22	−3.92	100.0	65.45	0.20
0	20	−4.45	100.4	70.00	0.19
0	18	−5.33	100.8	75.56	0.17
0	16	−8.16	100.7	82.50	0.12
0	15	−14.55	100.9	86.67	0.06
0	13	–	–	96.92	–

Table 14. *Measurement results in case* $x \approx 0.5$, $C_1' \approx 40\,\mathrm{pF}$ *:* $C_r = 6.1\,\mathrm{pF}$, $C_1 = 32\,\mathrm{pF}$, $C_2 = 78\,\mathrm{pF} \implies C_1' = 39.7\,\mathrm{pF}$, $C_2' = 78\,\mathrm{pF}$.

R_s (Ω)	R_p (Ω)	P_{SA} (dBm)	f (MHz)	G_L (mS)	$\hat{v}_{out}$ (V)
0	–	7.91	97.3	20.00	0.79
910	–	−9.74	96.3	1.04	1.98
620	–	−7.03	96.4	1.49	1.89
430	–	−4.48	96.5	2.08	1.81
360	–	−3.36	96.5	2.44	1.76
300	–	−1.92	96.6	2.86	1.77
240	–	−0.53	96.7	3.45	1.73
200	–	0.51	96.8	4.00	1.68
160	–	1.65	96.9	4.76	1.61
150	–	2.05	97.0	5.00	1.60
130	–	2.78	97.1	5.56	1.57
110	–	3.30	97.3	6.25	1.48
91	–	3.77	97.4	7.09	1.38
75	–	4.38	97.4	8.00	1.31
51	–	5.33	97.4	9.90	1.18
30	–	6.42	97.4	12.50	1.06
16	–	7.05	97.4	15.15	0.94
10	–	7.39	97.4	16.67	0.89
0	200	6.22	97.3	25.00	0.65
0	100	4.78	97.3	30.00	0.55
0	68	3.73	97.3	34.71	0.49
0	51	2.67	97.2	39.61	0.43
0	39	1.64	97.2	45.64	0.38
0	33	1.22	97.3	50.30	0.36
0	30	0.78	97.3	53.33	0.35
0	24	−0.25	97.4	61.67	0.31
0	22	−0.80	97.4	65.45	0.29
0	20	−1.23	97.5	70.00	0.27
0	18	−1.40	97.7	75.56	0.27
0	16	−2.45	97.7	82.50	0.24
0	15	−3.00	97.7	86.67	0.22
0	13	−3.79	98.0	96.92	0.20
0	12	−4.57	98.4	103.33	0.19
0	10	–	–	120.00	–

Table 15. *Measurement results in case* $x \approx 0.5$, $C_1' \approx 80\,\mathrm{pF}$ *:* $C_r = 5.1\,\mathrm{pF}$, $C_1 = 71\,\mathrm{pF}$, $C_2 = 160\,\mathrm{pF} \implies C_1' = 78.7\,\mathrm{pF}$, $C_2' = 160\,\mathrm{pF}$.

R_s (Ω)	R_p (Ω)	P_{SA} (dBm)	f (MHz)	G_L (mS)	$\hat{v}_{out}$ (V)
0	–	−1.22	98.0	20.00	0.27
910	–	−23.45	98.1	1.04	0.41
620	–	−20.68	98.1	1.49	0.39
430	–	−18.08	98.1	2.08	0.38
360	–	−16.89	98.1	2.44	0.37
300	–	−15.56	98.1	2.86	0.37
240	–	−14.13	98.1	3.45	0.36
200	–	−13.02	98.1	4.00	0.35
160	–	−11.55	98.0	4.76	0.35
150	–	−11.16	98.1	5.00	0.35
130	–	−10.36	98.0	5.56	0.35
110	–	−9.33	98.0	6.25	0.35
91	–	−8.39	98.0	7.09	0.34
75	–	−7.45	98.0	8.00	0.34
51	–	−5.88	98.0	9.90	0.32
30	–	−4.16	98.0	12.50	0.31
16	–	−2.94	98.0	15.15	0.30
10	–	−2.25	98.0	16.67	0.29
0	200	−1.79	98.0	25.00	0.26
0	100	−2.36	98.0	30.00	0.24
0	68	−2.84	98.0	34.71	0.23
0	51	−3.37	98.0	39.61	0.21
0	39	−4.04	98.0	45.64	0.20
0	33	−3.92	98.0	50.30	0.20
0	30	−4.24	98.0	53.33	0.19
0	24	−4.70	98.0	61.67	0.18
0	22	−5.02	98.0	65.45	0.18
0	20	−5.18	98.0	70.00	0.17
0	18	−5.09	98.0	75.56	0.18
0	16	−5.67	98.0	82.50	0.16
0	15	−6.01	98.0	86.67	0.16
0	13	−6.23	98.0	96.92	0.15
0	12	−5.95	98.1	103.33	0.16
0	10	−6.05	98.2	120.00	0.16
0	5.6	−7.26	98.5	198.57	0.14
0	3.3	−7.68	99.3	323.03	0.13
0	1	–	–	1020.00	–

Table 16. *Measurement results in case* $x \approx 0.5$, $C_1' \approx 160\,\mathrm{pF}$ *:* $C_r = 5.1\,\mathrm{pF}$, $C_1 = 150\,\mathrm{pF}$, $C_2 = 330\,\mathrm{pF} \implies C_1' = 157.7\,\mathrm{pF}$, $C_2' = 330\,\mathrm{pF}$.

R_s (Ω)	R_p (Ω)	P_{SA} (dBm)	f (MHz)	G_L (mS)	$\hat{v}_{out}$ (V)
0	–	−17.82	95.8	20.00	0.04
910	–	−42.50	95.9	1.04	0.05
620	–	−39.53	95.9	1.49	0.04
430	–	−36.71	95.9	2.08	0.04
360	–	−35.22	95.9	2.44	0.04
300	–	−33.62	95.9	2.86	0.05
240	–	−31.89	95.9	3.45	0.05
200	–	−30.68	95.9	4.00	0.05
160	–	−29.14	95.9	4.76	0.05
150	–	−28.61	95.9	5.00	0.05
130	–	−27.82	95.9	5.56	0.05
110	–	−26.77	95.9	6.25	0.05
91	–	−25.70	95.9	7.09	0.05
75	–	−24.76	95.9	8.00	0.05
51	–	−23.07	95.9	9.90	0.04
30	–	−21.22	95.9	12.50	0.04
16	–	−19.74	95.9	15.15	0.04
10	–	−19.01	95.9	16.67	0.04
0	200	−18.22	95.9	25.00	0.04
0	100	−18.62	95.9	30.00	0.04
0	68	−18.98	95.9	34.71	0.04
0	51	−19.38	95.9	39.61	0.03
0	39	−20.03	95.9	45.64	0.03
0	33	−20.07	95.9	50.30	0.03
0	30	−20.53	95.9	53.33	0.03
0	24	−21.14	95.9	61.67	0.03
0	22	−21.95	95.9	65.45	0.03
0	20	−22.40	95.9	70.00	0.02
0	18	−21.47	95.9	75.56	0.03
0	16	−23.75	95.9	82.50	0.02
0	15	−26.46	95.9	86.67	0.02
0	13	−26.25	95.9	96.92	0.02
0	12	−26.75	95.9	103.33	0.01
0	10	−26.05	95.9	120.00	0.02
0	5.6	–	–	198.57	–

APPENDIX C. SIMULATION CIRCUITS

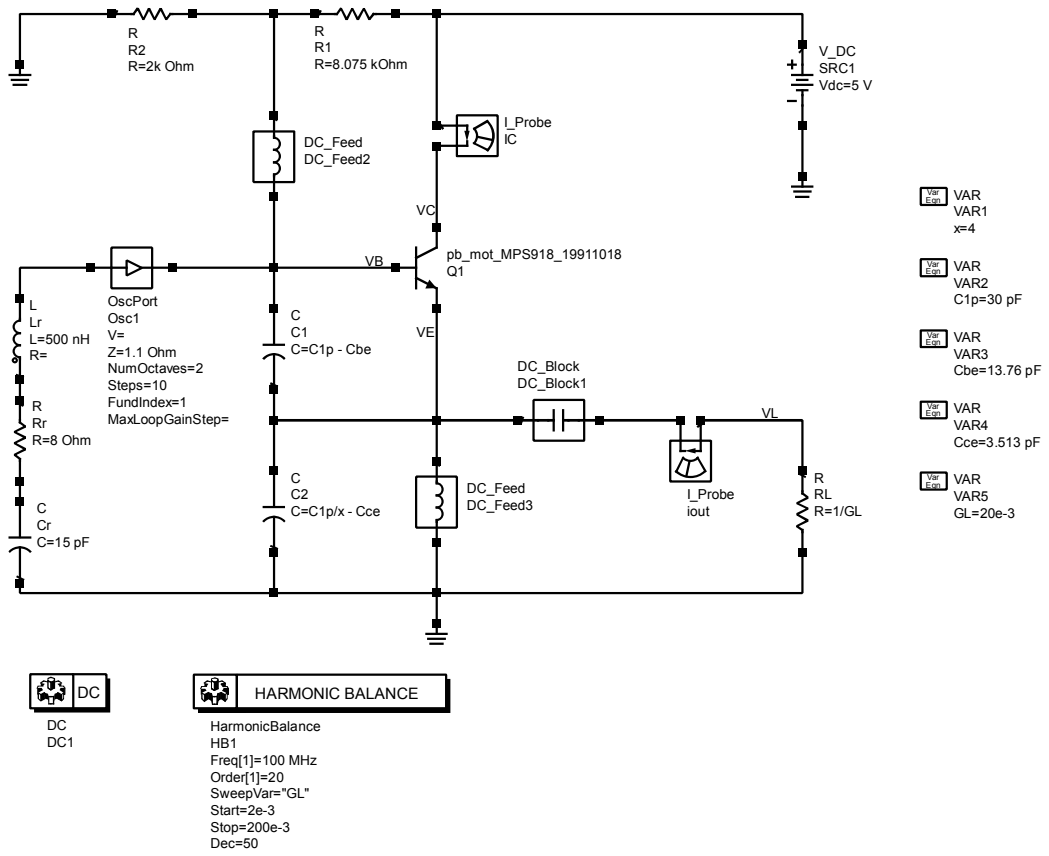

Figure 17. *The simulation circuit of the variable load method.*

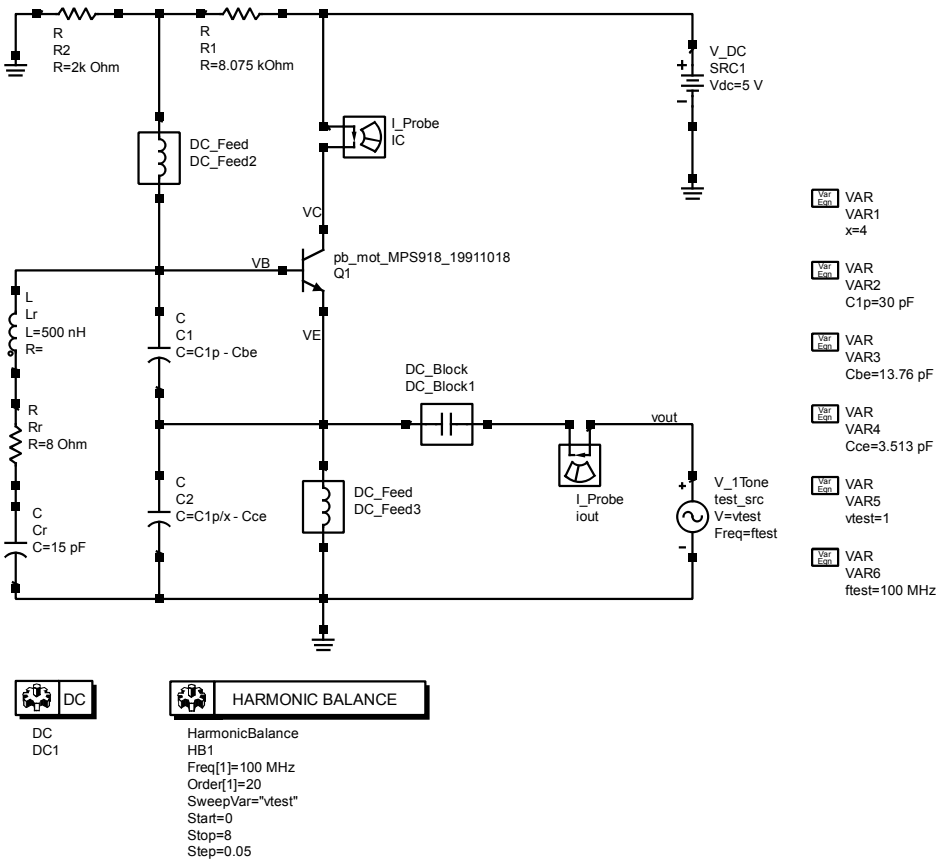

Figure 18. *The simulation circuit of the variable test voltage method.*